Dynamics of phase transitions in strings, beams and atomic chains

Thesis by

Prashant K. Purohit

In Partial Fulfillment of the Requirements

for the Degree of

Doctor of Philosophy

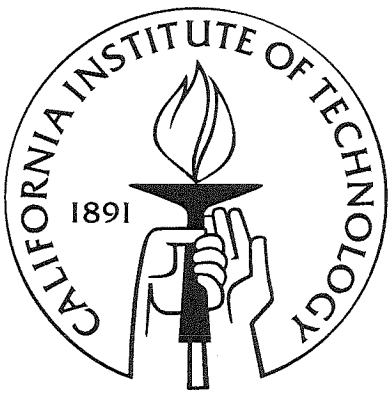

California Institute of Technology

Pasadena, California

2002

(Submitted November 08, 2001)

To my parents,

Sibanand Purohit and Sanjukta Purohit.

Acknowledgements

I am finding it particularly difficult to write this part. Is it because I was never too good at articulating my thoughts and feelings (Kaushik knows this very well) or is it because words can't express them, I do not know. But I must write, for a dissertation such as this is written only once in a person's life and I never could have done it without so many people that kept me going.

It has been such a pleasure to have Kaushik Bhattacharya as my advisor. I did not even think before I joined you Kaushik, but today as I stand ready to fly on my own, I know you are the one that prepared me. I wish you always remain my mentor and my friend.

I am grateful to Jim Knowles who took such an avid interest in my work and guided me all through these years. I also thank the National Science Foundation, the Air Force Office of Scientific Research and the California Institute of Technology who funded my research through various grants and fellowships.

I treasure the friendships with Amit Manwani, Nitin Deshpande, Pradeep Guduru, Ravinder Abrol and Sandeep Sane. You fellows made up my little India and were the cushion on which I landed when I came here as a new student.

I thank Gustavo Joseph, Michel Tanguay and Patrick Hung who have been with me in all those rigours that an engineering education at Caltech put us through. You fellows along with Dan Zimmerman and Guillaume Lessard are my connection to America.

I also thank my brother and my best friend, Prabir Purohit, for having stood with me as I went through the trials and tribulations of being away from my home and in a different country.

And finally, a word for Deepshikha Datta, the one that is so full of vitality and so full of energy. Over all these years and after endless cups of coffee I do not know when you became my source of inspiration and my source of motivation.

Abstract

This thesis presents a theory for dynamical martensitic phase transitions in strings and beams. Shape memory alloys that rely on such phase transitions for their unique properties are often used in slender configurations like beams and rods. Yet most studies of phase transformations are in one dimension and consider only extension. The theory presented in this thesis to model these slender structures is based on the general continuum mechanical framework of thermoelasticity with a non-convex Helmholtz free energy. This non-convexity allows for the simultaneous existence of several metastable phases in a material; in particular, it leads to the formation of phase boundaries. The study of the laws governing the propagation of phase boundaries is the object of this thesis.

Phase boundaries in strings are studied first. It is demonstrated that the motion of phase boundaries is not *fully* described by the usual balance laws of mass, momentum and energy. Additional constitutive information must be furnished from outside, and this additional information is referred to as the *kinetic relation.* While this notion is well-accepted in continuum theory, there is no definitive experiment or theoretical framework to determine the kinetic relation. This study of strings proposes a simple experiment to determine the kinetic relation. It also proposes a numerical method that accurately describes the complex behaviour of strings with phase boundaries.

The kinetic relation can also be viewed from the atomic scale. Phase transformations involve a complex rearrangemnet of the atoms the explicit details of which are averaged in a continuum theory. The kinetic relation may be viewed as an aggregate of those aspects of the atomistic rearrangement that have a bearing on macroscopic phenomena. This view is explored using a simple one dimensional model of an atomic chain with non-convex interaction potentials. A kinetic relation is obtained from dynamic simulations of impact experiments on the chain.

The latter part of this thesis studies beams made of materials capable of phase transi-

tions. It develops a conceptual framework that accounts for extension, shear and flexure in such beams using a non-convex stored energy function. Specific constitutive assumptions that relate to the underlying crystallography are developed. The theory is applied to design a simple experiment on single crystals of martensitic materials with the objective of measuring the kinetic relation.

Finally, propulsion at small scales is discussed as an application of beams made of phase transforming material. The goal is to mimic the flagellum of a micro-organism by propagating phase boundaries through a shearbale rod.

Contents

List of Figures

Chapter 1

Introduction

Various crystalline solids undergo a martensitic phase transformation that results in the formation of fascinating microstructures, and there has been much recent effort in understanding this microstructure and its evolution when subjected to thermal and mechanical loads. A continuum theory in the framework of thermoelasticity has emerged. The Helmholtz free energy density is non-convex in this theory, and this leads to a change of type in the governing equations, and this in turn leads to a rich but incompletely understood behaviour including phase boundaries and microstructure. Apart from this theoretical interest, growing applications of shape-memory alloys has provided a technological motivation.

It is now well-recognized that the usual balance laws of continuum mechanics do not completely determine the evolution or propagation of phase boundaries, and that one needs to provide additional constitutive information. This is usually done in the form of a *kinetic relation*: first, a thermodynamic driving force acting on the phase boundary is identified, and then a constitutive kinetic relation is postulated which gives the velocity of propagation of the phase boundary as a function of the driving force.

The notion of a driving force was first introduced from a variational point of view as the 'force on a defect' by Eshelby (1956). He subsequently discussed the concept of driving force in a very general context of field theories (Eshelby, 1975). Abeyaratne and Knowles (1990) introduced the driving force on any surface of discontinuity (not necessarily a phase boundary) associated with a thermo-mechanical process in an arbitrary continuum as the dynamic conjugate of the velocity of the discontinuity in the entropy inequality. In particular, they show that the driving force times the velocity divided by the absolute temperature is the rate of entropy production associated with the motion of the discontinuity. They also introduced the notion of a kinetic relation in this setting adapting ideas in Materi-

als Science (Abeyaratne and Knowles, 1991). More recently, Gurtin (1995) has developed a framework where such forces, referred to as configurational forces, are introduced and treated on par with the traditional deformational forces. The kinetic relation is then a part of the constitutive framework.

These works are largely conceptual as they set up the equations in a general setting, but do not study solutions. The detailed study of solutions has been carried out in the setting of bars, where Ericksen (1975) pointed out that non-convex energy leads to extreme non-uniqueness of equilibrium solutions. Abeyaratne and Knowles (1991) showed in a purely mechanical setting that a simple Riemann problem with initial data containing a phase boundary admits a one-parameter family of solutions, the parameter being the velocity of propagation of the phase boundary. They introduce the kinetic relation as an additional constitutive relation, and show that this naturally selects one amongst this family of solutions. They subsequently extended this framework to the thermoelastic setting and applied it to various problems (Abeyaratne and Knowles, 1993, 1994, 1997). One may regard the kinetic relation as the continuum manifestation of the microscopic physics at the phase boundary that are ignored in the continuuum theory. Slemrod (1983,1984), Truskinovsky (1998), and Turteltaub (1997) look for travelling wave solutions of an augmented set of governing equations which includes viscosity, capillarity and heat conduction and attempt to derive kinetic relations from them. The existence and derivation of kinetic relations from an atomistic model remains largely open though Puglisi and Truskinovsky (2000), Balk, Cherkaev and Slepyan (2001a,b) have studied phase boundary propagation in discrete nonlinear chains.

While the concept of kinetic relation as a constitutive degree of freedom has gained wide acceptance, there has yet to be a definitive experimental validation. A direct experimental measurement of the kinetic relation has also proved to be a daunting challenge, and is largely open. There have been some innovative and sophisticated attempts like those of Escobar and Clifton (1993), but the data collected is very limited.

This thesis studies the dynamics of phase phase transitions in strings and beams. We formulate a general continuum theory for both of them and then solve some problems using special constitutive relations. The need for kinetic relations is established for both but the theory does not furnish any information on the particular form of the kinetic relation. This has to be done through experiments. Keeping this in mind we suggest experiments to determine the kinetic relation governing the propapagation of phase boundaries in actual

martensitic materials.

The study of phase transforming strings and beams is also motivated by applications. Shape-memory alloys are being increasingly used in medical devices (such as stents, guide wires and dental arch-wires) and thermal actuators (such as thermostats and valves in IC engines and ventilation systems). In fact, the number of innovative products that exploit the unique properties of shape-memory materials is steadily increasing. Most of these devices are constructed from Nickel-Titanium (NiTi) wire, strips or tubes and they rely on the flexural (as in strips and tubes), torsional (as in wire springs) and extensional (as in wires and tubes) characteristics of the alloy. Proper design of these devices requires an understanding of the behaviour of these alloys in these long slender configurations (or more generally, in the form of lower dimensional structures). However, much of the current literature on shape-memory alloys, as noted earlier, focusses on uniaxial extension of bars or wires or full dimensional continua. Also these alloys in the form of wires or strips have noticeable shear and bending stiffness thereby requiring treatment as a beam or a rod. The available theories do not take these into account.

The thesis is organised into five chapters. Chapter 2 studies strings. We develop a thermomechanical framework for the dynamics of strings and demonstrate the need for a kinetic relation. We study specific problems analytically and numerically and propose a simple experiment to measure the kinetic relation.

Chapter 3 deals with atomistic simulations. We view the kinetic relation as an aggregate of those atomistic phenomena that have a bearing on the macroscopic behaviour. We obtain a kinetic realtion from dynamic simulations of impact experiments on one dimensioanl chains with non-convex interaction potentials.

Chapter 4 studies beams. We present a theory that accounts for extension, shear and flexure and thus goes beyond the one-dimensional framework of strings and bars. We develop specific constitutive relations that relate to the underlying crystallography. We also apply the theory to design a simple experiment on single crystals of martensitic materials with the objective of measuring the kinetic relation.

Finally, chapter 5 deals with a more esoteric application by studying the use of phase-transforming strings and beams for propulsion at small scales. Various microbes propel themselves with the use of flagella. This propulsion is generated from the reaction of the ambient viscous fluid to repeated deformation (beating) of the flagella. We examine if it

is possible to recreate such propulsion using strings made of phase transforming material. Since a string has no transverse stiffness, it can generate only longitudinal motions in a viscous medium. We show that longitudinal motions can not generate propulsion. We conclude that propulsion necessarily requires transverse deformation modes which in turn require beams or rods. The idea is to mimic microorganims and propagate bending waves through a beam. We propose a mechanism of doing this by propagating a large number of phase boundaries through a beam.

Chapter 2

Dynamics of strings

2.1 Introduction

In this chapter, we study the behaviour of strings made of a phase-transforming material. A string is a one-dimensional continuum moving in three dimensions. It can resist stretch, but not shear or curvature. It thus provides a simple generalization of the bar. The general thermo-mechanical theory is presented in Section 2.2. Some of this treatment is classical, especially the field equations for smooth motions, yet included for completeness.

We specialize to the purely mechanical setting in Section 2.3. We consider an up-down-up tension-stretch relation appropriate for the phase transforming materials with nonconvex energies. We begin by studying travelling waves and discontinuities. There are two types of travelling waves: longitudinal as in bars and also transverse (like for example the wave travelling down a taut rope). There are also two types of discontinuities: those with continuous tangent, and those with discontinuous tangent. The discontinuities with continuous tangent correspond to the bar discontinuities, and their behaviour in strings is very similar. In particular, the jump conditions determine the propagation velocity of the shocks (discontinuities where both sides are in the same phase), but the jump conditions alone are *insufficient* to determine the velocity of propagation of phase boundaries (discontinuities where the two sides are in different phases). The latter is a manifestation of the need for a kinetic relation.

The tangent discontinuities, however, reveal some surprises. Notably, the jump conditions alone are *sufficient* to determine the velocity of propagation of phase boundaries (discontinuities where the two sides are in different phases). Therefore no kinetic relation is necessary for such phase boundaries. It turns out that the jump conditions associated

with tangent discontinuities are vector valued, and contain more information than in the case with the tangent continuous. In fact, the state (stretch) on one side of this tangent discontinuity uniquely determines the velocity of propagation of this discontinuity as well as the state on the other. In particular, this gives a direct relation between the driving force and the velocity, and thus the jump conditions themselves imply a kinetic relation. We find that this kinetic relation is qualitatively different from those commonly accepted in the literature.

These phase boundaries with tangent discontinuities yield a definitive test of the notion of a kinetic relation. Notice that a kinetic relation rules out the existence of phase boundaries with tangent discontinuities unless the kinetic relation happens to coincide with that implied by the jump conditions!

To further understand these issues, we turn to some simple problems in Section 2.4. First we study Riemann problems and then we look at a Goursat-Riemann impact problem. A Riemann problem studies the evolution of an infinite string with a discontinuity at the origin. The discontinuity could be a phase boundary with or without a discontinuity in the tangent. The evolution of such problems is studied in Section 2.4.2. We find a one parameter family of solutions to this problem. Each solution in this family has the following features: there are two leading longitudinal shock waves moving in opposite directions followed by shock waves with tangent discontinuites also moving in opposite directions and a phase boundary whose velocity can be altered freely from zero (which corresponds to a solution with a contact discontinuity) to one where it moves faster than one of the tangent discontinuities. We conclude that we need a kinetic relation to choose from this family of solutions.

In a Goursat-Riemann problem a semi-infinite uniformly stretched string in the low strain phase is impacted with a constant velocity on one side. We find a one parameter family of solutions to this problem as well. It has exactly the same features as the Riemann problem discussed above. The study of these problems yields a simple experiment for measuring the kinetic relation. As explained in Section 2.4.3, it is possible to set up a simple experiment and infer the velocity of propagation of the phase boundary as well as the driving force acting on it by measuring the velocity of a clearly visible tangent discontinuity.

Section 2.5 builds on the solution of the Riemann and Goursat-Riemann problems to develop a numerical method for solving general initial and boundary value problems in phase

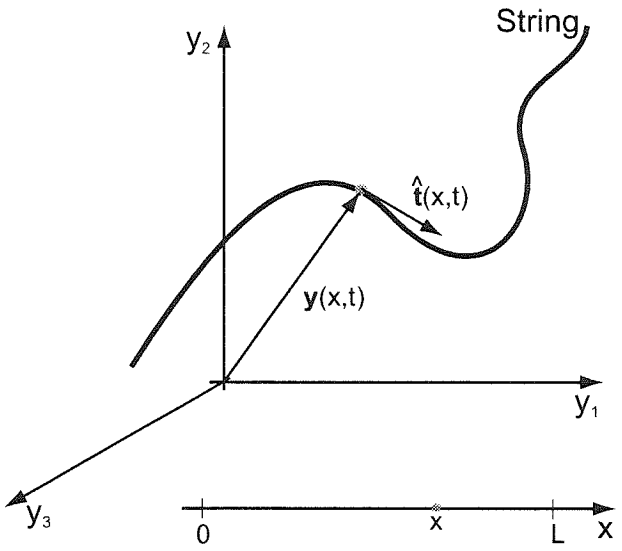

Figure 2.1: A string in a three-dimensional space.

transforming strings. This is a modified Godunov method following the work of Zhong, Hou and LeFloch (1996) which captures shocks, but explicitly tracks phase boundaries. We study several examples – a plucked string, a whipped string and a string with nucleating phase boundaries. The interactions between the various shocks bouncing off the ends of the finite strings and the phase boundaries are quite interesting.

2.2 Thermomechanics of strings

2.2.1 Kinematics

We consider a string as shown in Figure 2.1 that occupies the interval $(0, L)$ in the reference configuration. The position in the deformed configuration of a particle x at time t is given by the vector $\mathbf{y}(x,t)$. We use a superposed dot to denote material time derivative. So the particle velocity $\frac{\partial \mathbf{y}}{\partial t}$ is $\dot{\mathbf{y}}(x,t)$. We denote the stretch $|\frac{\partial \mathbf{y}}{\partial x}|$ by λ and the tangent $\frac{1}{\lambda}\frac{\partial \mathbf{y}}{\partial x}$ by $\hat{\mathbf{t}}$. In doing so, we have assumed sufficient smoothness on the displacement field of the string.

We are interested in shocks and phase boundaries which involve discontinuities in stretch, and hence we must relax some of the assumptions on smoothness. We require $\mathbf{y}(x,t)$ to be continuous in x and t, but allow the particle velocity $\dot{\mathbf{y}}$, the stretch λ and the tangent $\hat{\mathbf{t}}$ to jump across a finite number of points along the string. The points of discontinuity are allowed to move in the reference configuration. Consider one such discontinuity whose

position in the reference configuration is $x = s(t)$. We name $x > s(t)$ as the + side and $x < s(t)$ as the – side in the immediate vicinity of the discontinuity. For any quantity $f(x,t)$ which is smooth except at $x = s(t)$, we denote $f(x^+,t) - f(x^-,t)$ by $[\![f]\!]$. Therefore, continuity implies $[\![\mathbf{y}]\!] = 0$. Differentiating this equation with respect to time we find that

$$\dot{s}[\![\lambda\hat{\mathbf{t}}]\!] + [\![\dot{\mathbf{y}}]\!] = 0. \tag{2.1}$$

We call this the kinematic jump condition.

We also note the following for future use. If $f(x,t)$ is smooth in the interval (x_1, x_2) except for a single discontinuity whose position is given by $x = s(t)$. It is easy to see that

$$f(x_2) - f(x_1) = \int_{x_1}^{x_2} \frac{\partial f}{\partial x}\, dx + [\![f]\!]. \tag{2.2}$$

and

$$\frac{d}{dt}\int_{x_1}^{x_2} f\, dx = \int_{x_1}^{x_2} \dot{f}\, dx - \dot{s}[\![f]\!]. \tag{2.3}$$

2.2.2 Balance laws

The balance of *linear momentum* for a portion of the string occupying the interval (x_1, x_2) requires

$$\frac{d}{dt}\int_{x_1}^{x_2} \rho\dot{\mathbf{y}}\, dx = \mathbf{T}(x_2,t) - \mathbf{T}(x_1,t) + \int_{x_1}^{x_2} \mathbf{b}\, dx, \tag{2.4}$$

where

ρ denotes the mass per unit length of the string in the reference configuration (assumed constant),

$\mathbf{T} = \mathbf{T}(x,t)$ denotes the force acting at material point x in the deformed configuration at time t, and

$\mathbf{b} = \mathbf{b}(x)$ denotes a distributed load per unit reference length of the string at material point x.

If there are no discontinuities in the interval (x_1, x_2), we can localise (2.4) to get

$$\rho\ddot{\mathbf{y}} = \frac{\partial \mathbf{T}}{\partial x} + \mathbf{b}. \tag{2.5}$$

We need a jump condition if there is a discontinuity in the interval (x_1, x_2). This is obtained by applying (2.2) and (2.3) to (2.4). We have

$$\int_{x_1}^{x_2} \rho\ddot{\mathbf{y}}\, dx - \dot{s}[|\, \rho\dot{\mathbf{y}}\, |] = \int_{x_1}^{x_2} \frac{\partial \mathbf{T}}{\partial x}\, dx + [|\, \mathbf{T}\, |]\,.$$

Letting $x_1 \to s^-(t)$ and $x_2 \to s^+(t)$ we obtain

$$-\dot{s}[|\, \rho\dot{\mathbf{y}}\, |] = [|\, \mathbf{T}\, |]\,. \tag{2.6}$$

The balance of *angular momentum* for the same piece of the string requires

$$\frac{d}{dt}\Big(\int_{x1}^{x_2} \mathbf{y} \times \rho\dot{\mathbf{y}}\, dx\Big) = \mathbf{y}(x_2,t) \times \mathbf{T}(x_2,t) - \mathbf{y}(x_1,t) \times \mathbf{T}(x_1,t) + \int_{x_1}^{x_2} \mathbf{y} \times \mathbf{b}\, dx\,. \tag{2.7}$$

Localizing this relation and using (2.5), we get

$$\frac{\partial \mathbf{y}}{\partial x} \times \mathbf{T} = 0, \quad \text{or} \quad \mathbf{T} = T\hat{\mathbf{t}}\,. \tag{2.8}$$

where,

$T = T(x,t)$ is the scalar value of the tension at material point x in the string at time t, and

$\hat{\mathbf{t}} = \hat{\mathbf{t}}(x,t)$ is the unit vector along the tangent to the string at material point x at time t.

Therefore, the force at any point in the string is along the tangent to the string at that point. Hence, we can rewrite (2.5) and (2.6) as

$$\rho\ddot{\mathbf{y}} = \frac{\partial}{\partial x}(T\hat{\mathbf{t}}) + \mathbf{b}\,, \tag{2.9}$$

$$-\dot{s}[|\, \rho\dot{\mathbf{y}}\, |] = [|\, T\hat{\mathbf{t}}\, |]\,. \tag{2.10}$$

The jump condition corresponding to the conservation of angular momentum does not furnish any new information.

We can use (2.9) to derive a statement of the balance of *mechanical power* for the portion of the string between (x_1, x_2). Take the inner (dot) product of (2.9) with $\dot{\mathbf{y}}$ and integrate

from x_1 to x_2 to get

$$\int_{x_1}^{x_2} \rho\ddot{\mathbf{y}} \cdot \dot{\mathbf{y}}\, dx = \int_{x_1}^{x_2} \frac{\partial}{\partial x}(T\hat{\mathbf{t}}) \cdot \dot{\mathbf{y}}\, dx + \int_{x_1}^{x_2} \mathbf{b} \cdot \dot{\mathbf{y}}\, dx.$$

Assuming a single discontinuity at $x = s(t)$, we can use (2.2) and (2.3) to rewrite this as

$$\frac{d}{dt}\Big(\frac{1}{2}\int_{x_1}^{x_2} \rho|\dot{\mathbf{y}}|^2\, dx\Big) + \dot{s}[\,|\, \frac{1}{2}\rho|\dot{\mathbf{y}}|^2\,|\,] = T\hat{\mathbf{t}} \cdot \dot{\mathbf{y}}\,\Big|_{x_1}^{x_2} - [\,|\, T\hat{\mathbf{t}} \cdot \dot{\mathbf{y}}\,|\,] - \int_{x_1}^{x_2} T\hat{\mathbf{t}} \cdot \frac{\partial \dot{\mathbf{y}}}{\partial x}\, dx + \int_{x1}^{x_2} \mathbf{b} \cdot \dot{\mathbf{y}}\, dx\,.$$

Using the identities

$$[\,|\, \mathbf{a} \cdot \mathbf{b}\,|\,] = \langle \mathbf{a} \rangle \cdot [\,|\, \mathbf{b}\,|\,] + \langle \mathbf{b} \rangle \cdot [\,|\, \mathbf{a}\,|\,], \qquad \hat{\mathbf{t}} \cdot \frac{\partial \dot{\mathbf{y}}}{\partial x} = \dot{\lambda}$$

where $\langle \mathbf{a} \rangle = \frac{1}{2}(\mathbf{a}^+ + \mathbf{a}^-)$ etc., and by using the jump condition (2.10), we obtain the statement of the balance of mechanical power for the portion of the string between x_1 and x_2:

$$\frac{d}{dt}\Big(\frac{1}{2}\int_{x_1}^{x_2} \rho|\dot{\mathbf{y}}|^2\Big) = T\hat{\mathbf{t}} \cdot \dot{\mathbf{y}}\,\Big|_{x_1}^{x_2} - \int_{x_1}^{x_2} T\dot{\lambda}\, dx + \int_{x_1}^{x_2} \mathbf{b} \cdot \dot{\mathbf{y}}\, dx + \dot{s}[\,|\, \lambda\hat{\mathbf{t}}\,|\,] \cdot \langle T\hat{\mathbf{t}} \rangle\,. \tag{2.11}$$

The balance of *energy* for the portion of the string between x_1 and x_2 requires

$$\frac{d}{dt}\int_{x_1}^{x_2} \Big(\rho\varepsilon + \frac{1}{2}\rho|\dot{\mathbf{y}}|^2\Big)\, dx = -q\,\Big|_{x_1}^{x_2} + T\hat{\mathbf{t}} \cdot \dot{\mathbf{y}}\,\Big|_{x_1}^{x_2} - \int_{x_1}^{x_2} G(\theta)\, dx + \int_{x_1}^{x_2} \mathbf{b} \cdot \dot{\mathbf{y}}\, dx \tag{2.12}$$

where

$\varepsilon = \varepsilon(x,t)$ is the internal energy per unit mass at material point x at time t,

$q = q(x,t)$ is the heat flow in the tangential direction at the material point x at time t,

$\theta = \theta(x,t)$ is the temperature at the material point x at time t, and

$G(\theta)$ is the rate of heat lost per unit length from the string to the environment at any time.

Assuming a single discontinuity at $x = s(t)$, we can use the balance of mechanical power (2.11) to rewrite this as

$$\frac{d}{dt}\int_{x_1}^{x_2} \rho\varepsilon\, dx = \int_{x_1}^{x_2} \Big(-\frac{\partial q}{\partial x} - G(\theta) + T\dot{\lambda}\Big)\, dx - \dot{s}[\,|\, \lambda\hat{\mathbf{t}}\,|\,] \cdot \langle T\hat{\mathbf{t}} \rangle - [\,|\, q\,|\,]\,. \tag{2.13}$$

Localizing this equation away from $x = s(t)$, we obtain

$$\rho\dot{\varepsilon} = -\frac{\partial q}{\partial x} - G(\theta) + T\dot{\lambda}\,. \tag{2.14}$$

Localizing at $x = s(t)$, we have

$$\dot{s}\Big(\rho[\![\,\varepsilon\,]\!] - \langle T\hat{\mathbf{t}}\rangle \cdot [\![\,\lambda\hat{\mathbf{t}}\,]\!]\Big) = [\![\,q\,]\!]\,. \tag{2.15}$$

We finally turn to the *entropy* inequality. For (x_1, x_2), this requires

$$\frac{d}{dt}\int_{x_1}^{x_2} \rho\eta\, dx \geq -\frac{q}{\theta}\Big|_{x_1}^{x_2} - \int_{x_1}^{x_2} \frac{G(\theta)}{\theta}\, dx\,. \tag{2.16}$$

Localizing this away from any discontinuities, we get

$$\rho\dot{\eta} + \frac{\partial}{\partial x}\Big(\frac{q}{\theta}\Big) + \frac{G(\theta - \theta_0)}{\theta} \geq 0\,. \tag{2.17}$$

Multiplying the equation above by θ and using (2.14), we get

$$\rho(\theta\dot{\eta} - \dot{\varepsilon}) + T\dot{\lambda} - \frac{q}{\theta}\frac{\partial\theta}{\partial x} \geq 0\,.$$

Introducing the Helmholtz free energy $\psi = \varepsilon - \theta\eta$, we can finally write

$$\rho\dot{\psi} + \rho\dot{\theta}\eta - T\dot{\lambda} + \frac{q}{\theta}\frac{\partial\theta}{\partial x} \leq 0\,. \tag{2.18}$$

Localizing to a discontinuity at $x = s(t)$, we get

$$-\rho\dot{s}\theta[\![\,\eta\,]\!] + [\![\,q\,]\!] \geq 0\,. \tag{2.19}$$

Using (2.15) above, we obtain

$$\dot{s}\Big(\rho[\![\,\psi\,]\!] - \langle T\hat{\mathbf{t}}\rangle \cdot [\![\,\lambda\hat{\mathbf{t}}\,]\!]\Big) \geq 0\,. \tag{2.20}$$

Notice that this is of the form $f\dot{s} \geq 0$ where

$$f(\lambda, \theta) = \rho[\![\,\psi\,]\!] - \langle T\hat{\mathbf{t}}\rangle \cdot [\![\,\lambda\hat{\mathbf{t}}\,]\!]\,. \tag{2.21}$$

The quantity f is the dynamic conjugate of the velocity of the discontinuity and is therefore called the *driving force* on the discontinuity. This derivation of the driving force follows the work of Abeyaratne and Knowles (1990) who introduced it on a surface of discontinuity (not necessarily a phase boundary) associated with a thermomechanical process in an arbitrary continuum. They show that $f\dot{s}/\theta$ is the entropy production rate associated with the motion of a discontinuity. The origins of the concept of the driving force, however, are more ancient. It was introduced (from a variational point of view) as the 'force on a defect' by Eshelby (1956). Eshelby (1975) has also discussed the concept of driving force in a very general context of field theories. More recently, Gurtin (2000) has developed a framework where such forces, referred to as configurational forces, are introduced and treated on par with the traditional deformational forces.

We conclude by looking at the dissipation inequality in three settings. First, thermodynamic or *local equilibrium*. Here we set $f = 0$ so that

$$\rho\dot{s}\theta[\![\,\eta\,]\!] = [\![\,q\,]\!]\,. \tag{2.22}$$

Trivially then $f\dot{s} = 0$. Second, we have the *adiabatic* setting where $[\![\,q\,]\!] = 0$ so that jump conditions (2.15) and (2.19) will now read

$$\dot{s}\Big(\rho[\![\,\psi + \theta\eta\,]\!] - \langle T\hat{\mathbf{t}}\rangle \cdot [\![\,\lambda\hat{\mathbf{t}}\,]\!]\Big) = 0\,, \tag{2.23}$$

$$\rho\dot{s}\theta[\![\,\eta\,]\!] \leq 0\,. \tag{2.24}$$

Remembering the definition of the driving force from (2.21), we can rewrite the above equations more conveniently as

$$f\dot{s} = -\rho\dot{s}\theta[\![\,\eta\,]\!] \geq 0\,. \tag{2.25}$$

Finally, we have the *isothermal* case $\theta = const$ which means that $\frac{\partial\theta}{\partial x} = 0$ everywhere. Equations (2.15) and (2.19) merely tell us that

$$f\dot{s} \geq 0\,. \tag{2.26}$$

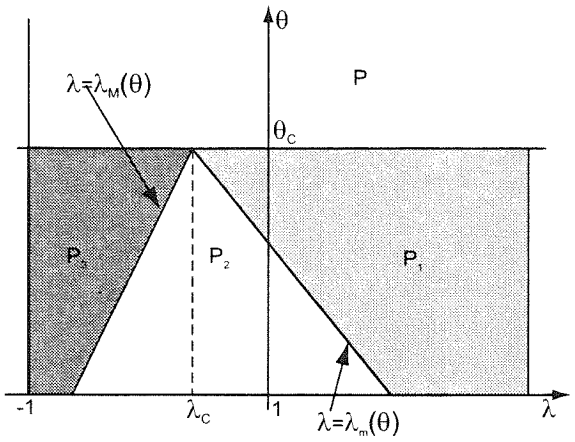

Figure 2.2: The $\lambda - \theta$ plane.

2.2.3 Constitutive assumptions

We assume that T,ψ and η are constitutive functions of λ and θ, and that $q = -k\frac{\partial\theta}{\partial x}$ where k is a material constant. The entropy inequality (2.18) now becomes

$$\Big(\rho\frac{\partial\psi}{\partial\lambda} - T\Big)\dot{\lambda} + \rho\Big(\frac{\partial\psi}{\partial\theta} + \eta\Big) - \frac{k}{\theta}\Big|\frac{\partial\theta}{\partial x}\Big|^2 \leq 0\,.$$

Arguing in the spirit of Coleman and Noll (1963), we conclude

$$T = \rho\frac{\partial\psi}{\partial\lambda}\,, \qquad \eta = -\frac{\partial\psi}{\partial\theta}\,, \qquad k \geq 0\,.$$

Therefore we only have to specify a constitutive relation for ψ.

We now provide a simple example of a constitutive law suitable for a phase transforming material with two stable phases: a *low strain* phase with a stress-free stretch equal to 1 and a *high strain* phase with a stress-free stretch equal to $(1 + \gamma_T)$ where $\gamma_T > 0$ is the transformation stretch. The two phases are linear with elastic modulus $E > 0$ which is assumed to be constant and equal in both phases. We assume that the low strain phase is preferred at high temperatures (so that the free energy is lower at $\lambda = 1$ than at $\lambda = (1+\gamma_T)$ at high temperatures), while the high strain phase is preferred at low temperatures, with the exchange of stability occurring at the transformation temperature θ_T. Abeyaratne and Knowles (1997) have proposed a constitutive relation with similar properties for bars. We

adapt this to strings and we have

$$\psi(\lambda,\theta) = \begin{cases} \frac{E}{2\rho}(\lambda-1)^2 - c\theta\log\frac{\theta}{\theta_T} & \text{if } \lambda < \lambda_M(\theta), \\ \frac{E}{2\rho}(\lambda-1)^2 - \frac{E\gamma_T}{2\rho}\frac{[\lambda-\lambda_M(\theta)]^2}{\lambda_m(\theta)-\lambda_M(\theta)} - c\theta\log\frac{\theta}{\theta_T} & \text{if } \lambda_M(\theta) \le \lambda \le \lambda_m(\theta), \\ \frac{E}{2\rho}(\lambda-(1+\gamma_T))^2 + \frac{E\gamma_T}{2\rho}[\lambda_m(\theta)+\lambda_M(\theta)-(2+\gamma_T)] & \\ -c\theta\log\frac{\theta}{\theta_T} + \lambda_T\frac{\theta-\theta_T}{\theta_T} & \text{if } \lambda > \lambda_m(\theta), \end{cases} \tag{2.27}$$

where c is the specific heat at constant stretch (assumed to be constant and equal in both phases),

$$\lambda_m(\theta) = \lambda_C + m(\theta-\theta_C)\,, \tag{2.28}$$

$$\lambda_M(\theta) = \lambda_C + M(\theta-\theta_C) \tag{2.29}$$

for materials constants λ_C, θ_C, M and m $(M > m)$.

At any given temperature θ, ψ is piecewise quadratic in λ. It is convex on $(0,\lambda_M(\theta))$ which corresponds to the region of stability of the low strain phase and on $(\lambda_m(\theta),\infty)$ which corresponds to the region of stability of the high strain phase, but concave on $(\lambda_M(\theta),\lambda_m(\theta))$ which corresponds to the unstable region that separates the two phases. This is shown in Figure 2.2 . Note that the unstable branch shrinks linearly with increasing temperature and vanishes at the critical temperature $\theta = \theta_C$. This model breaks down at this and higher temperatures.

For this choice of ψ,

$$T(\lambda,\theta) = \begin{cases} E(\lambda-1) & \text{if } \lambda < \lambda_M(\theta), \\ T_u(\lambda,\theta) & \text{if } \lambda_M(\theta) \le \lambda \le \lambda_m(\theta), \\ E(\lambda-1-\gamma_T) & \text{if } \lambda > \lambda_m(\theta), \end{cases} \tag{2.30}$$

$$\eta(\lambda,\theta) = \begin{cases} c(1+\log\frac{\theta}{\theta_T}) & \text{if } \lambda < \lambda_M(\theta), \\ \eta_u(\lambda,\theta) & \text{if } \lambda_M(\theta) \le \lambda \le \lambda_m(\theta), \\ c(1+\log\frac{\theta}{\theta_T}) - \frac{\lambda_T}{\theta_T} & \text{if } \lambda > \lambda_m(\theta), \end{cases} \tag{2.31}$$

where we have not displayed the formulae for the middle (unstable) branch.

2.2.4 Summary

It is useful to collect the governing equations and jump conditions.

Governing equations

$$\rho\ddot{\mathbf{y}} = \frac{\partial}{\partial x}(T\hat{\mathbf{t}}) + \mathbf{b}\,, \tag{2.32}$$

$$\rho\theta\dot{\eta} = k\frac{\partial^2\theta}{\partial x^2} - G(\theta)\,, \tag{2.33}$$

$$T = \rho\frac{\partial\psi}{\partial\lambda} \qquad \eta = -\frac{\partial\psi}{\partial\theta}\,, \tag{2.34}$$

where

$\mathbf{y} = \mathbf{y}(x,t)$ is the position vector at time t of a point on the string with reference position x,

$\lambda = |\frac{\partial\mathbf{y}}{\partial x}|$ is the stretch at a point on the string with position vector $\mathbf{y}$,

$\hat{\mathbf{t}} = \frac{1}{\lambda}\frac{\partial\mathbf{y}}{\partial x}$ is the tangent at a point on the string with position vector $\mathbf{y}$,

$\theta = \theta(x,t)$ is the temperature at time t of a point on the string with reference position x,

$\psi = \psi(\lambda,\theta)$ is the Helmholtz free energy density of the material of the string,

$\mathbf{b} = \mathbf{b}(x)$ is the body force density as a function of the reference position,

$G = G(\theta)$ is the rate of heat lost from the string per unit reference length,

and the density ρ as well as the thermal conductivity k are positive constants.

Jump conditions

$$\dot{s}[|\,\lambda\hat{\mathbf{t}}\,|] + [|\,\dot{\mathbf{y}}\,|] = 0\,. \tag{2.35}$$

$$\dot{s}[|\,\rho\dot{\mathbf{y}}\,|] + [|\,T\hat{\mathbf{t}}\,|] = 0\,. \tag{2.36}$$

$$\dot{s}\Big(\rho[|\,\psi + \theta\eta\,|] - \langle T\hat{\mathbf{t}}\rangle\cdot[|\,\lambda\hat{\mathbf{t}}\,|]\Big) = [|\,q\,|] = -k[|\,\frac{\partial\theta}{\partial x}\,|]\,. \tag{2.37}$$

$$\rho\dot{s}\theta[|\,\eta\,|] \le [|\,q\,|]\,. \tag{2.38}$$

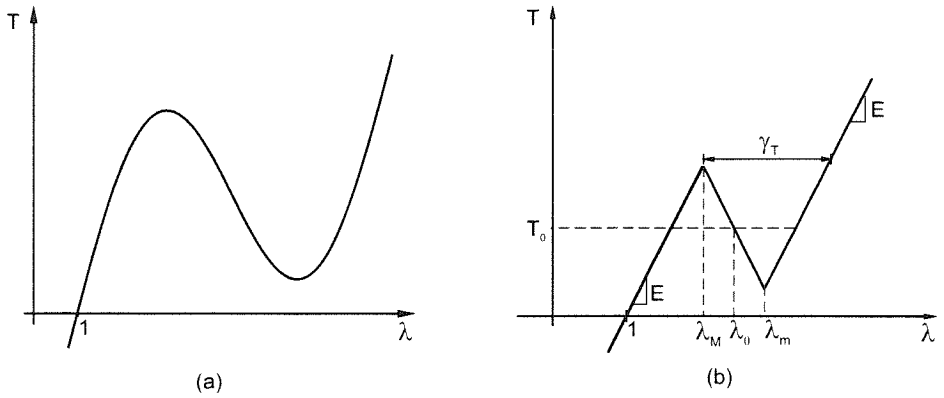

Figure 2.3: (a) The general phase transforming material. (b) The trilinear material.

2.3 Purely mechanical string

Suppose we fix the temperature at some given temperature θ ($< \theta_C$) and consider the isothermal situation. We obtain a purely mechanical string, where the only equation we need to solve is the momentum equation (2.32), the jump conditions (2.35) and (2.36), in addition to suitable initial and boundary values. We shall also assume for simplicity that the body force $\mathbf{b} = \mathbf{0}$. This section studies some basic properties of travelling waves and discontinuities in this setting. Sections 2.3.1 and 2.3.2 use a generic *up-down-up* material (Figure 2.3(a), while the rest of the chapter specializes to the *trilinear* material (Figure 2.3(b) and equation (2.30)).

2.3.1 Travelling waves and sound waves

It is useful to start by looking at travelling waves i.e., solutions of the form $\mathbf{y}(x,t) = \mathbf{y}(x-ct)$ for (2.32). For solutions of this form, (2.32) reduces to

$$\rho c^2 \mathbf{y}'' = \left(\frac{\hat{T}(\lambda)}{\lambda}\mathbf{y}'\right)' \tag{2.39}$$

where the prime denotes differentiation with respect to $\xi = x - ct$. We can rewrite this equation as

$$\rho c^2 \mathbf{y}'' = \mathbf{A}\mathbf{y}'' \tag{2.40}$$

where the matrix $\mathbf{A}$ is defined by

$$\mathbf{A} = \frac{\hat{T}(\lambda)}{\lambda}\mathbf{I} + \frac{1}{\lambda^2}\Big(\frac{d\hat{T}(\lambda)}{d\lambda} - \frac{\hat{T}(\lambda)}{\lambda}\Big)\mathbf{y}' \otimes \mathbf{y}'.$$

Matrix $\mathbf{A}$ turns out to have the following two eigenvalues,

$\frac{dT}{d\lambda}$ with eigenvector $\frac{\mathbf{y}'}{|\mathbf{y}'|} = \hat{\mathbf{t}}$,

$\frac{T}{\lambda}$ with eigenvector being any vector perpendicular to $\hat{\mathbf{t}}$ (repeated).

The first system corresponds to the familiar longitudinal waves in bars and strings. The second corresponds to transverse travelling waves where the displacement is perpendicular to the tangent to the string at any point. Also note that for the system to be hyperbolic both these eigenvalues should be positive. Thus, hyperbolicity is lost when the material is in the unstable branch of the stress-strain curve or when the string is compressed. We shall assume henceforth that $T > 0$.

2.3.2 Study of discontinuities

Two kinds of strain discontinuities occur in strings. There are *shocks*, both sides of which are in the same phase and there are *phase boundaries*, the two sides of which are in different phases. We now make some general observations about both shocks and phase boundaries. We also make a further classification - continuous tangent and discontinuous tangent, since it will be seen that there is a marked difference in their behaviour.

Before we begin, it is useful to eliminate $[\![\, \dot{\mathbf{y}} \,]\!]$ between the jump conditions (2.35) and (2.36) to obtain

$$[\![\, T\hat{\mathbf{t}} \,]\!] = \rho\dot{s}^2[\![\, \lambda\hat{\mathbf{t}} \,]\!]\,. \tag{2.41}$$

This of course holds for all discontinuities.

Continuous tangent: We begin by looking at discontinuities with continuous tangent, i.e., the situation $[\![\, \hat{\mathbf{t}} \,]\!] = \mathbf{0}$. Equation (2.41) simplifies under this assumption to

$$[\![\, T \,]\!]\hat{\mathbf{t}} = \rho\dot{s}^2[\![\, \lambda \,]\!]\hat{\mathbf{t}}$$

. Since $\hat{\mathbf{t}} \neq \mathbf{0}$, we obtain

$$\rho \dot{s}^2 = \frac{[\![T]\!]}{[\![\lambda]\!]}. \tag{2.42}$$

This relation tell us that speed of a discontinuity is proportional to the ratio of the jump in tension to the jump in stretch.

Discontinuous tangent: We now assume that $[\![\hat{\mathbf{t}}]\!] \neq \mathbf{0}$. Taking the inner product of (2.41) with $< \hat{\mathbf{t}} >$, we obtain

$$([\![T]\!] - \rho \dot{s}^2 [\![\lambda]\!])(1 + k) = 0$$

where $k = \hat{\mathbf{t}}^+ \cdot \hat{\mathbf{t}}^-$. We note that $k \neq -1$ since that would mean that $\hat{\mathbf{t}}^+$ and $\hat{\mathbf{t}}^-$ are antiparallel and that in turn implies that either the mapping $\mathbf{y} = \mathbf{y}(x,t)$ is not globally one-to-one or that the string has a cusp. We conclude that

$$\rho \dot{s}^2 = \frac{[\![T]\!]}{[\![\lambda]\!]}. \tag{2.43}$$

This is the same information as we obtained in the case of continuous tangent.

Now taking the inner product of (2.41) with $[\![\hat{\mathbf{t}}]\!]$,

$$(T^+ \hat{\mathbf{t}}^+ - T^- \hat{\mathbf{t}}^-) \cdot (\hat{\mathbf{t}}^+ - \hat{\mathbf{t}}^-) = \rho \dot{s}^2 (\lambda^+ \hat{\mathbf{t}}^+ - \lambda^- \hat{\mathbf{t}}^-) \cdot (\hat{\mathbf{t}}^+ - \hat{\mathbf{t}}^-).$$

We can rewrite this as

$$(< T > - \rho \dot{s}^2 < \lambda >)(1 - k) = 0.$$

We note that $k \neq 1$ since $[\![\hat{\mathbf{t}}]\!] \neq \mathbf{0}$, and conclude that

$$\rho \dot{s}^2 = \frac{< T >}{< \lambda >}. \tag{2.44}$$

This is more information than we had in the case of a continuous tangent.

Equations (2.44) and (2.43) together imply that

$$\rho \dot{s}^2 = \frac{T^+}{\lambda^+} = \frac{T^-}{\lambda^-}. \tag{2.45}$$

Therefore, if we have a discontinuity in a string with a discontinuous tangent, then the end

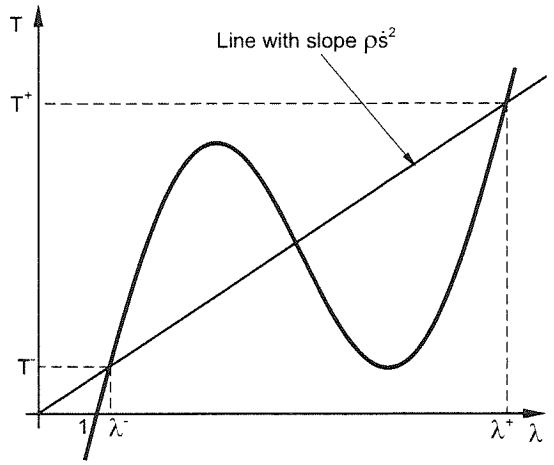

Figure 2.4: Kinetic relation obatined from the string. This assumes that the phase boundary coincides with a tangent discontinuity.

states (λ^-, T^-) and (λ^+, T^+) must lie on a straight line with slope $\rho\dot{s}^2$ that goes through the origin in the $\lambda - T$ plane. This is shown in Figure 2.4. It is important to note that we did not use any specific constitutive relation to obtain this result and it holds for all materials, phase transforming or not.

It has important implications, in particular, for phase transforming materials. Assume as shown in Figure 2.4 that any straight line going through the origin in the $\lambda - T$ plane intersects each stable (up) branches at most once. Then, (2.45) states that the shocks with discontinuous tangent have the same stretch (and tension) on both sides. In other words, either the tangent or the stretch, but *not* both can jump across a shock in these materials. Now turning to a phase boundary with a discontinuous tangent, (2.45) gives a complete link between each end state and the phase boundary velocity. Therefore, if we choose one end state, the other end state as well as the phase boundary velocity is uniquely determined. Alternately, if we choose the phase boundary velocity, both end states are completely determined. Recall that the driving force on an interface is determined by the end states. Thus (2.45) gives us an unique relation between the driving force and the phase boundary velocity. Such a relation is called a *kinetic relation.* Therefore, we see that in strings, the jump conditions give us a kinetic relation when the tangent is discontinuous across a phase boundary. This is in remarkable variance with our experience in bars, where this information can *not* be obtained from the jump conditions, and has to be prescribed externally as a constitutive relation.

2.3.3 Discontinuities in the trilinear material

We examine these issues closely by specializing to a trilinear material whose tension-stretch relation is given in (2.30) and shown in Figure 2.3(b) . The temperature θ is a constant and we suppress it from our notation.

2.3.3.1 Shocks

Continuous tangent: For shocks with continuous tangent in strings made of trilinear materials, equation (2.42) specializes to

$$\rho\dot{s}^2 = \frac{E(\lambda^+ - \lambda^-)}{\lambda^+ - \lambda^-} \qquad \text{or,} \qquad \dot{s}^2 = \frac{E}{\rho} = c^2 \,. \tag{2.46}$$

We now show that the converse of this statement is also true, i.e., $\dot{s}^2 = c^2$ for a discontinuity implies that $[\![\, \hat{\mathbf{t}} \,]\!] = \mathbf{0}$. To see this subsitute for T given by (2.30) in the combined jump condition (2.41)

$$E(\lambda^+ - 1)\hat{\mathbf{t}}^+ - E(\lambda^- - 1)\hat{\mathbf{t}}^- = \rho\dot{s}^2(\lambda^+\hat{\mathbf{t}}^+ - \lambda^-\hat{\mathbf{t}}^-).$$

After some algebra we get,

$$(c^2 - \dot{s}^2)[\![\, \lambda\hat{\mathbf{t}} \,]\!] + c^2[\![\, \hat{\mathbf{t}} \,]\!] = \mathbf{0} \,. \tag{2.47}$$

Thus, $\dot{s}^2 = c^2$ implies $[\![\, \hat{\mathbf{t}} \,]\!] = \mathbf{0}$, and the tangent is continuous. Notably, such shocks have particle displacements parallel to the tangent to the string and hence they are nothing but the longitudinal waves as in bars.

Discontinuous tangent: The more unusual shocks are the ones where the tangent is allowed to have a jump discontinuity. For such shocks (2.45) dictates that either

$$\rho\dot{s}^2 = \frac{E(\lambda^+ - 1)}{\lambda^+} = \frac{E(\lambda^- - 1)}{\lambda^-}$$

if material is in the low strain phase, or

$$\rho\dot{s}^2 = \frac{E(\lambda^+ - 1 - \gamma_T)}{\lambda^+} = \frac{E(\lambda^- - 1 - \gamma_T)}{\lambda^-}$$

if material is in the high strain phase. This is possible if and only if $\lambda^+ = \lambda^- = \lambda$, i.e., if and only if the stretch is continuous across the shock. Further,

$$\rho \dot{s}^2 = \frac{E(\lambda - 1)}{\lambda} \qquad \text{or} \qquad \frac{\dot{s}^2}{c^2} = 1 - \frac{1}{\lambda} \tag{2.48}$$

if material is in the low strain phase, and

$$\rho \dot{s}^2 = \frac{E(\lambda - 1 - \gamma_T)}{\lambda} \qquad \text{or} \qquad \frac{\dot{s}^2}{c^2} = 1 - \frac{1 + \gamma_T}{\lambda} \tag{2.49}$$

if material is in the high strain phase. Once again, we note that these shocks are essentially the same as transverse travelling waves. They propagate with velocity smaller than the stretch discontinuity.

Combining the results of the continuous and discontinuous shocks, we note that for shocks in our trilinear material,

$$[\![\, \lambda \,]\!][\![\, \hat{\mathbf{t}} \,]\!] = \mathbf{0} \qquad \text{or} \qquad [\![\, \lambda \,]\!](k - 1) = 0 \tag{2.50}$$

as we discussed in Section 2.3.2.

2.3.3.2 Phase boundaries

Continuous tangent: For phase boundaries with continuous tangent, we only have (2.42) which reduces to

$$\begin{aligned} \rho \dot{s}^2 &= \frac{E(\lambda^+ - 1 - \gamma_T) - E(\lambda^- - 1)}{\lambda^+ - \lambda^-} \\ \text{or} \qquad [\![\, \lambda \,]\!] &= \frac{\gamma_T}{1 - \frac{\dot{s}^2}{c^2}} \end{aligned} \tag{2.51}$$

Thus when the + side is in the high strain phase and the − side is in the low strain phase we have one equation to determine both the jump in stretch as well as the phase boundary velocity. Therefore, we need some additional information – from outside the balance laws – to determine the phase boundary velocity. This can in fact be demonstrated using Riemann problems. The situation is similar to that of a bar, where one specifies this additional information as a kinetic relation.

Discontinuous tangent: For definiteness, let us assume that the material on the + side is in the high strain phase and that on the − side is in the low strain phase. Then, we can write (2.45) as

$$\rho \dot{s}^2 = \frac{E(\lambda^+ - 1 - \gamma_T)}{\lambda^+} = \frac{E(\lambda^- - 1)}{\lambda^-}.$$

It follows

$$\lambda^+ = \frac{1+\gamma_T}{1-\frac{\dot{s}^2}{c^2}}, \qquad \lambda^- = \frac{1}{1-\frac{\dot{s}^2}{c^2}}. \tag{2.52}$$

Clearly, knowledge of any one among λ^+, λ^- and $\dot{s}$ determines the rest.

We need to ensure that λ^+ lies in the high strain phase and that λ^- lies in the low strain phase. So, we require

$$\lambda^+ \geq \lambda_m = \lambda_0 + \frac{\gamma_T}{4},$$

$$\lambda^- \leq \lambda_M = \lambda_0 - \frac{\gamma_T}{4}$$

where $\lambda_0 = \frac{\lambda_m + \lambda_M}{2}$ is the stretch corresponding to the Maxwell stress. These two inequalities together imply

$$\frac{\lambda_0 - 1 - \frac{3\gamma_T}{4}}{\lambda_0 + \frac{\gamma_T}{4}} \leq \frac{\dot{s}^2}{c^2} \leq \frac{\lambda_0 - 1 - \frac{\gamma_T}{4}}{\lambda_0 + \frac{\gamma_T}{4}}. \tag{2.53}$$

Recall that T cannot be compressive, and hence

$$\lambda^+ = \frac{1+\gamma_T}{1-\frac{\dot{s}^2}{c^2}} > 1 + \gamma_T \qquad \text{or,} \quad \frac{\dot{s}^2}{c^2} > 0$$

$$\lambda^- = \frac{1}{1-\frac{\dot{s}^2}{c^2}} > 1 \qquad \text{or,} \quad \frac{\dot{s}^2}{c^2} > 0$$

Putting everything together, we assert that the phase boundary velocity $\dot{s}$ in strings made of our special trilinear material must be bounded such that

$$0 < \frac{\dot{s}^2}{c^2} \leq \alpha^2 \leq 1 \qquad \text{where} \qquad \alpha^2 = \frac{\lambda_0 - 1 - \frac{\gamma_T}{4}}{\lambda_0 + \frac{\gamma_T}{4}}. \tag{2.54}$$

A summary of the behaviour of different types of discontinuities can be found in Table 2.1.

	Continuous tangent	Discontinuous tangent
Shock	$\dot{s} = \pm c$	$\dot{s} = \pm\sqrt{\frac{T^-}{\rho\lambda^-}}$
Phase boundary	Indeterminate	$\dot{s} = \pm\sqrt{\frac{T^+}{\rho\lambda^+}} = \pm\sqrt{\frac{T^-}{\rho\lambda^-}}$

Table 2.1: Behaviour of discontinuities.

2.3.3.3 Driving force on shocks and phase boundaries

Let us now calculate the driving force (2.21) for various discontinuities in an isothermal string. We can expand (2.21) and write

$$f = \rho[|\,\psi\,|] - \frac{1}{2}(T^+\lambda^+ - T^-\lambda^-) + \frac{k}{2}(T^-\lambda^+ - T^+\lambda^-) \tag{2.55}$$

where $k = \hat{\mathbf{t}}^+ \cdot \hat{\mathbf{t}}^-$ as before. For a continuous tangent, $k = 1$, and therefore this reduces to

$$f = \rho[|\,\psi\,|] - \frac{1}{2}(T^+ + T^-)(\lambda^+ - \lambda^-)\,. \tag{2.56}$$

We will now show that this is true even for a discontinuous tangent. In such a situation, we have from (2.45) that $T^-\lambda^+ - T^+\lambda^- = 0$. Therefore, we can add $\frac{1}{2}(1-k)(T^-\lambda^+ - T^+\lambda^-)$ to the right -hand side of (2.55) and obtain (2.56).

We now specialize to the trilinear material. Going through a lengthy calculation which is omitted for brevity, we find that the driving force on a shock is given by

$$\begin{aligned} f(t) &= E[|\,\lambda\,|]\Big(\frac{k-1}{2}\Big) && \text{for material in low strain phase,} \\ f(t) &= E[|\,\lambda\,|]\Big(\frac{k-1}{2}\Big)(1+\gamma_T) && \text{for material in high strain phase.} \end{aligned} \tag{2.57}$$

Combining this with (2.50), we see that the driving force on a shock is always zero. Turning now to the phase boundary, and assuming that the high strain phase is on the + side, we obtain from (2.56) again after a lengthy calculation that

$$f = E\gamma_T(\lambda_0 - < \lambda >)\,. \tag{2.58}$$

We observe that the driving force is determined by the average value of stretch across a phase boundary regardless of whether or not the tangent is continuous.

2.3.4 Kinetics of phase boundaries

We saw above that the speed of a phase boundary with continuous tangent can not be determined from the jump conditions alone. This is also true of phase boundaries in bars. In fact, in bars, Abeyaratne and Knowles (1990) have shown that the field equations and jump conditions give a one parameter family (parameter $\dot{s}$) of solutions to Riemann problems that involve a phase boundary. In other words, we have a severe lack of uniqueness and Abeyaratne and Knowles remedy it by introducing a constitutive assumption called a *kinetic relation* which states that the phase boundary velocity is a given constitutive function of the driving force:

$$\dot{s} = V(f)\,. \tag{2.59}$$

The entropy inequality (2.26) provides a restriction on this function V:

$$fV(f) \geq 0\,. \tag{2.60}$$

This formalism of relating the rate of progression of a local microstructural rearrangement within the material to the corresponding thermodynamic force conjugate to the extent of that rearrangement is again rather old and has been prevalent in material science for long. For instance, in metal plasticity this principle boils down to the conventional notion that the velocity of a given segment of a dislocation line is stress-state dependent only through the glide force per unit length of that line. In Rice (1971) microstructural details such as these are described by internal variables and the above formalism is used to conveniently incorporate them into a continuum theory for plasticity. Abeyaratne and Knowles adopt a similar point of view when they regard the position of the phase boundary as an internal variable and postulate that its rate of change (i.e., its speed) should be related to the corresponding conjugate thermodynamic force (or the driving force) through a function V which they regard as a given.

Going back to strings, we saw that the velocity of the phase boundary with a discontinuous tangent is determined by the jump conditions alone. In fact, (2.58) and (2.52) define a kinetic relation for phase boundaries with tangent discontinuities. When we substitute

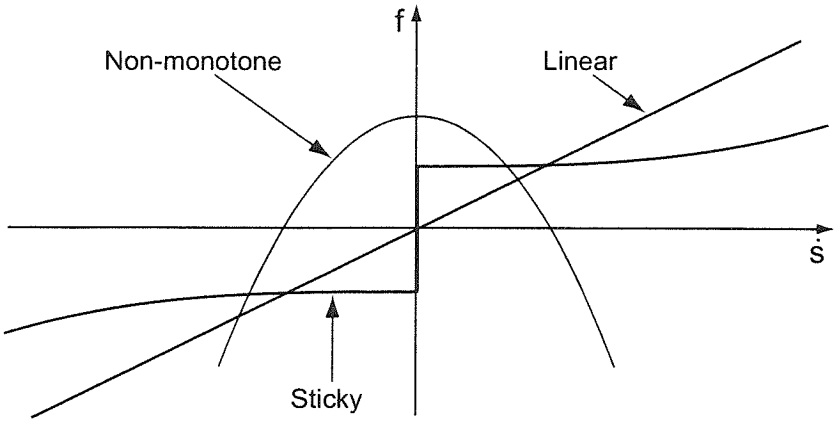

Figure 2.5: Various kinetic relations. The non-monotone kinetic relation is obtained from the balance laws for phase boundaries with discontinuous tangent. The vectorial nature of the jump conditions implies such a relation. The linear and sticky kinetic relations are more conventional and have traditionally been given as constitutive information.

for $< \lambda >$ in (2.58) using (2.52) we get

$$f = E\gamma_T\Big(\lambda_0 - \frac{1 + \frac{\gamma_T}{2}}{1 - \frac{\dot{s}^2}{c^2}}\Big). \tag{2.61}$$

This is plotted in Figure 2.5 as the non-monotone kinetic relation. The restriction (2.60) states that we need to consider only those parts that are in the first and the third quadrant. It is also interesting that the portion in the first quadrant has a negative slope. Such kinetic relations were shown by Rosakis and Knowles (1997) to be unstable in the sense that some phase boundaries propagating under such a law could display stick-slip behaviour.

It is significant that the kinetic relation (2.61) depends only on the material properties, and is independent of the angle between the tangents as long as it is non-zero. One may argue then, that by extension, this kinetic relation should also hold for the case of a continuous tangent. This presumes that the phase boundaries with continuous tangent are identical to those with discontinuous ones in some more fundamental mathematical or physical sense. This remains an open question.

Also plotted in Figure 2.5 are two other kinetic relations. The linear kinetic relation explores only the first and third quadrants of the $f - \dot{s}$ plane. It has been used in the past principally because it facilitates easy computation and helps in building intuition. The sticky kinetics, on the other hand, is motivated from experimental observations. It has been found that phase boundaries tend to move in a jerky fashion - something very characteristic

of sticky kinetics similar to what is seen in frictional contact problems. A little later in this chapter we set up a boundary value problem that brings out the qualitative differences in these kinetic relations.

2.4 Riemann problems

We study Riemann problems for the trilinear material in this section to further investigate the need for a kinetic relation in strings. We consider an infinite string and prescribe a piecewise constant initial data (stretch λ, tangent $\hat{\mathbf{t}}$ and particle velocity $\dot{\mathbf{y}}$). We show that the solution to the Riemann problem is uniquely determined by the balance laws and a kinetic relation.

Consider an infinite string made of a trilinear material subject to the following initial conditions:

$$\begin{aligned} &\lambda(x,0) = \lambda_L, \hat{\mathbf{t}}(x,0) = \hat{\mathbf{t}}_L, \dot{\mathbf{y}}(x,0) = \mathbf{v}_L \quad \text{for } x < 0, \\ &\lambda(x,0) = \lambda_R, \hat{\mathbf{t}}(x,0) = \hat{\mathbf{t}}_R, \dot{\mathbf{y}}(x,0) = \mathbf{v}_R \quad \text{for } x > 0 \end{aligned} \tag{2.62}$$

where λ_L, λ_R, $\mathbf{v}_L$, $\mathbf{v}_R$, $\hat{\mathbf{t}}_L$ and $\hat{\mathbf{t}}_R$ are given constants. We assume λ_L and λ_R to be such that the string is not in compression. We also assume that λ_L and λ_R are not in the unstable region of the trilinear stress-strain curve. In other words, we assume that

$$1 < \lambda_L, \lambda_R \leq \lambda_M \quad \text{or} \quad \lambda_L, \lambda_R > 1 + \gamma_T.$$

We seek solutions $\lambda(x,t), \hat{\mathbf{t}}(x,t), \dot{\mathbf{y}}(x,t)$ to (2.32),(2.35),(2.36) subject to initial conditions (2.62). It is natural to look for solutions where $\lambda, \hat{\mathbf{t}}$ and $\mathbf{v}$ are piecewise constant in the x,t-plane. These satisfy (2.32) trivially and we are left with the two jump conditions (2.35) and (2.36) at each discontinuity.

There are two useful results that one can prove for this Riemann problem. First, if the unstable phase is absent initially, as we have assumed, then it is absent for all subsequent times. Second, the number N of phase boundaries in any solution is necessarily either 0,1 or 2. These results can be proved by adapting the arguments of Abeyaratne and Knowles (1991) who proved them for bars. Their arguments use only equations (2.51), (2.56) and the dissipation inequality; as these equations hold in identical form for bars and strings, the

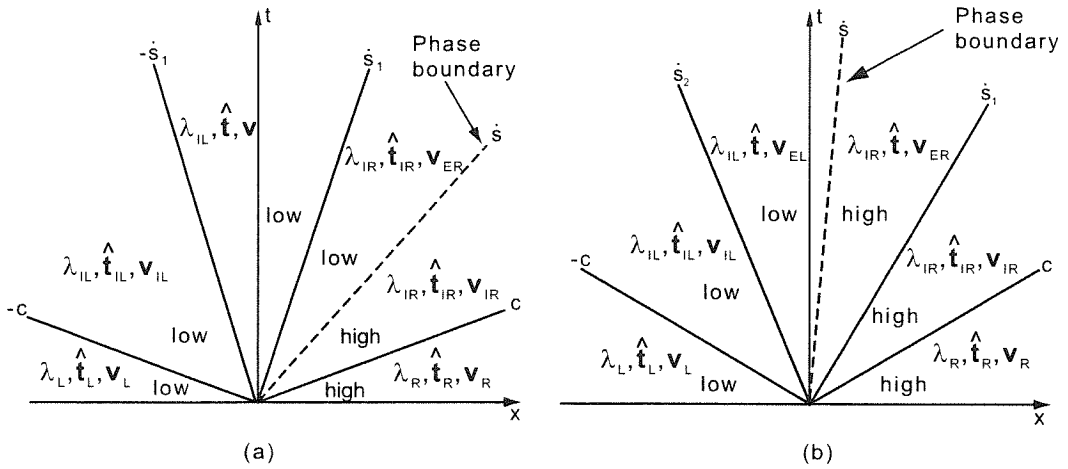

Figure 2.6: Possible solutions to the low-high Riemann problem. (a) Phase boundary moving faster than kink. (b) Phase boundary sandwiched between kinks.

argument of Abeyaratne and Knowles also hold for strings.

Depending on the prescribed values for λ_L, λ_R, we have three cases - low-low, low-high, high-high. We discuss only the first and the second since the third is very similar to the first. We also assume that $\hat{\mathbf{t}}_L \neq \hat{\mathbf{t}}_R$ since the case $\hat{\mathbf{t}}_L = \hat{\mathbf{t}}_R$ reduces to the Riemann problem in bars which has been studied by Abeyaratne and Knowles (1991).

2.4.1 Low-high problem

Suppose that the prescribed initial data is such that λ_L is in the low strain phase and λ_R is in the high strain phase. In other words, we already have a phase boundary in the initial data. We look for solutions of the form shown in Figure (2.6). There are five discontinuities:

Two shocks with continuous tangent necessarily propagating with velocity $\pm c$.

Two shocks with discontinuous tangent, one propagating to the right with velocity $\dot{s}_1$ and another to the left with velocity $-\dot{s}_2$ (we assume $\dot{s}_1, \dot{s}_2 > 0$). We know that the stretch has to be continuous across each of these shocks.

One phase boundary with continuous tangent with velocity $\dot{s}$ which could either be positive or negative.

Let us assume for now that the phase boundary moves slower than the tangent discontinuities so that $\dot{s}^2 \leq \min\{s_1^2, s_2^2\}$. The $x-t$ plane in such a situation looks as shown in Figure 2.6(b). We assume that the solution is constant in each of the six sectors of the $x-t$ plane. This trivially satisfies the field equations, and we need to worry about the jump conditions only. The jump conditions at each of the five discontinuities can be written as

$$c\hat{\mathbf{t}}_R(\lambda_R - \lambda_{IR}) + \mathbf{v}_R - \mathbf{v}_{IR} = \mathbf{0}, \tag{2.63}$$

$$\dot{s}_1\lambda_{IR}(\hat{\mathbf{t}}_R - \hat{\mathbf{t}}) + \mathbf{v}_{IR} - \mathbf{v}_{ER} = \mathbf{0}, \tag{2.64}$$

$$\dot{s}(\lambda_{IR} - \lambda_{IL})\hat{\mathbf{t}} + \mathbf{v}_{ER} - \mathbf{v}_{EL} = \mathbf{0}, \tag{2.65}$$

$$-\dot{s}_2\lambda_{IL}(\hat{\mathbf{t}} - \hat{\mathbf{t}}_L) + \mathbf{v}_{EL} - \mathbf{v}_{IL} = \mathbf{0}, \tag{2.66}$$

$$-c\hat{\mathbf{t}}_L(\lambda_{IL} - \lambda_L) + \mathbf{v}_{IL} - \mathbf{v}_L = \mathbf{0}. \tag{2.67}$$

In addition we have the following from (2.48), (2.49) and (2.51).

$$\lambda_{IL} = \frac{1}{1 - \frac{\dot{s}_2^2}{c^2}}, \quad \lambda_{IR} = \frac{1+\gamma_T}{1 - \frac{\dot{s}_1^2}{c^2}}, \tag{2.68}$$

$$\lambda_{IR} - \lambda_{IL} = \frac{\gamma_T}{1 - \frac{\dot{s}^2}{c^2}}. \tag{2.69}$$

Adding equations (2.63) to (2.67) and substituting from (2.68) and (2.69), we obtain the following two equations in the three unknowns $z = \frac{\dot{s}}{c}$, $z_1 = \frac{\dot{s}_1}{c}$ and $z_2 = \frac{\dot{s}_2}{c}$.

$$\mathbf{Q} - \frac{1+\gamma_T}{1+z_1}\hat{\mathbf{t}}_R - \frac{1}{1+z_2}\hat{\mathbf{t}}_L = ((z_1 - z)\frac{1+\gamma_T}{1-z_1^2} + (z+z_2)\frac{1}{1-z_2^2})\hat{\mathbf{t}}, \tag{2.70}$$

$$\frac{1+\gamma_T}{1-z_1^2} - \frac{1}{1-z_2^2} = \frac{\gamma_T}{1-z^2} \tag{2.71}$$

where $\mathbf{Q} = \lambda_R\hat{\mathbf{t}}_R + \lambda_L\hat{\mathbf{t}}_L + \frac{\mathbf{v}_R - \mathbf{v}_L}{c}$ is determined completely from the initial conditions. We can eliminate $\hat{\mathbf{t}}$ by squaring both sides of (2.70) and noticing that $|\hat{\mathbf{t}}| = 1$. We obtain

$$\left|\mathbf{Q} - \frac{1}{1-z_1^2}(1-z_1)\hat{\mathbf{t}}_R - \frac{1+\gamma_T}{1-z_2^2}(1-z_2)\hat{\mathbf{t}}_L\right|^2 = \left|\frac{1}{1-z_1^2}(z_1 - z) + \frac{1+\gamma_T}{1-z_2^2}(z-z_2)\right|^2 \tag{2.72}$$

(2.71) and (2.72) are not sufficient to solve for all the three unknowns. Clearly, these equations have a one parameter (parameter $\dot{s}$) family of solutions much like we see in bars. We demonstrate this by showing how a solution can be obtained if $\dot{s}$ (or z) is given.

Solution Procedure for a given z.

1. Solve equations (2.71) and (2.72) simultaneously for $z_1, z_2 \in [0,1]$. Note that these roots will only depend on the initial data.

2. We can now obtain $\lambda_{IR}, \lambda_{IL}$ from (2.68) and (2.69), and $\hat{\mathbf{t}}$ from (2.70).

3. We can now obtain $\mathbf{v}_{IR}$, $\mathbf{v}_{ER}$, $\mathbf{v}_{EL}$ and $\mathbf{v}_{IL}$ from (2.63) through (2.67).

The main difficulty, of course, is step 1 which calls for solving simultaneously an eighth and a fourth order polynomial. These equations have to be solved numerically. It is difficult to prove existence (or lack thereof) of roots. However, experience with numerical solutions suggests that one does indeed find unique roots in the interval $[0,1]$.

If the phase boundary moves faster than one of the tangent discontinuities, then the $x-t$ plane and jump conditions look slightly different. Figure 2.6(a) depicts the situation when the phase boundary moves faster than the right tangent discontinuity. The jump conditions in this case may be summarized as follows

$$c\hat{\mathbf{t}}_R(\lambda_R - \lambda_{IR}) + \mathbf{v}_R - \mathbf{v}_{IR} = \mathbf{0}, \tag{2.73}$$

$$\dot{s}(\lambda_{IR} - \lambda_{IL})\hat{\mathbf{t}}_R + \mathbf{v}_{IR} - \mathbf{v}_{ER} = \mathbf{0}, \tag{2.74}$$

$$\dot{s}_1\lambda_{IL}(\hat{\mathbf{t}}_R - \hat{\mathbf{t}}) + \mathbf{v}_{ER} - \mathbf{v} = \mathbf{0}, \tag{2.75}$$

$$-\dot{s}_1\lambda_{IL}(\hat{\mathbf{t}} - \hat{\mathbf{t}}_L) + \mathbf{v} - \mathbf{v}_{IL} = \mathbf{0}, \tag{2.76}$$

$$-c\hat{\mathbf{t}}_L(\lambda_{IL} - \lambda_L) + \mathbf{v}_{IL} - \mathbf{v}_L = \mathbf{0}. \tag{2.77}$$

Also from (2.48), (2.49) and (2.51), we have

$$\lambda_{IL} = \frac{1}{1 - \frac{\dot{s}_1^2}{c^2}}, \quad \lambda_{IR} - \lambda_{IL} = \frac{\gamma_T}{1 - \frac{\dot{s}^2}{c^2}}. \tag{2.78}$$

Once again, adding equations (2.73) to (2.77), using (2.78) we get

$$\mathbf{Q} - \frac{\hat{\mathbf{t}}_R + \hat{\mathbf{t}}_L}{1 + z_1} - \frac{\gamma_T\hat{\mathbf{t}}_R}{1 + z} = \frac{2z_1\hat{\mathbf{t}}}{1 - z_1^2}. \tag{2.79}$$

Squaring both sides to eliminate $\hat{\mathbf{t}}$, we get

$$\left|\mathbf{Q} - \frac{\hat{\mathbf{t}}_R + \hat{\mathbf{t}}_L}{1 + z_1} - \frac{\gamma_T\hat{\mathbf{t}}_R}{1 + z}\right|^2 = \frac{4z_1^2}{(1 - z_1^2)^2}. \tag{2.80}$$

The unknowns in the above equation are z and z_1 and just as in the previous case one can determine z_1 if z is given. We thus obtain a one-parameter (parametrized by $\dot{s}$ or z) family of solutions to the Riemann problem. In order to choose a unique solution among these we now prescribe a kinetic relation. The driving force (2.58) on the phase boundary can be written as

$$f = E\gamma_T(\lambda_0 - < \lambda >) = \frac{E\gamma_T}{2}(2\lambda_0 - \lambda_{IR} + \lambda_{IL}).$$

The kinetic relations in Figure 2.4 give the velocity as a function of the driving force. Thus, we may regard the kinetic relation as an equation of the form

$$z = G(\lambda_{IR}, \lambda_{IL})$$

or invoking (2.68), (2.69),

$$z = g(z_1, z_2)\,. \tag{2.81}$$

Once again, we outline the method for solving the equations.

Solution Procedure with a Kinetic relation.

1. Solve equations (2.71), (2.72) and (2.81) or (2.80) and (2.81) as appropriate, simultaneously for $z, z_1, z_2 \in [0, 1]$. Note that these roots will only depend on the initial data.

2. We can now obtain $\lambda_{IR}, \lambda_{IL}$ from (2.68) and (2.69) or (2.78), and $\hat{\mathbf{t}}$ from (2.70) or (2.79).

3. An then we can obtain $\mathbf{v}_{IR}$, $\mathbf{v}_{ER}$, $\mathbf{v}_{EL}$ and $\mathbf{v}_{IL}$ from (2.63) through (2.67) or (2.73) through (2.77).

Note in the above that we do not preclude the possibility of the phase boundary being a contact discontinuity. (Contact discontinuities can occur, for instance, when we use 'sticky' kinetic relations.) Neither does it preclude the phase boundary coinciding with the tangent discontinuity if it is consistent with the kinetic relation.

2.4.2 Low-low problem

Suppose that the prescribed initial data is such that both λ_L and λ_R are in the low-strain phase. We then have two classes of solutions. Solutions in class 1 have the form shown in figure 2.7(a). We have

Two shocks with continuous tangent moving at velocities $\pm c$.

Two tangent discontinuities moving at velocities $\pm\dot{s}$ where $|\dot{s}| < c$.

Recall from Section 2.3.3 that shocks with continuous tangent necessarily travel with velocity $\pm c$. Again from Section 2.3.3, recall that the stretch on one side of a shock with discontinuous tangent determines the velocity of the shock (upto sign). We can conclude, therefore, that if one tangent discontinuity travels at a velocity $\dot{s}$, then the other necessarily travels at a velocity $-\dot{s}$. Note that this solution of the low-low problem does not involve phase boundaries.

The four discontinuities of figure 2.7(a) divide the (x,t) plane into five sectors; the stretch, the tangent and the particle velocity is constant in each sector with values as marked in the figure. We have to solve for the unknowns λ_{IR}, λ_{IL}, λ, $\hat{\mathbf{t}}$, $\mathbf{v}_{IR}$, $\mathbf{v}_{IL}$ and $\dot{s}$ from the jump conditions.

$$c\hat{\mathbf{t}}_R(\lambda_R - \lambda_{IR}) + \mathbf{v}_R - \mathbf{v}_{IR} = \mathbf{0}, \tag{2.82}$$

$$\dot{s}(\lambda_{IR}\hat{\mathbf{t}}_R - \lambda\hat{\mathbf{t}}) + \mathbf{v}_{IR} - \mathbf{v} = \mathbf{0}, \tag{2.83}$$

$$-\dot{s}(\lambda\hat{\mathbf{t}} - \lambda_{IL}\hat{\mathbf{t}}_L) + \mathbf{v} - \mathbf{v}_{IL} = \mathbf{0}, \tag{2.84}$$

$$-c\hat{\mathbf{t}}_L(\lambda_{IL} - \lambda_L) + \mathbf{v}_{IL} - \mathbf{v}_L = \mathbf{0}. \tag{2.85}$$

For future use, we add equations (2.82) through (2.85) and then divide through by c to obtain

$$\left(\frac{\dot{s}}{c} - 1\right)(\lambda_{IR}\hat{\mathbf{t}}_R + \lambda_{IL}\hat{\mathbf{t}}_L) + \mathbf{Q} = 2\lambda\frac{\dot{s}}{c}\hat{\mathbf{t}} \tag{2.86}$$

where

$$\mathbf{Q} = \lambda_R\hat{\mathbf{t}}_R + \lambda_L\hat{\mathbf{t}}_L + \frac{\mathbf{v}_R - \mathbf{v}_L}{c}$$

is a quantity determined entirely from the initial conditions.

We have assumed that the tangent discontinuities are both shocks so that λ, λ_{IL} and λ_{IR} are all in the low strain phase. Then, (2.50) implies that the stretch is continuous

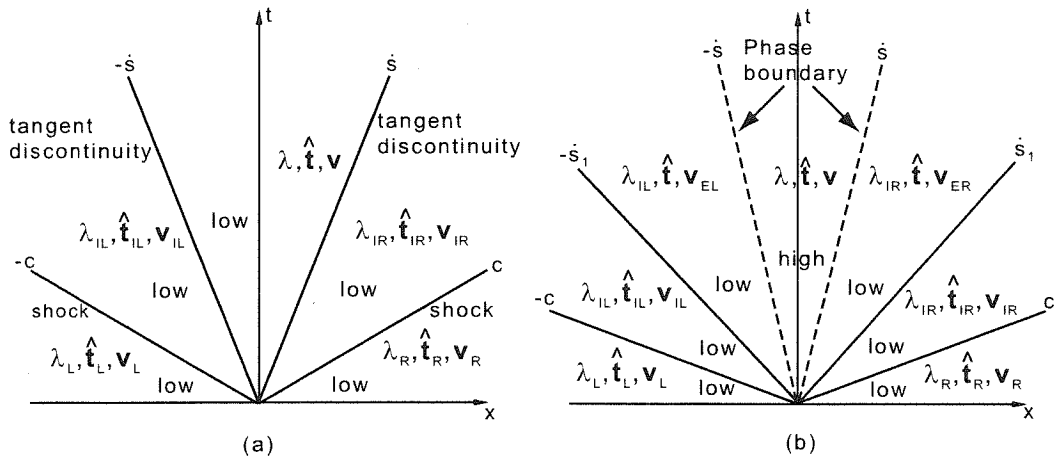

Figure 2.7: Possible solutions to the low-low Riemann problem.(a) A solution without nucleation of the high strain phase is the simplest Riemann solution involving only four shocks. (b) Nucleation in a low-low problem. This solution involves six discontinuities, two of which are phase boundaries. The phase boundaries can move faster or slower than the tangent discontinuities.

across these tangent discontinuities. We therefore have from (2.48) that

$$\lambda_{IR} = \lambda = \lambda_{IL} = \frac{1}{1 - \frac{\dot{s}^2}{c^2}}. \tag{2.87}$$

We substitute this into (2.86), and rewrite it as

$$\frac{1}{1 - \frac{\dot{s}^2}{c^2}} \left(\frac{\dot{s}}{c} - 1 \right) (\hat{\mathbf{t}}_R + \hat{\mathbf{t}}_L) + \mathbf{Q} = 2 \frac{1}{1 - \frac{\dot{s}^2}{c^2}} \frac{\dot{s}}{c} \hat{\mathbf{t}}. \tag{2.88}$$

We eliminate $\hat{\mathbf{t}}$ by taking the inner product of the above equation with itself and using the fact $|\,\hat{\mathbf{t}}\,| = 1$. After some algebra we get the following equation for $z = \frac{\dot{s}}{c}$.

$$|\mathbf{Q}|^2(1 - z^2)^2 - 2\mathbf{Q} \cdot (\hat{\mathbf{t}}_R + \hat{\mathbf{t}}_L)(1 - z)(1 - z^2) + 2(1 + k)(1 - z)^2 - 4z^2 = 0 \tag{2.89}$$

where $k = \hat{\mathbf{t}}_R \cdot \hat{\mathbf{t}}_L$. This is a quartic equation in z, whose coefficients are completely determined by the initial data. We seek a root of this equation between 0 and α (defined in 2.54). This root determines the velocity of the tangent discontinuity $\dot{s}$. We can then determine the other unknowns from (2.82) through (2.85).

It can be shown that this equation has one and only one root in the interval $[0, 1]$. For some initial data this root is also in $[0, \alpha]$, but it is not for others. When the root is not in $[0, \alpha]$ we must explore the possibility of *nucleation* of the high strain phase at $x = 0$ and this is class 2. As shown in Figure 2.7(b) this class of solutions has six discontinuities:

Two shocks with continuous tangent propagating with velocity $\pm c$.

Two shocks with discontinuous tangent propagating with velocities $\pm \dot{s}_1$.

Two phase boundaries with continuous tangent propagating with velocity $\pm \dot{s}$.

The methods to solve this problem are exactly the same as before – write the kinematic jump condition for each discontinuity, add all the equations, eliminate $\hat{\mathbf{t}}$, invoke a kinetic relation for each of the phase boundaries and solve for the speeds of the phase boundaries and tangent discontinuities numerically.

We have found that a low-low problem, in general, could have two solutions, one with no nucleation and one with nucleation of the high strain phase. The phase boundary velocity for the solution with nucleation is uniquely determined. There are some initial data for which we have one of these solutions, and some for which we have both. We should note here that we have been unable to prove that for any given (reasonable) initial data we always have at least one of these solutions. However, our numerical investigations suggest that this is so.

It remains to choose a solution when both are possible. We do so using a *nucleation criterion.* Following Abeyaratne and Knowles (1991), we propose the following: we pick the one with nucleation if the driving force exceeds a critical amount and the one without nucleation if it does not.

2.4.3 Goursat-Riemann problem

We conclude this section by looking at the Goursat-Riemann initial-boundary value problem. This is a special case of an impact problem where we consider a semi-infinite string with constant initial and boundary data. In particular, we seek a solution $(\lambda(x,t), \hat{\mathbf{t}}(x,t), \dot{\mathbf{y}}(x,t))$ of the field equation (2.32) and jump conditions (2.35) and (2.36) in the first quadrant of

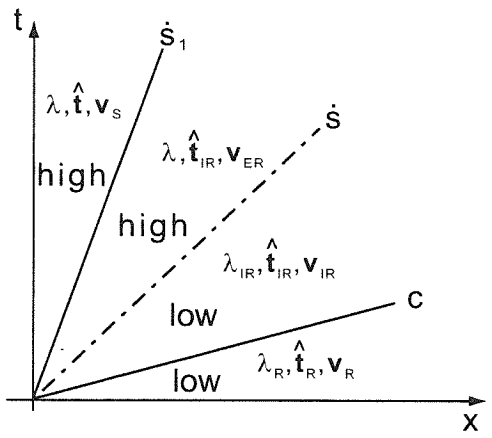

Figure 2.8: The Goursat-Riemann problem.

the $x - t$ plane subject to the following initial and boundary conditions:

$$\begin{aligned} &\lambda(x,0) = \lambda_R, \mathbf{y}(x,0) = \mathbf{v}_R, && \text{for } x > 0, \\ &\hat{\mathbf{t}}(x,0) = \hat{\mathbf{t}}_R, && \text{for } x > 0, \\ &\dot{\mathbf{y}}(0,t) = \mathbf{v}_S && \text{for } t > 0. \end{aligned} \tag{2.90}$$

We assume that the string is initially in the low strain phase, so that $1 < \lambda_R < \lambda_M$. We seek a solution with three discontinuities.

One shock with continuous tangent. This necessarily propagates with velocity c.

One shock with discontinuous tangent propagating with the velocity $\dot{s}_1$ $(0 \leq \dot{s}_1 \leq c)$.

One phase boundary with continuous tangent propagating with the velocity $\dot{s} > 0$.

The phase boundary could be moving faster or slower than the tangent discontinuity, but for the present we assume that it moves faster.

We know from (2.48) and (2.51) that

$$\lambda = \frac{1 + \gamma_T}{1 - z_1^2}, \tag{2.91}$$

$$\lambda_{IR} = \frac{1 + \gamma_T}{1 - z_1^2} - \frac{\gamma_T}{1 - z^2}. \tag{2.92}$$

Above, we have introduced the notation

$$z_1 = \frac{\dot{s}_1}{c}, \quad z = \frac{\dot{s}}{c}. \tag{2.93}$$

We have to satisfy only one jump condition for each discontinuity. Writing the kinematic jump condition (2.35) at each discontinuity,

$$c\hat{\mathbf{t}}_R(\lambda_R - \lambda_{IR}) + \mathbf{v}_R - \mathbf{v}_{IR} = \mathbf{0}, \tag{2.94}$$

$$cz\hat{\mathbf{t}}_R(\lambda_{IR} - \lambda) + \mathbf{v}_{IR} - \mathbf{v}_{ER} = \mathbf{0}, \tag{2.95}$$

$$cz_1\lambda(\hat{\mathbf{t}}_R - \hat{\mathbf{t}}) + \mathbf{v}_{ER} - \mathbf{v}_S = \mathbf{0}. \tag{2.96}$$

It can be easily shown that given z (i.e., given $\dot{s}$), we can solve (2.91) through (2.96) for our unknowns:

$$z_1, \lambda_{IR}, \lambda, \hat{\mathbf{t}}, \mathbf{v}_{IR}, \mathbf{v}_{ER}.$$

To this end, add equations (2.94) through (2.96) and divide by c to obtain

$$\mathbf{q} - \lambda_{IR}\hat{\mathbf{t}}_R(1 - z) + \lambda\hat{\mathbf{t}}_R(z_1 - z) = z\lambda\hat{\mathbf{t}} \tag{2.97}$$

where

$$\mathbf{q} = \lambda_R\hat{\mathbf{t}}_R + \frac{\mathbf{v}_R - \mathbf{v}_S}{c}$$

is a quantity determined from the initial and boundary conditions. We eliminate $\hat{\mathbf{t}}$ by squaring both sides of (2.97) and noticing that $|\hat{\mathbf{t}}| = 1$, and substitute from (2.92), (2.91) to obtain

$$\left|\mathbf{q} - \frac{1 + \gamma_T}{1 + z}\hat{\mathbf{t}}_R + \frac{\gamma_T}{1 + z_1}\hat{\mathbf{t}}_R\right|^2 = \left|\frac{(1 + \gamma_T)z}{1 - z^2}\right|^2 \tag{2.98}$$

Given a kinetic relation (which will be of the form $g(z, z_1) = 0$) this equation can be solved in exactly the same manner as we saw for the Riemann problem with a single phase boundary. We can also go about the whole exercise assuming that the phase boundary moves slower than the tangent discontinuity. In this case a phase boundary velocity equal to zero would simply mean that the high strain phase did not nucleate.

2.4.4 Experimental determination of kinetic relation

The presence of a tangent discontinuity in the solution to this problem can be exploited in experiments to determine the kinetic relation. The tangent discontinuity is easily visible and can be accurately tracked to determine its velocity. This information can be used to deduce the velocity and driving force on the phase boundary as we saw above. Of course,

the solution above is valid only at the very early stages when the reflected shocks from the other end of the string have not arrived. We can ensure that this time is long enough by using a sufficiently long string. The experiment can then be performed as follows:

1. Set up an impact with given $\mathbf{q}, \hat{\mathbf{t}}_R$, and measure the velocity of the tangent discontinuity z_1.

2. Solve (2.98) for phase boundary velocity z.

3. Use (2.92) and (2.91) to calculate λ_{IR} and λ.

4. Calculate the driving force from the result

$$f = E\gamma_T \left(\lambda_0 - \frac{\lambda + \lambda_{IR}}{2} \right).$$

2.5 Numerical method and examples

In this section we introduce a numerical method used for solving initial-boundary value problems following Zhong, Hou and LeFloch (1996). Godunov-type schemes (which is the basis of their scheme) have been used for solving hyperbolic problems and they follow as natural extensions to the solutions of the Riemann problems that we found in the previous section. They, however, need to be modified to deal with problems in phase boundary propagation where one has a change in type. We describe the modified method and present some examples.

2.5.1 Godunov methods

We begin by discretizing our reference configuration into a series of cells. On each of these cells we specify the stretch λ, the tangent $\hat{\mathbf{t}}$, and the velocity $\mathbf{v}$. We also specify the boundary data which consists of the stretch and tangent (if it is a force boundary condition) or the velocity (if it is a displacement boundary condition). Assuming that we begin our computation at time t_n, we have a series of Riemann problems at each of the cell interfaces. We can solve the Riemann problems and propagate the discontinuities to a time $t_n + \Delta t$ such that the discontinuities emerging from two adjacent cell-interfaces do not intersect. This has been illustrated in the Figure 2.9 below. We now have another series of Riemann

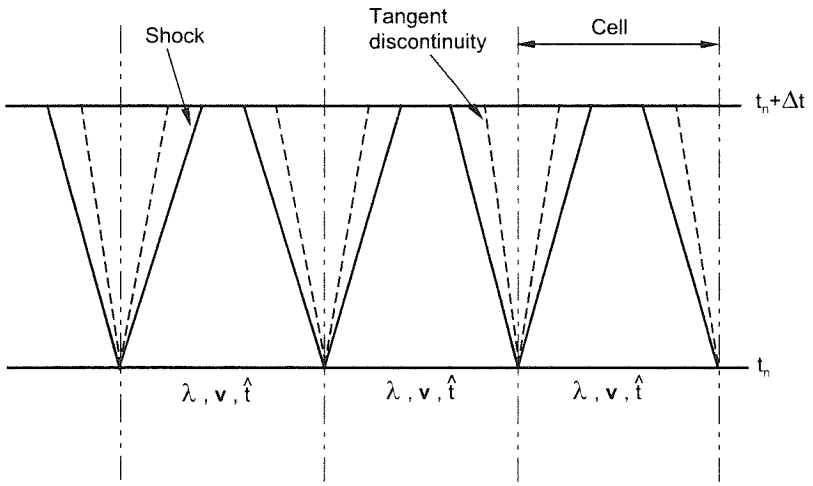

Figure 2.9: The principle of a Riemann solver.

problems at time $t_n + \Delta t$. However, we have produced much smaller cells and hence the next time-step we take will have to be much smaller. To circumvent this problem we average the data over each cell at time $t_n + \Delta t$ and then repeat the whole process as we march ahead in time. By averaging over a cell we smear out the discontinuities and this introduces some numerical dissipation. In other words, we are 'capturing' the discontinuities as opposed to 'tracking' them. The dissipation associated with smearing of the discontinuities can be reduced by using a fine grid. We demonstrate this through the example of the vibrating string made of a linearly elastic material. In its initial configuration the string is stretched between the two fixed ends. At time $t = 0$ it is plucked at the centre and let go. Figure 2.10 shows its deformed configuration at a later time. The exact profile is shown along with one obtained from a computation with grid-size of 1.25×10^{-3}. A blow-up of the profiles near the kink (boxed region in Figure 2.10) obtained from several computations (with different grid-sizes) can be seen in the inset. It is evident that as the mesh is refined the tangent discontinuity at the kink is less smeared out. In other words the error decreases as we refine the mesh. The convergence is to first order as expected for 'shock-capturing' methods.

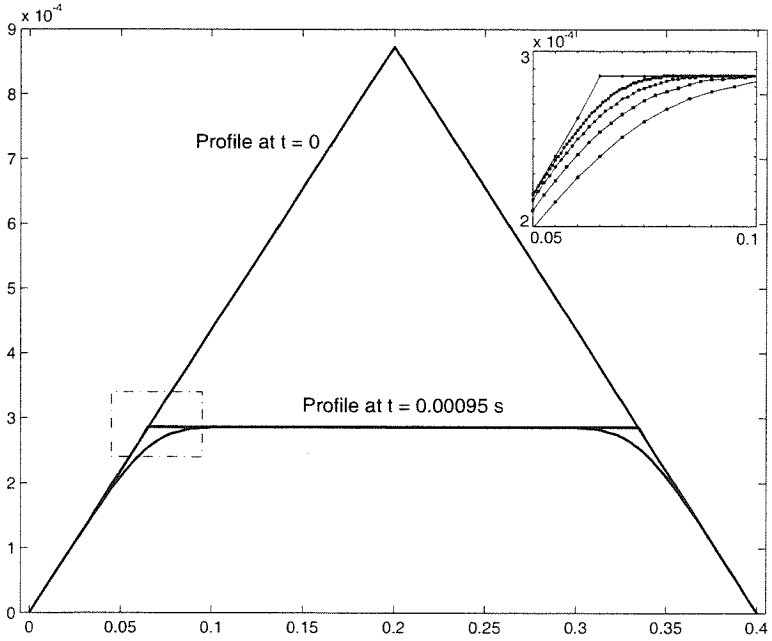

Figure 2.10: Exact and computed shapes of a vibrating elastic string. The inset shows the deformed shapes with different grid sizes. The grid size decreases from 5.0×10^{-3} to 6.25×10^{-4} as we go from the bottom right to the top left.

However, the Godunov method in this form cannot be used for problems involving changes of phase. The reason is that averaging over a cell with multiple phases can lead to values of the stretch λ in the unstable region of the stress-strain curve rendering the system non-hyperbolic. We therefore have to avoid averaging over multiple phases. Following Zhong, Hou and LeFloch (1996) we accomplish this by individually tracking the phase boundaries as they move in the reference configuration. The shocks are captured in the conventional manner.

2.5.2 Propagation, nucleation and interaction

In order to track a phase boundary, we discretize the reference configuration in such a way that each phase boundary lies on grid-point or a cell interface. We start our computation at time t_n by solving Riemann problems at each of the interfaces. By solving the Riemann problems we know the phase boundary velocity and we can determine its position at time $t_n + \Delta t$. So at the next time step we shift the grid-point so that the phase boundary still coincides with it. We thus have a locally non-uniform grid. There are certain subtleties associated with such non-uniform moving grids that we shall address below.

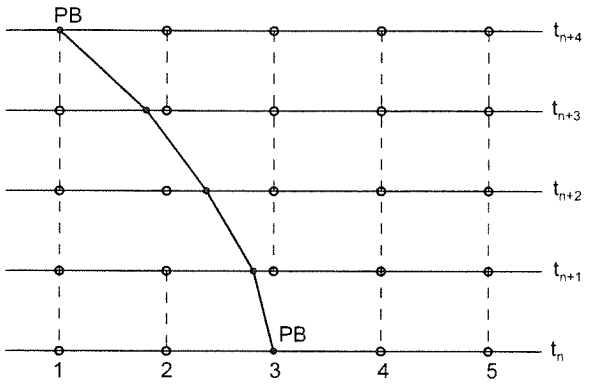

Figure 2.11: Modified Riemann solver. We always have a grid point moving with the phase boundary.

If we have a moving grid then it is possible that two grid-points come very close causing some of the cells to shrink. This would lead to a small time-step and will also result in a disproportionately large contribution to the error from the small cells. We therefore have to avoid the situation of having very small cells. In our computations we do this by enforcing the condition that $|\frac{c\Delta t}{h}| < \frac{1}{4}$. By doing so we have restricted the minimum cell size to $h/2$. To see how this is implemented, consider a uniform grid (cell-size h) at time t_n as shown in figure. The phase boundary sitting on point 3 has been labelled PB. At time t_{n+1} the phase boundary has moved to the left and the distance between it and point 3 is less than $h/2$. So, while averaging over the reference configuration we place a grid point on PB and leave out point 3. When we go to time t_{n+2} we find that PB is too close to point 2. So, we remove point 2 and reinsert point 3 while calculating the averages. At time t_{n+3} PB has moved to the left of point 2 but it is still too close. So, we do not reinsert point 2. At time t_{n+4} when the phase boundary has reached point 1 we reinsert point 2 and remove point 1. The calculation carries on in this manner.

Interaction and nucleation of phase boundaries is handled in a similar manner. If the distance between two phase bounadries is less than $h/2$ then we let them coalesce and have only one grid point replacing them. When we know that nucleation is to occur at a given grid point we replace the grid point with two phase boundaries moving in opposite directions separated by $h/2$ in the reference configuration.

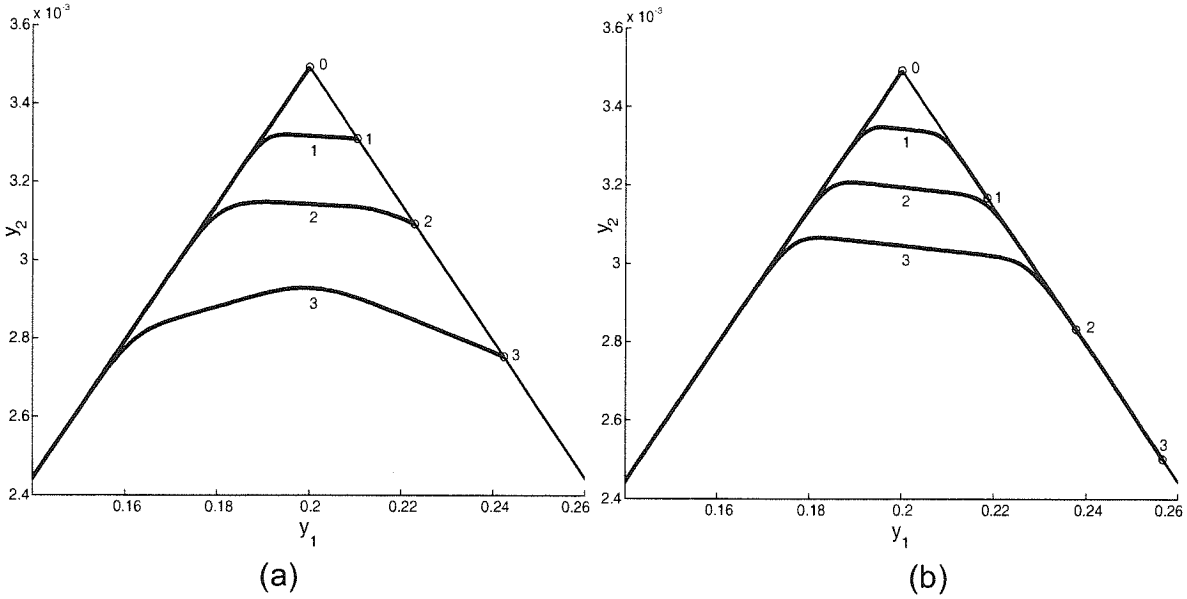

Figure 2.12: (a) Snapshots of a plucked string with a phase boundary calculated using two different kinetic relations. The circle shows the location of the phase boundary. (a) Non-monotone strign kinetic relation. The phase boundary follows the kink until the reflected shock interferes with it. (b) Sticky kinetic relation. Phase boundary moves independently of the kink.

2.5.3 Examples

2.5.3.1 Plucked string

Our first example is again a plucked string. This time, however, we have a phase boundary sitting exactly on top of the kink at time $t = 0$. At time $t = 0^+$ we let go of the string and observe how the phase boundary moves under the influence of the kinks and the shocks. We choose this example as a means to contrast the qualitative features of the kinetic relations that we discussed earlier. Figure 2.12(a) shows snapshots of the deformed shape of the string under the non-monotone kinetic relation. We saw earlier that this kinetic relation is obtained from the balance laws under the assumption that a phase boundary coincides with a tangent discontinuity. In fact, it can be shown that the following is also true – if the initial data in a Riemann problem is such that we have a tangent discontinuity coinciding with a phase boundary then the non-monotone kinetic relation forces the phase boundary to remain with the tangent discontinuity as the system evolves. It is clear from Figure 2.12(a) that this is the case at least in the initial stages (before the interaction with the shocks). In Figure 2.12(b), on the other hand, the phase boundary moves independently of (in this

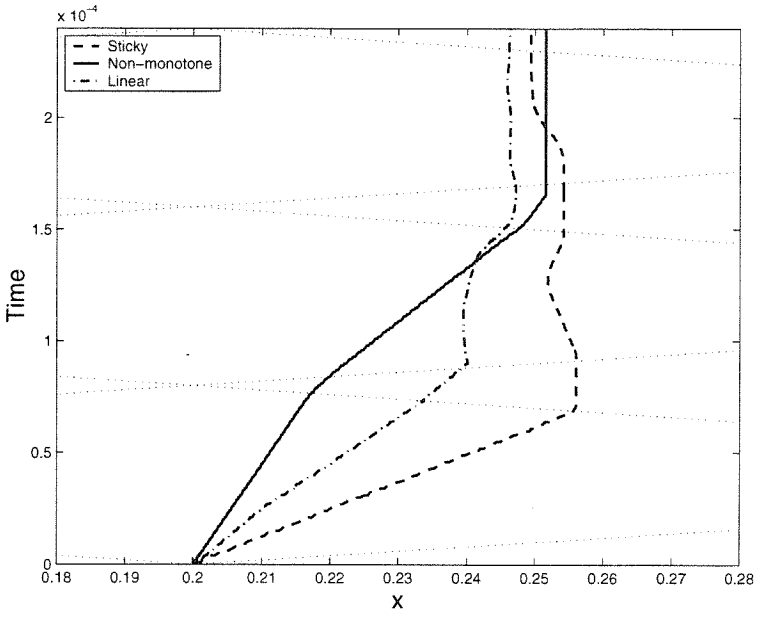

Figure 2.13: The trajectories of the phase boundary in a snapped string for different kinetic relations. The light dotted lines are the shocks. Interaction with shocks results in changes in the speed of the phase boundary.

case faster than) the tangent discontinuity. Here we assume that the phase boundary obeys a sticky kinetic relation. The results from the linear kinetic relation are very similar.

The figures above illustrate the beahviour of the phase boundary before it collides with the shocks that reflect off the fixed ends of the string. Figure 2.13 shows the trajectory of the phase boundary in the reference configuration over a time period of four shock reflections. We notice that significant changes in the speed of the phase boundary occur as a result of interaction with shocks. The phase boundary with the sticky kinetic relation shows a tendency to become a stationary contact discontinuity. The linear kinetic relation does not have a sticky region, so although we see a change in the speed of the phase boundary it never becomes a contact discontinuity. The non-monotone kinetic relation also results in 'stick-slip' motion of the phase boundary but this behaviour is quite different from that obtained from the sticky kinetic relation.

2.5.3.2 Whipped string

Our next example is a stretched string with a single phase boundary that is 'whipped' at the left end at $t = 0$. In other words we apply the following boundary condition at $x = 0$.

$$\begin{aligned} \dot{y}_1 = 0.0, \quad \dot{y}_2 = 100.0 m/s \qquad & 0 \leq t < 1.6 \times 10^{-4}, \\ \dot{y}_1 = 0.0, \quad \dot{y}_2 = -100.0 m/s \qquad & 1.6 \times 10^{-4} \leq t < 3.2 \times 10^{-4}, \\ \dot{y}_1 = 0.0, \quad \dot{y}_2 = 0.0 \qquad & 3.2 \times 10^{-4} \leq t < 1.2 \times 10^{-3}. \end{aligned}$$

The deformed configuration of the string has been plotted in Figure 2.14. The travelling wave propagating through the length of the string is clearly discernible. The wave gets smeared out by a small amount as it passes through. This is an effect of numerical dissipation associated with shock capturing methods. The trajectory of the phase boundary and the shocks have been plotted in Figure 2.15. We have used the sticky kinetic relation for this calculation. We find as a result that the phase boundary remains stationary for most of the time. Interaction with the shocks causes it to move by a small amount. From the figure we observe that abrupt changes in the mobility of the phase boundary do not coincide exactly with the arrival of the shocks. The reason again is that the shocks are spread out as opposed to being sharp discontinuities.

2.5.3.3 Nucleating string

This last example is a little artificial but we have chosen it to show how the deformed shape of a string can become so non-trivial in the presence of nucleation. The example also demonstrates annihilation of phase boundaries as the simulation is carried until a long enough time to let the entire string change phase. The problem is set up as follows. Initially there is a tangent discontinuity at the centre of the string. There are two phase boundaries flanking the tangent discontinuity on either side. The portion of the string between these phase boundaries is in the high strain phase and the rest of it is in the low strain phase. The string is initially held taut but at time $t = 0$ the tension applied at the ends is suddenly changed. This results in nucleation of the high strain phase at both ends and the resulting phase boundaries eat into the rest of the string. Eventually, the entire string changes into the high strain phase. The deformation of the string as this happens is depicted in Figure 2.16.

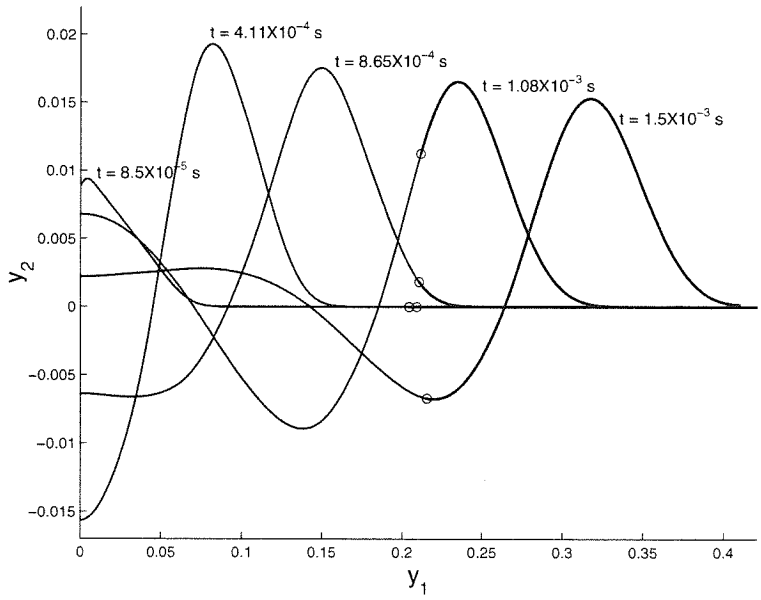

Figure 2.14: Travelling wave on a whipped string with a phase boundary. For this calculation the grid size is 1.25×10^{-3}.

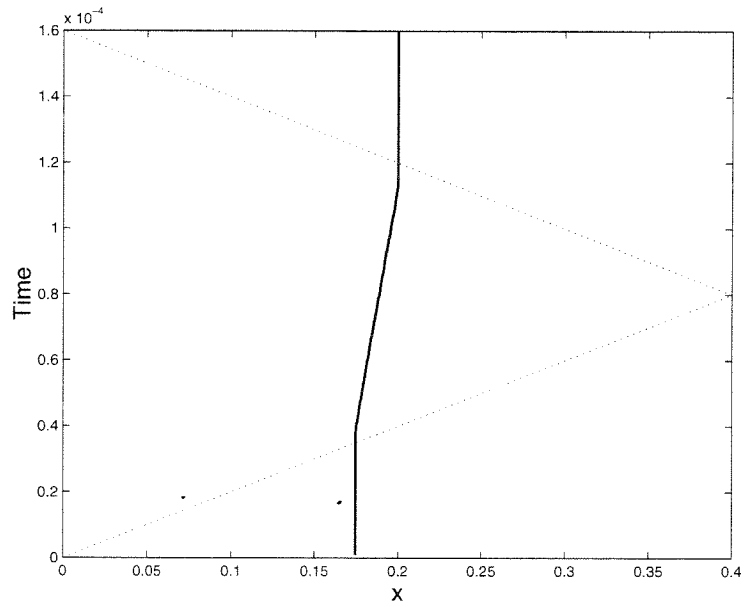

Figure 2.15: Trajectory of the phase boundary in the whipped string with a sticky kinetic relation. The heavy line gives the location of the phase boundary whereas the dotted lines determine the position of the shocks.

The trajectory of the four phase boundaries can be found in Figure 2.17. Once again we find that significant changes in the speed of the phase boundaries occur when they collide with shocks.

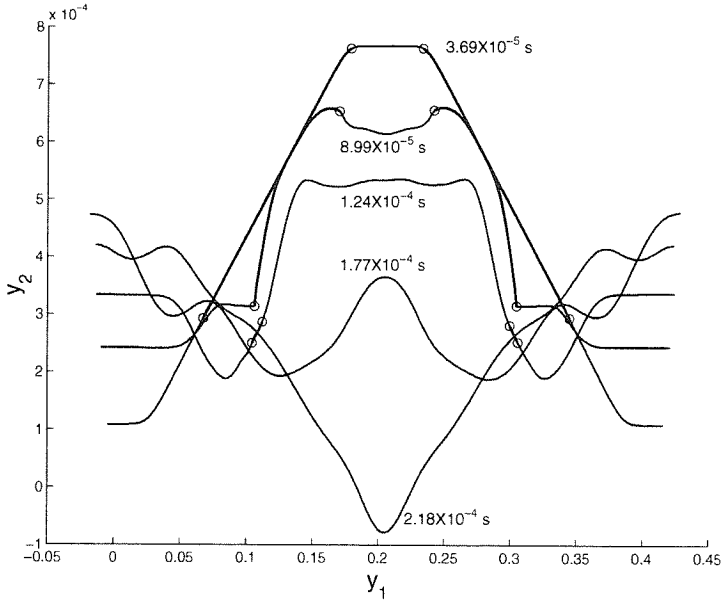

Figure 2.16: Deformed shape of a string with several phase boundaries. The shapes are quite non-intuitive.

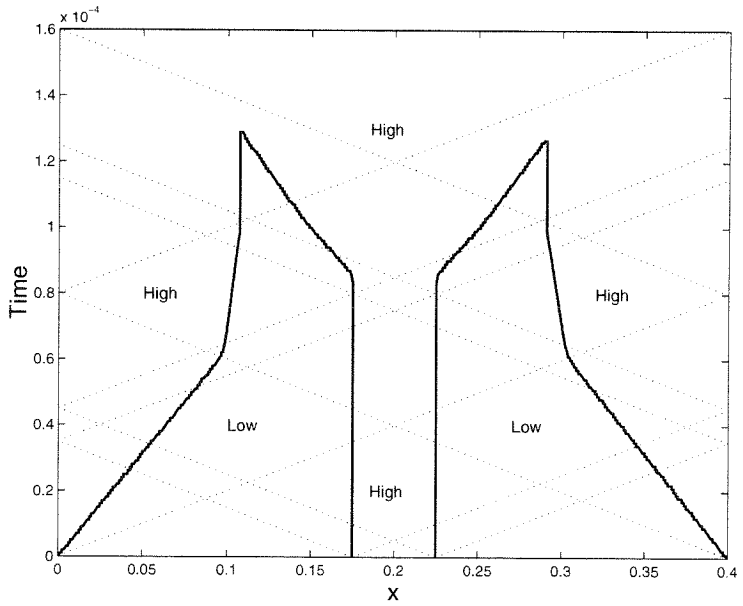

Figure 2.17: Trajectories of the phase boundaries in the nucleating string. After a short time the phase boundaries coalesce and the entire string is in the high strain phase.

Chapter 3

Atomistics

3.1 Introduction

We have seen that kinetic relations are needed to determine the mobility of phase boundaries in strings and bars. This is true in quasistatic as well as dynamic problems. The need for kinetic relations has also been demonstrated for phase boundaries in three-dimensional continua (see Abeyaratne and Knowles (1990) and Gurtin (1995)). While this has now become a generally accepted point of view there is no systematic understanding regarding specific kinetic relations that govern phase boundaries in actual materials. We examine the issue from the atomistic point of view in this chapter. By doing so we hope to unravel the processes that occur at the atomic level but affect the mechanics at the macroscopic level. The details of these processes are ignored in a continuum theory but their collective effect is embodied in the kinetic relation.

Atomistic studies of phase transitions are not new. Krumhansl and Schrieffer (1975) considered a one-dimensional model of masses interacting through quartic double well potentials and studied travelling wave solutions to the governing equations in a continuum approximation. They demonstrated that one could have thermal oscillations (just like those observed with harmonic potentials) and also moving domain walls as a result of the non-convex potential. More recent examples of atomistic studies can be found in Puglisi and Truskinovsky (2000) and Balk *et al.* (2001). Puglisi and Truskinovsky (2000) explore the energy landscape of a chain with cubic and tri-linear elastic springs. The unstable (or spinodal) region is given special attention. The authors consider quasi-static evolution paths and analyze the effect of the shape of the spinodal region on the hysteresis associated with the force-displacement curve. While Puglisi and Truskinovsky focus on the static

and quasi-static characteristics of discrete chains Balk *et al.* (2001) concentrate on their dynamic behaviour. They perform numerical experiments on a chain with piecewise linear elements and find analytical solutions describing the frequency, kinetic energy and speed of the waves of phase transition. A significant finding in their numerical experiments is that a part of the energy stays in the form of high frequency oscillations. This motion becomes 'invisible' in the continuum limit and one can say that the corresponding kinetic energy is transferred into heat. Such high frequency oscillations cause an energy cascade towards the smaller scales and are highly dissipative. None of these studies, however, yield a specific kinetic relation. That is the goal of our work. We construct a simple one-dimensional model mass and spring model with a bistable potential as in the papers above and perform several numerical experiments involving dynamically propagating phase boundaries. We find that the results of these computations can be collected in a single kinetic relation that depends only on the macroscopic material properties of the chain, such as the elastic modulus, the transformation strain, and the Maxwell strain and is apparently independent of the extent of the second neighbour interaction and temperature (at least for moderate temperatures).

3.2 Equilibrium

Consider a series of N masses as shown in Figure 3.1. The masses interact with each other through non-linear springs whose potential energy is described by a quartic expression.

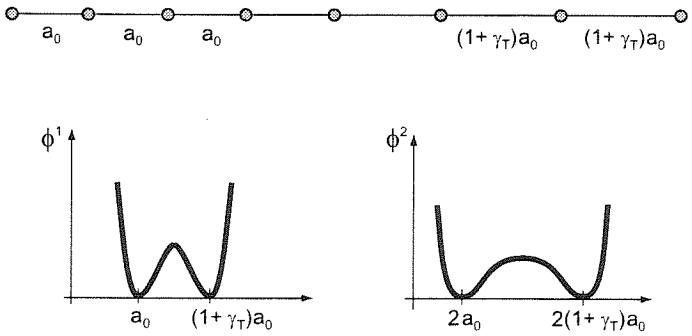

Figure 3.1: One-dimensional chain of interacting masses. The graphs below show the interaction potentials with the first and second nearest neighbours. Second neighbour interactions are used to crudely account for the effects of interfacial energy.

The interactions are limited to the first and second nearest neighbours so that the potential

energy of the springs can be written as

$$\phi = \sum_{i=1}^{N-1} \phi^1(x_i) + \sum_{j=1}^{N-2} \phi^2(y_j) \tag{3.1}$$

where

$$\phi^1(x) = (x - a_0)^2(x - (1 + \gamma_T)a_0)^2, \tag{3.2}$$

$$\phi^2(y) = (y - 2a_0)^2(y - 2(1 + \gamma_T)a_0)^2, \tag{3.3}$$

and

$$x_i = u_{i+1} - u_i, \quad y_j = u_{j+2} - u_j, \tag{3.4}$$

where

u_i is the position of mass i at any time,

a_0 is the equlibrium separation between two adjacent masses in the low strain phase,

$(1 + \gamma_T)a_0$ is the equlibrium separation between them in the high strain phase, and

C_1 and C_2 are certain moduli satisfying $C_2 \leq C_1$.

When forces f_i are applied to the masses, the potential energy ψ is given by

$$\psi = \phi - \sum_{i=1}^{N} f_i u_i \tag{3.5}$$

and equilibrium requires

$$\frac{\partial \phi}{\partial u_i} = f_i, \quad i = 1, ..., N, \tag{3.6}$$

which is a set of N non-linear equations. We wish to determine the force *vs.* displacement characteristics of a one -dimensional chain. To this end we assume $N = 20$ and then apply a displacement u_{20} to mass 20 holding mass 1 fixed so that $u_1 = 0$. No external forces are applied to the other masses. This corresponds to a hard loading device. The problem reduces to a solution of 20 non-linear equations (3.6) in the 20 variables $u_i, i = 2, \ldots, 19$, f_1 and f_{20}. We solve this using a Newton-Raphson method and plot the force f_{20} vs. the displacement $u_{20} - 19a_0$. We start with $u_{20} = (19 - 1.6\gamma_T)a_0$ and an initial guess

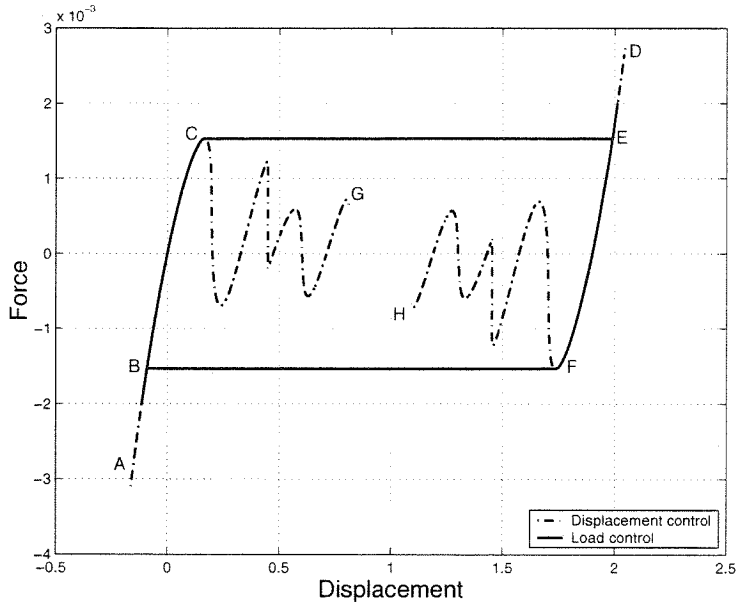

Figure 3.2: Hard and soft loading on a chain of 20 masses. The hysterisis is evident.

$u_i = \left[\frac{i-1}{19}\right] u_{20}, i = 1, \ldots, 20$. We iterate holding u_{20} fixed. The method is guaranteed to give the correct solution with this initial guess because there is only a unique set of displacements that will satisfy (3.6) for this boundary condition. Once we have obtained this solution we increase u_{20} by a small amount and redo the calculation. The initial guess for the Newton-Raphson method is the previous equilibrium state. The method converges since our initial guess is very close to the solution. We continue in this manner even after the force rises above point B, that is, after we have entered the region of multiple equilibria. We find that the calculation proceeds smoothly with the springs staying in the low strain phase till we reach C. Beyond this, there is no stable equilibrium in the low strain phase. The calculation becomes unstable and the results follow the curve CG crossing the zero force line several times. The calculations become extremely unstable beyond that and the results are not shown. We restart the calculation by applying a very large u_{20} so that there is a unique equilibrium solution in the high strain phase. This is shown as point D. We proceed as before, but by decreasing u_{20} in small decrements. The results are stable along DEF in the high strain phase and becomes unstable beyond and proceed as shown in FH.

One can also load the chain in a 'soft' device by applying a force instead of a displacement at mass 20. The results of doing so are plotted in Figure 3.2 as the solid line. It is evident that the solid line coincides with the dotted line everywhere except the region $BCEF$.

As one *loads* the chain upto point C, it suddenly changes phase and jumps to point E. Similarly, as one *unloads* it upto point F, it suddenly jumps to point B. This shows that the force-displacement curve of the chain is *hysteretic* – something characteristic of materials with multi-well energies. Similar curves can be obtained by starting with a chain that is entirely in the high strain phase in the beginning or with several phase boundares located at different positions. These results are consistent with the detailed analysis of Puglisi and Truskinovsky (2000) for smaller chains.

3.3 Dynamics with the chain

We now study the dynamics to understand the kinetic relations for moving phase boundaries. In particular, we simulate impact experiments on the chain and compare the results obtained with those in the continuum theory. Impact problems on atom chains are easy to simulate owing to the uncomplicated nature of the boundary conditions. Moreover, continuum solutions of impact problems on bars and strings are already available for ready comparison. The presence of propagating discontinuities in the solution to these problems provides a benchmark test for the correctness of the algorithm. Also, in a few cases one can actually obtain analytical solutions for the waves in the chain. Considerations such as these prompted us to perform numerical studies of impacts on atom chains. In order to facilitate quantitative comparison of the continuum and atomic descriptions, we switch to different potentials ϕ^1 and ϕ^2 such that the resulting force-displacement (or stress-strain) relation is trilinear as in Figure 2.3(b). So

$$\phi^1(\epsilon) = \begin{cases} \frac{E}{2}\epsilon^2 & \text{if } 1+\epsilon < \lambda_0 - \frac{\gamma_T}{4}, \\ \frac{E}{2}\epsilon^2 - E(1+\epsilon-\lambda_0+\frac{\gamma_T}{4})^2 & \text{if } \lambda_0 - \frac{\gamma_T}{4} \le 1+\epsilon \le \lambda_0 + \frac{\gamma_T}{4}, \\ \frac{E}{2}(\epsilon-\gamma_T)^2 + \frac{E\gamma_T}{2}[2\lambda_0 - (2+\gamma_T)] & \text{if } 1+\epsilon > \lambda_0 + \frac{\gamma_T}{4}, \end{cases} \tag{3.7}$$

where

$$\epsilon_i = \frac{u_{i+1} - u_i}{a_0} - 1 \tag{3.8}$$

will be called the strain and

$$\phi^2(\gamma) = \begin{cases} \frac{E}{2}\gamma^2 & \text{if } 1+\gamma < \lambda_0 - \frac{\gamma_T}{4}, \\ \frac{E}{2}\gamma^2 - E(1+\gamma-\lambda_0+\frac{\gamma_T}{4})^2 & \text{if } \lambda_0 - \frac{\gamma_T}{4} \leq 1+\gamma \leq \lambda_0 + \frac{\gamma_T}{4}, \\ \frac{E}{2}(\gamma-\gamma_T)^2 + \frac{E\gamma_T}{2}[2\lambda_0 - (2+\gamma_T)] & \text{if } 1+\gamma > \lambda_0 + \frac{\gamma_T}{4}, \end{cases} \tag{3.9}$$

where

$$\gamma_j = \frac{u_{j+1} - u_j}{2a_0} - 1. \tag{3.10}$$

In other words, the force-displacement relation is characterised by the transformation strain γ_T and the Maxwell stretch λ_0. Hence, the potential is still a double-well potential but it is piecewise parabolic. This is true of the potentials describing the first neighbour interaction as well as the second neighbour interaction.

The dynamics of the chain is governed by the following system of ordinary differential equations.

$$m_i \ddot{u}_i = \frac{\partial \psi}{\partial u_i}, \quad i = 1, ..., N, \tag{3.11}$$

where m_i is the mass of particle i. We assume for simplicity that $m_i = m$. The problem is to determine the evolution in time of the variables $u_i(t)$ given certain initial conditions $u_i(0) = u_i^0, i = 1, ..., N$ and boundary conditions $u_0 = u^0(t)$ and $u_N = u^N(t)$. This is done using a Newmark explicit time-stepping algorithm.

Our model consists of 300 atoms, all of them in the energy well corresponding to the low-strain phase. For now we assume that the atoms are static; in other words they are at zero temperature. At time $t = 0^+$ we apply a velocity v_I to atom 300 at the extreme right. Atom 1 at the extreme left is held fixed. A small impact velocity results in the propagation of a sonic wave into the medium. Since the stress-strain curve corresponding to the material is trilinear, the speed of this sonic wave is constant. The profile of this wave is depicted in Figure 3.3. The solution to this problem is explicitly known (Chin (1975)) and we find good agreement between this and our numerical results.

This is the case, however, only for small impact velocities. If the impact velocity v_I is large enough, we nucleate a phase boundary at the point of impact. The phase boundary then moves into the medium at a speed lower than the sonic wave. Two snapshots of the

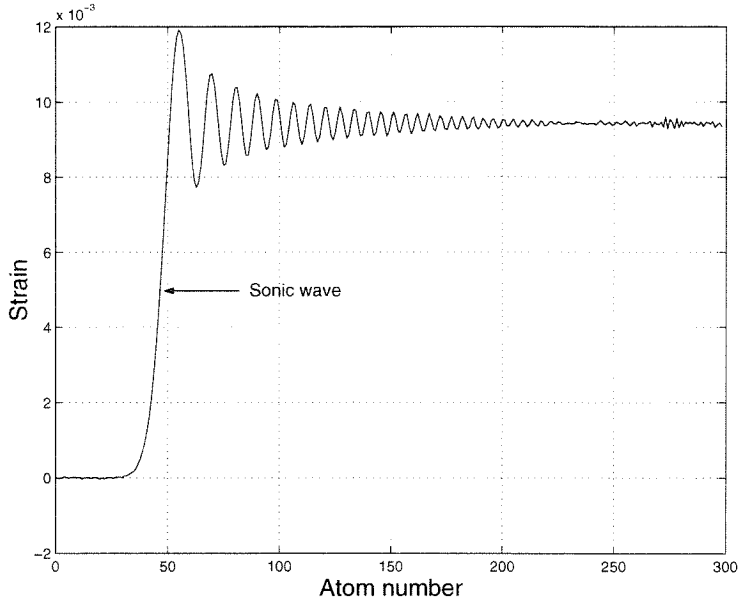

Figure 3.3: Sonic wave moving through an atom chain.

strain profile with a moving phase boundary is depicted in Figure 3.4. As can be easily seen, the phase boundary manifests itself as a sharp strain discontinuity. The sonic wave, on the other hand is spread over several atoms. There are some marked differences between sonic waves and phase boundaries that come to light from this plot. Sonic waves are relatively long wave-length waves. Phase boundaries on the other hand have short wavelength waves associated with them. It can also be seen that the passage of the phase boundary causes the atoms to go over the hump in the energy curve (causing one of the springs to become unstable) and leaves them vibrating more vigorously. This becomes clear in Figure 3.5 which depicts the strain histories at two of the atoms at the extreme right. Also note that the difference in arrival times of the sonic wave is smaller than the difference in arrival times of the phase boundary. This is expected since the sonic wave travels faster than the phase boundary.

3.3.1 Determining the kinetic relation

An examination of the strain profiles in the reference coordinate and the time coordinate reveals that one can approximate it as being piecewise constant with superimposed thermal oscillations. This is exactly what we get from a continuum theory of bars. Once we know the strains ahead and behind the phase boundary, we can calculate the driving force on it

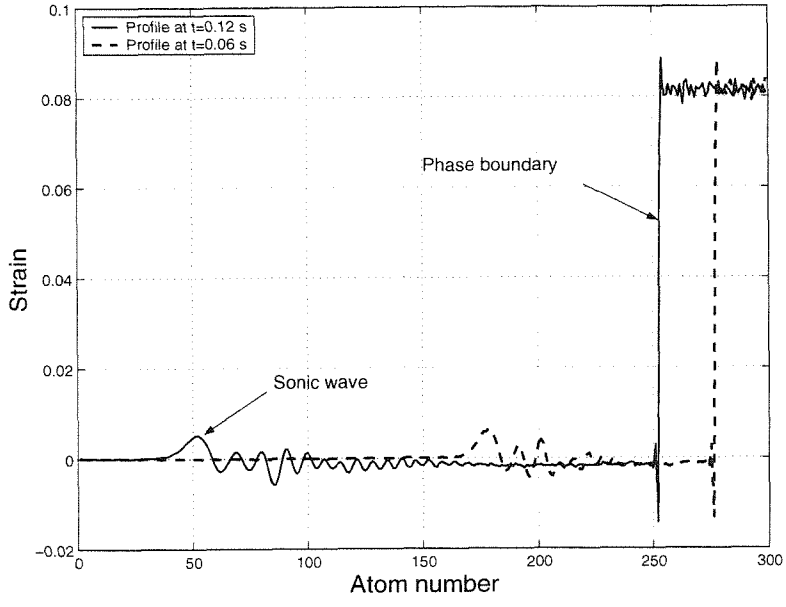

Figure 3.4: Snapshots of the strain profile with a moving phase boundary.

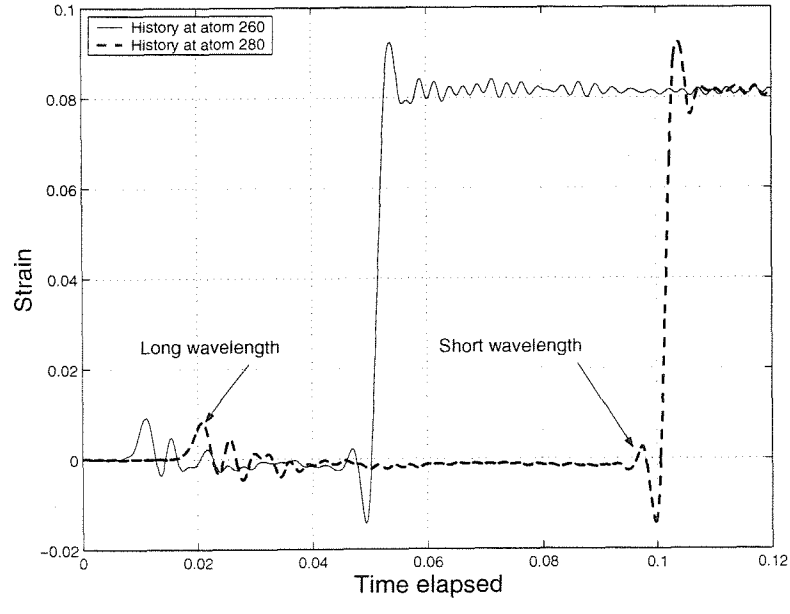

Figure 3.5: Strain histories at atoms 260 and 280.

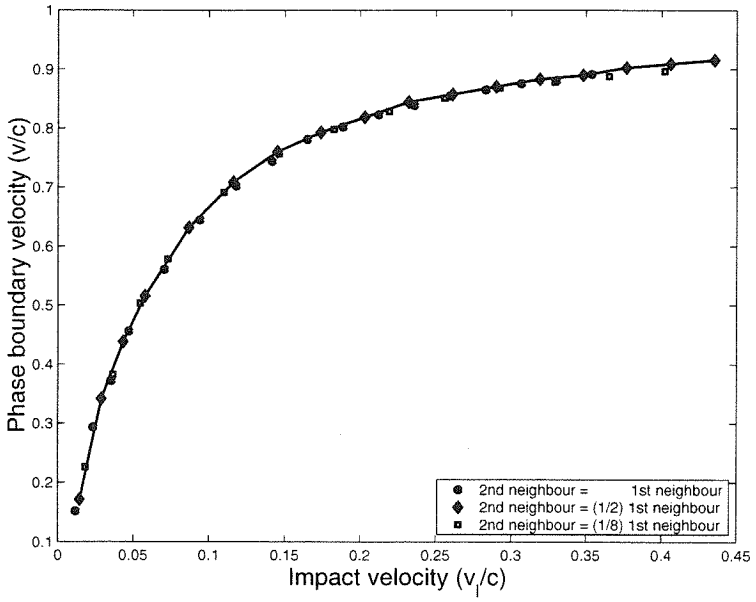

Figure 3.6: Results of simulations at high impact velocities. The phase boundary velocity tends to asymptote towards the sonic speed.

using the following expression from continuum theory

$$f = \frac{E\gamma_T}{2}(2\lambda_0 - \lambda^+ - \lambda^-), \tag{3.12}$$

where λ^+ and λ^- are the stretches ahead and behind the phase boundary respectively. In fact we can determine the entire $x-t$ plane once we know the velocity of the phase boundary. We can determine this velocity from plots like Figure 3.5 which give us the time elapsed between the arrival of the waves at two fixed locations. We need to do this for several different phase boundary velocities in order to determine the underlying kinetic relation. The phase boundary velocity can be varied by changing the impact velocity. We went through this exercise for several combinations of first and second neighbour spring stiffness. The results have been plotted in Figure 3.6. The figure plots the non-dimensionalized phase boundary velocity v/c against the non-dimensionalized impact velocity v_I/c (where c is the sonic speed) for different ratios of second neighbour to first neighbour interaction. It is quite remarkable that all the data collapses into a single master curve that is independent of the details of nearest neighbour interaction. We also see from this plot that for each of the materials the phase boundary velocity tends to asymptote towards the sonic speed as we increase the impact velocity. Continuum theory gives similar predictions for phase

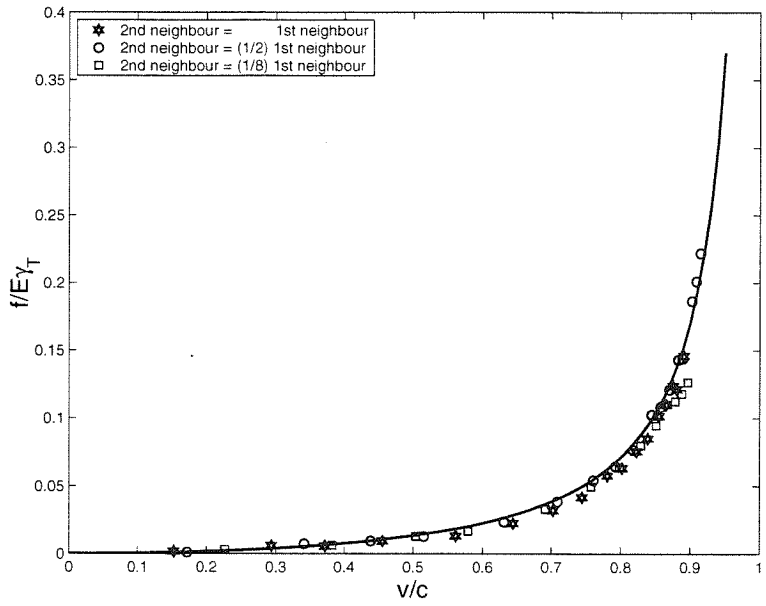

Figure 3.7: Kinetic relation obtained from computations.

boundaries in bars with a trilinear stress-strain law, but the specific curve depends on the assumed kinetic relation.

We calculated the driving force on the phase boundary using the data from our numerical experiments. Figure 3.7 shows plots of the non-dimensionalized driving force as a function of the non-dimesionalized phase boundary velocity. It is to be expected (in view of Figure 3.6) that the relation between $f/E\gamma_T$ and v/c is quite independent of the amount of interaction with the second nearest neighbour. However, the most remarkable fact about this data is that the following curve is an excellent fit to the points obtained from the atomistic simulations.

$$\frac{f}{E\gamma_T} = (\lambda_0 - 1) + \frac{\gamma_T/2}{1 - \frac{v^2}{c^2}} \tag{3.13}$$

This has been plotted as the heavy line in Figure 3.7.

3.3.2 Effects of finite temperature

The results above were obtained for $T = 0$. We have made an attempt to incorporate the effects of temperature in our simulations. The temperature T of our system is interpreted as being proportional to the mean kinetic energy of the masses in the system. In other

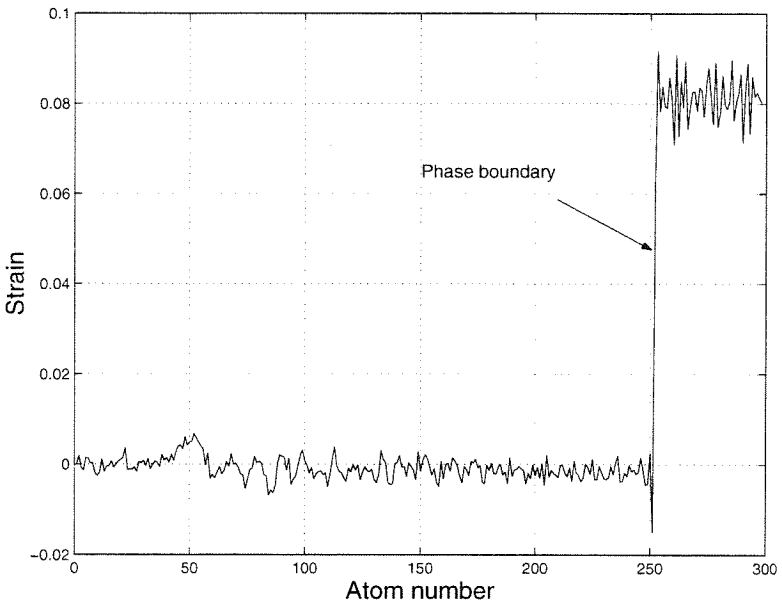

Figure 3.8: Phase boundary in a thermalized atom chain. There is a big jump in strain at the phase boundary.

words, we assume

$$\frac{T_1}{T_2} = \frac{\sum_{i=1}^{N} m_i \mathbf{v}_{1i}^2}{\sum_{i=1}^{N} m_i \mathbf{v}_{2i}^2}. \tag{3.14}$$

Given a certain initial temperature T the initial velocities of the masses have to be assigned randomly while also making sure that the chain has no net momentum. In other words, the initial velocities must have a zero mean. Once we have such a set of initial velocities, say $\mathbf{v}_0$, we calculate the corresponding temperature T_0. This is done as follows.

$$kT_0 = 2\sum_{i=1}^{M} m_i \mathbf{v}_{0i}^2, \tag{3.15}$$

where k is some constant. Finally, we scale up the velocities $\mathbf{v}_{0i}$ by the amount $\sqrt{\frac{T}{T_0}}$ to obtain a velocity distribution consistent with the temperature T.

We have performed some preliminary simulations with such thermalized chains. The results from one of them has been plotted in Figure 3.8. It is an impact experiment with a phase boundary moving in. We see that while the phase boundary is clearly discernible as a big strain discontinuity the leading shock wave has been completely overwhelmed by the thermal oscillations. In order to eliminate the thermal oscillations we take an ensemble average of several experiments with the same boundary conditions but different initial velocity

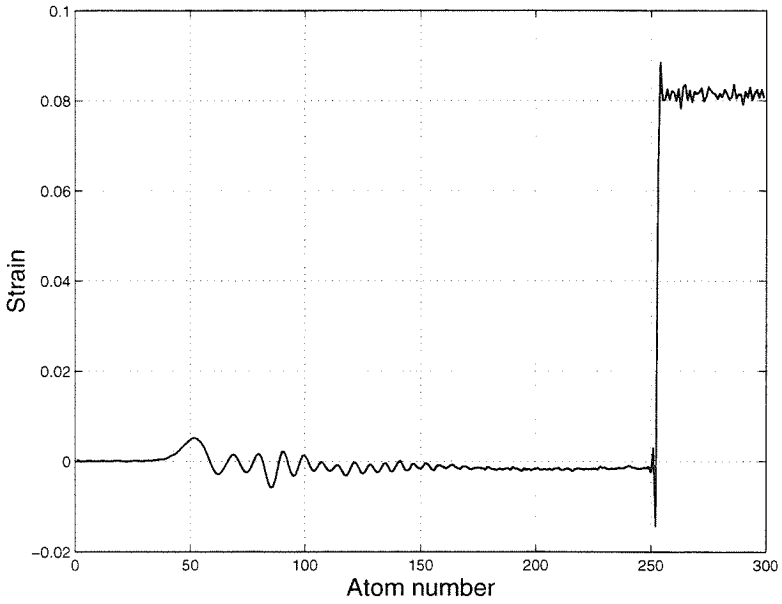

Figure 3.9: Ensemble averaged strain profile from 100 experiments on a thermalized chain.

distributions. All the initial velocity distributions are consistent with a given temperature. In Figure 3.9 we have plotted the ensemble average corresponding to the experiment of Figure 3.8. The leading shock wave is now clearly visible. We have found that the kinetic relation is not affected by moderate temperatues.

Chapter 4

Mechanics of beams

4.1 Introduction

In this chapter, we study the mechanics of beams made of a single crystal of a shape-memory alloy. Of particular interest are the laws that govern the propagation and evolution of phase boundaries. We have extensively studied this issue in strings (without bending and shear) and have found that the *kinetic relation* plays a central role in determining the dynamics. While this theoretical framework has gained wide acceptance, it has proved to be difficult to measure it experimentally (see for example Escobar and Clifton (1993)). We find that the notion of kinetic relation is relevant even in beams, and propose a *simple* experiment to measure this kinetic relation.

The basic theory – the kinematics, the balance laws, dissipation inequality and the constitutive assumptions – are presented in detail in Section 4.2. We allow our beams to stretch, shear and bend, and assume following Bhattacharya (2001) that the energy is non-convex in stretch and shear, but convex in the moment. The kinematics which follow a one director or one Cosserat vector formulation and the balance laws are classical (we refer the reader to Antman (1995) for background and detailed bibliographic notes). The constitutive relations are not. Therefore a detailed discussion of the motivation and relation of the constitutive constants to crystallographically measurable quantities is given. Anticipating the role of phase boundaries, the treatment of the dissipation inequality is more general, and leads to a notion of driving force on interfaces.

The equilibria of such beams are studied in Section 4.3. We show that equilibria which involve phase boundaries are characterized by discontinuities in tangent as well sharp changes in curvature of the centerline of the beam. The role of the kinetic relation in quasistatic

evolution of phase boundaries is discussed, and a *simple* experiment based on a cantilever to measure the kinetic relation is described. We turn to dynamics in Section 4.4, and show that the jump conditions do not *uniquely* determine the velocity of the phase boundaries and that there is indeed room for a kinetic relation.

It would be desirable to confirm the need for a kinetic realtion through the solution of simple initial-boundary value problems like Riemann or impact problems. For example, in bars Abeyaratne and Knowles (1991) have shown that these problems admit a one parameter family of solutions, and the kinetic relation provides a selection criterion. We saw in chapter 2 that strings behave in exactly the same manner. Unfortunately, even Riemann and impact problems are too complicated to solve explicitly in beams. In particular, in contrast to bars and strings, the solutions are not piecewise constant in strain, etc. since the coupling between the linear and angular momentum equations does not allow us to reduce them to wave equations. We have been able to identify some special boundary conditions in impact problems when this coupling vanishes, and one is able to write a one-parameter family of solutions. Unfortunately, these boundary conditions are physically difficult to achieve, and hence the calculations are not very illuminating. We therefore do not include these here.

4.2 Basic Equations

4.2.1 Kinematics

Consider a beam of length L and constant cross-sectional area A in the reference configuration. Let x be a typical point on the centerline $(0, L)$ of the reference configuration and t denote an instant of time. We assume that the diameter of the cross-section is much smaller than the length of the beam. Therefore, we assume that during any deformation of the beam, planar cross-sections of the beam remain planar (but not necessarily normal to the centerline). We further assume in this chapter that the deformation of the center-line is planar. Therefore, we use a one-director Cosserat description where the deformation is described by two vector fields:

$\mathbf{y}(x,t)$ which describes the deformation of the centerline of the beam and

$\hat{\mathbf{b}}(x,t), \quad |\hat{\mathbf{b}}| = 1$ which describes the orientation of the cross-section.

Above, both $\mathbf{y}$ and $\hat{\mathbf{b}}$ are two-vectors. This is illustrated in Figure 4.1 . We note that the assumption $|\hat{\mathbf{b}}| = 1$ does *not* mean that the cross-sectional area of the beam is assumed to be constant as it deforms. Instead, it is assumed that the cross-sectional area is completely determined by the axial stretch and shear and thus no independent kinematic variable is necessary to describe it. Since $\hat{\mathbf{b}}$ is a planar unit-vector, it can be described uniquely by the angle θ it makes with the horizontal:

$$\hat{\mathbf{b}}(x,t) = \cos(\theta(x,t))\hat{\mathbf{i}} + \sin(\theta(x,t))\hat{\mathbf{j}}.$$

We will use the notations $\hat{\mathbf{b}}$ and θ interchangeably.

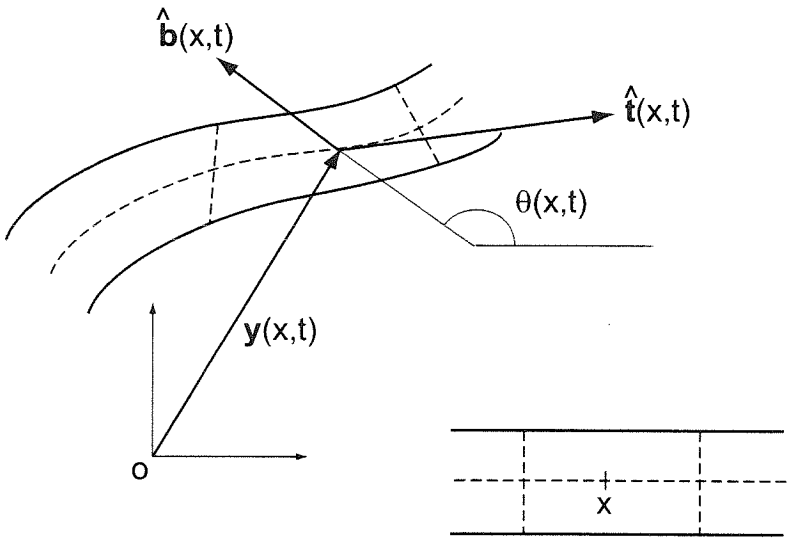

Figure 4.1: Reference (bottom right) and deformed (top left) configuration of the beam.

A super-posed dot will denote material time derivative, i.e., partial derivative with respect to t holding x fixed. Therefore, the velocity of a particle on the center-line is $\dot{\mathbf{y}}(x,t)$ while the rate of rotation of the director is $\dot{\theta}(x,t)$. We shall denote the stretch and the tangent to the centerline respectively as

$$\lambda = |\frac{\partial \mathbf{y}}{\partial x}|, \quad \hat{\mathbf{t}} = \frac{1}{\lambda}\frac{\partial \mathbf{y}}{\partial x}; \quad \text{so} \quad \frac{\partial \mathbf{y}}{\partial x} = \lambda \hat{\mathbf{t}}.$$

It is useful to write this with respect to the orthonormal basis $\{\hat{\mathbf{b}}^{\perp}, \hat{\mathbf{b}}\}$:

$$\lambda \hat{\mathbf{t}} = \alpha \hat{\mathbf{b}}^{\perp} + \gamma \hat{\mathbf{b}}.$$

Clearly $\lambda = \sqrt{\alpha^2 + \gamma^2}$ is the stretch and γ is the shear. We also introduce the angle β as the angle between $\hat{\mathbf{b}}$ and $\hat{\mathbf{t}}$ ($\cos\beta = \hat{\mathbf{t}} \cdot \hat{\mathbf{b}}$). We have

$$\alpha = \lambda \cos\beta, \quad \gamma = \lambda \sin\beta.$$

Finally we define $\kappa = \frac{\partial\theta}{\partial x}$ to be the curvature of the beam. The primary measures of strain in the beam are α, γ and κ.

We are interested in studying shocks and phase boundaries. We will therefore consider deformations $\mathbf{y}(x,t)$ and $\theta(x,t)$ that are not smooth, but only continuous in x and t with possible discontinuities in the velocities $\dot{\mathbf{y}}$ and $\dot{\theta}$, the stretch λ, the tangent $\hat{\mathbf{t}}$ and the curvature κ at a finite number of points. Continuity of $\mathbf{y}(x,t)$ and $\theta(x,t)$ implies that these jumps can not be arbitrary but satisfy the some jump conditions. If we have discontinuities in the quantities listed above at the point $s(t)$ in the reference configuration, then

$$-\dot{s}[|\, \lambda\hat{\mathbf{t}} \,|] = [|\, \dot{\mathbf{y}} \,|], \tag{4.1}$$

$$-\dot{s}[|\, \kappa \,|] = [|\, \dot{\theta} \,|] \tag{4.2}$$

where $\dot{s}$ is the velocity of the discontinuity in the reference configuration.

4.2.2 Conservation laws

The balance of *linear momentum* for a part of the beam occupying the interval (x_1, x_2) requires

$$\frac{d}{dt}\int_{x_1}^{x_2} \rho A\dot{\mathbf{y}}\, dx = \mathbf{T}(x_2,t) - \mathbf{T}(x_1,t) + \int_{x_1}^{x_2} \mathbf{f}\, dx, \tag{4.3}$$

where

ρ is the density of the beam in the reference configuration,

A is its cross-sectional area in the reference configuration,

$\mathbf{T}(x,t)$ is the force acting at material point x at time t, and

$\mathbf{f}(x)$ is the body force per unit reference length at material point x.

For future use. we will denote $T_\perp = \mathbf{T} \cdot \hat{\mathbf{b}}^\perp$ and $T_b = \mathbf{T} \cdot \hat{\mathbf{b}}$ to be the components of $\mathbf{T}$ with respect to the orthonormal basis $\{\hat{\mathbf{b}}^\perp, \hat{\mathbf{b}}\}$.

If there are no discontinuities in the interval (x_1, x_2) then (4.3) can be localized to

$$\rho A \ddot{\mathbf{y}} = \frac{\partial \mathbf{T}}{\partial x} + \mathbf{f}. \tag{4.4}$$

If there is a discontinuity in the interval (x_1, x_2), then we also need a jump condition. If we have a discontinuity at $x = s(t)$ in the reference configuration, then the required jump condition may be easily derived by dividing each integral in (4.3) into two: one from x_1 to $s(t)$ and the other from $s(t)$ to x_2. We obtain

$$-\dot{s}[|\, \rho A \dot{\mathbf{y}} \,|] = [|\, \mathbf{T} \,|].$$

We assume henceforth that ρ and A are constant and therefore we conclude that

$$-\dot{s}\rho A[|\, \dot{\mathbf{y}} \,|] = [|\, \mathbf{T} \,|]. \tag{4.5}$$

Similarly, the balance of *angular momentum* for the part of the beam in the interval (x_1, x_2) requires

$$\begin{aligned} \frac{d}{dt}\int_{x_1}^{x_2} \mathbf{y} \times \rho A \dot{\mathbf{y}}\, dx + \frac{d}{dt}\int_{x_1}^{x_2} \hat{\mathbf{b}} \times \rho I \dot{\hat{\mathbf{b}}}\, dx = M(x_2,t) - M(x_1,t) \\ + \mathbf{y}(x_2,t) \times \mathbf{T}(x_2,t) - \mathbf{y}(x_1,t) \times \mathbf{T}(x_1,t) + \int_{x_1}^{x_2} \mathbf{y} \times \mathbf{f}\, dx + \int_{x_1}^{x_2} l\, dx, \end{aligned}$$

where

I is the second moment of area of the cross-section of the beam about an axis that causes the first moment to vanish,

$M(x,t)$is the moment acting at material point x at time t, and

$l(x)$ is the body moment per unit reference length of the beam at material point x.

Note in the above expression that we write the cross-product as a scalar since we are working in two dimensions. We will use this convention throughout this chapter. The statement above can be localized in the absence of discontinuities to

$$\mathbf{y} \times \rho A \ddot{\mathbf{y}} + \hat{\mathbf{b}} \times \rho I \ddot{\hat{\mathbf{b}}} = \frac{\partial M}{\partial x} + \frac{\partial}{\partial x}(\mathbf{y} \times \mathbf{T}) + \mathbf{y} \times \mathbf{f} + l.$$

Recalling the definition of θ and using (4.4), this can be simplified to obtain

$$\begin{aligned} \rho I\ddot{\theta} &= \frac{\partial M}{\partial x} + \frac{\partial \mathbf{y}}{\partial x} \times \mathbf{T} + l, \\ \text{or,} \quad \rho I\ddot{\theta} &= \frac{\partial M}{\partial x} + \lambda \hat{\mathbf{t}} \times \mathbf{T} + l. \end{aligned} \tag{4.6}$$

When we have a discontinuity at $x = s(t)$, we also obtain the following jump condition,

$$-\dot{s}\rho I[\,|\,\dot{\theta}\,|\,] = [\,|\,M\,|\,]. \tag{4.7}$$

In summary, the equations (4.4), (4.6) along with the jump conditions (4.5), (4.7) describe the balance of linear and angular momentum in the beam.

We now turn to the dissipation inequality. Since we are considering a purely mechanical theory, we can not write a balance of energy, but can write a dissipation inequality: rate of work being done by external forces (and moments) on any part of the body is greater than or equal to the rate of change of kinetic and potential energy in the same part of the body. Consider a portion of the beam in the interval (x_1, x_2). The rate of work being done by external forces (and moments) on this part of the body is

$$\begin{aligned} P^{ext} = & \int_{x_1}^{x_2} \{\dot{\mathbf{y}} \cdot \mathbf{f} + l(\hat{\mathbf{b}} \times \dot{\hat{\mathbf{b}}})\}\, dx + \dot{\mathbf{y}}(x_2, t) \cdot \mathbf{T}(x_2, t) - \dot{\mathbf{y}}(x_1, t) \cdot \mathbf{T}(x_1, t) \\ & + M(x_2, t)\hat{\mathbf{b}}(x_2, t) \times \dot{\hat{\mathbf{b}}}(x_2, t) - M(x_1, t)\hat{\mathbf{b}}(x_1, t) \times \dot{\hat{\mathbf{b}}}(x_1, t). \end{aligned} \tag{4.8}$$

Similarly, the rate of change of kinetic and potential energy in the same part of the body is given by

$$P^{int} = \frac{d}{dt} \int_{x_1}^{x_2} \left\{ \frac{\rho}{2} |\dot{\mathbf{y}}|^2 + \frac{\rho I}{2} |\hat{\mathbf{b}} \times \dot{\hat{\mathbf{b}}}|^2 + \Phi \right\} dx \tag{4.9}$$

where $\Phi = \Phi(x, t)$ is the energy stored in the beam per unit reference length. We define the power dissipated as

$$P^{diss} = P^{ext} - P^{int}. \tag{4.10}$$

The dissipation inequality states that

$$P^{diss} \geq 0 \qquad \text{or} \qquad P^{ext} \geq P^{int}. \tag{4.11}$$

For smooth motions,

$$P^{int} = \int_{x_1}^{x_2} \left\{ \dot{\mathbf{y}} \cdot \rho \ddot{\mathbf{y}} + (\hat{\mathbf{b}} \times \dot{\hat{\mathbf{b}}})(\hat{\mathbf{b}} \times \rho I \ddot{\hat{\mathbf{b}}}) + \dot{\Phi} \right\} dx.$$

Therefore,

$$\begin{aligned} P^{diss} &= \int_{x_1}^{x_2} \left\{ \dot{\mathbf{y}} \cdot (\mathbf{f} - \rho \ddot{\mathbf{y}}) + (\hat{\mathbf{b}} \times \dot{\hat{\mathbf{b}}})(l - \hat{\mathbf{b}} \times \rho I \ddot{\hat{\mathbf{b}}}) - \dot{\Phi} \right\} dx \\ &\quad + \dot{\mathbf{y}}(x_2, t) \cdot \mathbf{T}(x_2, t) - \dot{\mathbf{y}}(x_1, t) \cdot \mathbf{T}(x_1, t) \\ &\quad + M(x_2, t)\hat{\mathbf{b}}(x_2, t) \times \dot{\hat{\mathbf{b}}}(x_2, t) - M(x_1, t)\hat{\mathbf{b}}(x_1, t) \times \dot{\hat{\mathbf{b}}}(x_1, t). \end{aligned}$$

Using the balance of momenta, (4.4) and (4.6), this can be rewritten as

$$\begin{aligned} P^{diss} &= -\int_{x_1}^{x_2} \left\{ \frac{\partial \mathbf{T}}{\partial x} \cdot \dot{\mathbf{y}} + \Big(\frac{\partial M}{\partial x} + \lambda \hat{\mathbf{t}} \times \mathbf{T} \Big)(\hat{\mathbf{b}} \times \dot{\hat{\mathbf{b}}}) + \dot{\Phi} \right\} dx \\ &+ \dot{\mathbf{y}}(x_2, t) \cdot \mathbf{T}(x_2, t) - \dot{\mathbf{y}}(x_1, t) \cdot \mathbf{T}(x_1, t) \\ &+ M(x_2, t)\hat{\mathbf{b}}(x_2, t) \times \dot{\hat{\mathbf{b}}}(x_2, t) - M(x_1, t)\hat{\mathbf{b}}(x_1, t) \times \dot{\hat{\mathbf{b}}}(x_1, t). \end{aligned}$$

We can now integrate by parts to obtain

$$P^{diss} = \int_{x_1}^{x_2} \left\{ \mathbf{T} \cdot \frac{\partial \dot{\mathbf{y}}}{\partial x} + M \frac{\partial}{\partial x}(\hat{\mathbf{b}} \times \dot{\hat{\mathbf{b}}}) - (\lambda \hat{\mathbf{t}} \times \mathbf{T})(\hat{\mathbf{b}} \times \dot{\hat{\mathbf{b}}}) - \dot{\Phi} \right\} dx;$$

or

$$P^{diss} = \int_{x_1}^{x_2} \left\{ \mathbf{T} \cdot \Big(\frac{\partial \dot{\mathbf{y}}}{\partial x} - (\hat{\mathbf{b}} \times \dot{\hat{\mathbf{b}}}) \lambda \hat{\mathbf{t}}^{\perp} \Big) + M \frac{\partial}{\partial x}(\hat{\mathbf{b}} \times \dot{\hat{\mathbf{b}}}) - \dot{\Phi} \right\} dx$$

since $\mathbf{T} \times \lambda \hat{\mathbf{t}} = -\mathbf{T} \cdot \lambda \hat{\mathbf{t}}^{\perp}$ for $\lambda \hat{\mathbf{t}}^{\perp} = -\gamma \hat{\mathbf{b}}^{\perp} + \alpha \hat{\mathbf{b}}$. Further, since $\hat{\mathbf{b}} \times \dot{\hat{\mathbf{b}}} = \dot{\theta}$, and therefore the above expression can be rewritten as

$$P^{diss} = \int_{x_1}^{x_2} \left\{ \mathbf{T} \cdot \Big(\frac{\partial \dot{\mathbf{y}}}{\partial x} - \dot{\theta} \lambda \hat{\mathbf{t}}^{\perp} \Big) + M \dot{\kappa} - \dot{\Phi} \right\} dx. \tag{4.12}$$

We now show that

$$\frac{\partial \dot{\mathbf{y}}}{\partial x} - \dot{\theta} \lambda \hat{\mathbf{t}}^{\perp} = \dot{\gamma} \hat{\mathbf{b}} + \dot{\alpha} \hat{\mathbf{b}}^{\perp}. \tag{4.13}$$

First,

$$\dot{\gamma} = \dot{\overline{\lambda \hat{\mathbf{t}} \cdot \hat{\mathbf{b}}}} = \dot{\overline{\lambda \hat{\mathbf{t}}}} \cdot \hat{\mathbf{b}} + \lambda \hat{\mathbf{t}} \cdot \dot{\hat{\mathbf{b}}} = \dot{\overline{\lambda \hat{\mathbf{t}}}} \cdot \hat{\mathbf{b}}^{\perp} - \dot{\theta} \lambda \hat{\mathbf{t}} \cdot \hat{\mathbf{b}}^{\perp} = \dot{\overline{\lambda \hat{\mathbf{t}}}} \cdot \hat{\mathbf{b}}^{\perp} - \dot{\theta} \alpha.$$

Similarly,

$$\dot{\alpha} = \dot{\overline{\lambda \hat{\mathbf{t}}}} \cdot \hat{\mathbf{b}} + \dot{\theta}\gamma.$$

Therefore,

$$\dot{\gamma}\hat{\mathbf{b}} + \dot{\alpha}\hat{\mathbf{b}}^{\perp} = (\dot{\overline{\lambda \hat{\mathbf{t}}}} \cdot \hat{\mathbf{b}})\hat{\mathbf{b}} + (\dot{\overline{\lambda \hat{\mathbf{t}}}} \cdot \hat{\mathbf{b}}^{\perp})\hat{\mathbf{b}}^{\perp} - \dot{\theta}(\alpha\hat{\mathbf{b}} - \gamma\hat{\mathbf{b}}) = \dot{\overline{\lambda \hat{\mathbf{t}}}} - \dot{\theta}(\alpha\hat{\mathbf{b}} - \gamma\hat{\mathbf{b}})$$

which is (4.13).

Using (4.13), we can rewrite (4.12) as

$$P^{diss} = \int_{x_1}^{x_2} \left\{ T_b\dot{\gamma} + T_{\perp}\dot{\alpha} + M\dot{\kappa} - \dot{\Phi} \right\} dx. \tag{4.14}$$

Therefore, the dissipation inequality for smooth motions after localiization says

$$T_b\dot{\gamma} + T_{\perp}\dot{\alpha} + M\dot{\kappa} - \dot{\Phi} \geq 0. \tag{4.15}$$

We now consider a deformation with a discontinuity at $s(t)$. Starting from (4.11), we obtain the following condition in addition to (4.15).

$$\begin{aligned} -\dot{s}[|\,\Phi\,|] - \rho A\dot{s}[|\,\dot{\mathbf{y}}\,|]\cdot <\dot{\mathbf{y}}> - \rho I\dot{s}[|\,\dot{\theta}\,|] <\dot{\theta}> \quad \geq \quad & [|\,\mathbf{T}\,|]\cdot <\dot{\mathbf{y}}> + <\mathbf{T}>\cdot[|\,\dot{\mathbf{y}}\,|] \\ & + [|\,M\,|] <\dot{\theta}> + <M> [|\,\dot{\theta}\,|]. \end{aligned}$$

Using the jump conditions (4.5) and (4.7), we get

$$-\dot{s}[|\,\Phi\,|] \geq <\mathbf{T}>\cdot[|\,\dot{\mathbf{y}}\,|] + <M> [|\,\dot{\theta}\,|]. \tag{4.16}$$

Finally using the kinematic conditions (4.1) and (4.2) we get

$$\dot{s}\Big([|\,\Phi\,|] - <\mathbf{T}>\cdot[|\,\lambda\hat{\mathbf{t}}\,|] - <M> [|\,\kappa\,|] \Big) \geq 0. \tag{4.17}$$

We thus notice that the term in parentheses is the force conjugate to the velocity of the discontinuity. Therefore, following Abeyaratne and Knowles (1990) (and Eshelby (1956, 1975)), we define it to be the thermodynamic driving force:

$$f = [|\,\Phi\,|] - <\mathbf{T}>\cdot[|\,\lambda\hat{\mathbf{t}}\,|] - <M> [|\,\kappa\,|]. \tag{4.18}$$

Therefore, the dissipation inequality becomes

$$f\dot{s} \geq 0. \tag{4.19}$$

4.2.3 Constitutive assumptions

We now make the following consitutitve assumptions.

$$\begin{aligned} \Phi &= \Phi(\alpha, \gamma, \kappa) \\ \mathbf{T} &= \mathbf{T}(\alpha, \gamma, \kappa) \\ M &= M(\alpha, \gamma, \kappa) \end{aligned}$$

Substiting these into (4.15), we write it as

$$\left(T_\perp - \frac{\partial \Phi}{\partial \alpha}\right)\dot{\alpha} + \left(T_b - \frac{\partial \Phi}{\partial \gamma}\right)\dot{\gamma} + \left(M - \frac{\partial \Phi}{\partial \kappa}\right)\dot{\kappa} \geq 0.$$

Following Coleman and Noll (1963), we can argue that this inequality has to be true for all smooth motions (since we can arbitrarily choose the body forces and moments). In particular, we can choose a class of motions where (γ, α, κ) are the same, but $(\dot{\gamma}, \dot{\alpha}, \dot{\kappa})$ take arbitrary values. The above inequality has to hold for each of these motions. Therefore, we conclude that

$$T_\perp = \frac{\partial \Phi}{\partial \alpha}, \quad T_b = \frac{\partial \Phi}{\partial \gamma}, \quad M = \frac{\partial \Phi}{\partial \kappa}. \tag{4.20}$$

Therefore, we only need to specify a constitutive relation for Φ. We note that this also implies that the dissipation is zero for any smooth motion, and that the only possible source of dissipation in these beams is at the discontinuities.

We now specialize to a specific constitutive relation, appropriate for beams made of single crystals of materials undergoing martensitic phase transformation. We will argue shortly that it is appropriate in such situations to assume that the energy is a non-convex function of the stretch and the shear, but a convex function of the curvature. We assume that there are two natural or stress-free states for the beam:

low strain state $\quad \alpha = \alpha_l, \quad \gamma = \gamma_l, \quad \kappa = 0,$

high strain state $\quad \alpha = \alpha_h, \quad \gamma = \gamma_h, \quad \kappa = 0.$

Above, α_l and α_h are the axial transformation stretches, stress-free stretches or eigen-stretches in the two phases and γ_l and γ_h are the transformation strains, stress-free strains

or eigen-strains in shear. The free energy Φ has local minima at these states and grows away from it. In order to keep things simple, we shall assume that Φ is quadratic near these states. We assume therefore that

$$\Phi = \begin{cases} \frac{1}{2}EA(\alpha-\alpha_l)^2 + \frac{1}{2}\mu A(\gamma-\gamma_l)^2 + \frac{1}{2}EI\kappa^2 & \text{in the low strain phase,} \\ \Phi_u(\gamma,\alpha) + \frac{1}{2}EI\kappa^2 & \text{in the unstable phase,} \\ \frac{1}{2}EA(\alpha-\alpha_h)^2 + \frac{1}{2}\mu A(\gamma-\gamma_h)^2 + \frac{1}{2}EI\kappa^2 + \Phi_0 & \text{in the high strain phase,} \end{cases} \tag{4.21}$$

for a suitable Φ_u. Above, E is the Young's modulus, μ the shear modulus and Φ_0 the difference in the ground state energies of the two phases. Note that we have assumed that both phases have the same moduli. This is not true in actual materials, but it simplifies many subsequent calculations. Φ_0 determines which phase would be more stable in a completely stress-free situation. We have not explicitly specified the regions of validity of the expressions for the low strain phase and high strain phase, neither have we given any explicit expression for the unstable phase Φ_u. We note that it is possible to specify these in such a manner that Φ is smooth and has no additional local minima. The details are cumbersome and omitted.

The expressions for the force $\mathbf{T}$ and the moment M follow immediately from (4.20). Omitting the expressions in the unstable phase, we can write

$$\mathbf{T} = EA(\lambda\hat{\mathbf{t}}\cdot\hat{\mathbf{b}}^{\perp} - \alpha^*)\hat{\mathbf{b}}^{\perp} + \mu A(\lambda\hat{\mathbf{t}}\cdot\hat{\mathbf{b}} - \gamma^*)\hat{\mathbf{b}}, \tag{4.22}$$

where

$$\alpha^* = \begin{cases} \alpha_l & \text{low strain phase,} \\ \alpha_h & \text{high strain phase;} \end{cases}$$

$$\gamma^* = \begin{cases} \gamma_l & \text{low strain phase,} \\ \gamma_h & \text{high strain phase;} \end{cases}$$

and

$$M = EI\kappa. \tag{4.23}$$

We now discuss the justification for choosing an energy that is nonconvex in stretch and shear but convex in the curvature. This follows from the work of Bhattacharya (2001), where a theory for rods made of martensitic material has been derived starting from a fully

three-dimensional theory without the use of any apriori ansatz about the deformation. This derivation is in a variational setting appropriate for the study of equilibria, and follows the methods of Bhattacharya and James (1999).

In martensitic materials, we have a high temperature austenite phase, and a low temperature martensite phase. Typically, the symmetry of the austenite is greater than that of the martensite and this gives rise to multiple variants of martensite. There is now a well-developed continuum framework for modeling such materials (see for example, Ball and James (1992), Bhattacharya (1991)), where one describes different configurations of the crystal as deformations of some fixed reference configuration. It is conventional to choose the austenite phase as the reference, so the identity corresponds to the austenite. Each variant of martensite can be obtained by an affine deformation of the austenite, and therefore we can describe the variants through fixed transformation stretch $\mathbf{U}_j$ which takes the austenite lattice to the martensite lattice. We assume that these are positive-definite and symmetric.

For example, there are three variants of martensite in a material undergoing cubic to tetragonal transformation, with

$$\mathbf{U}_1 = \begin{pmatrix} \eta_2 & 0 & 0 \\ 0 & \eta_1 & 0 \\ 0 & 0 & \eta_1 \end{pmatrix}, \quad \mathbf{U}_2 = \begin{pmatrix} \eta_1 & 0 & 0 \\ 0 & \eta_2 & 0 \\ 0 & 0 & \eta_1 \end{pmatrix}, \quad \mathbf{U}_3 = \begin{pmatrix} \eta_1 & 0 & 0 \\ 0 & \eta_1 & 0 \\ 0 & 0 & \eta_2 \end{pmatrix}$$

where the measured values in NiAl are $\eta_1 = 0.9392, \eta_2 = 1.1302$. Similarly there are six variants of martensite in a material undergoing cubic to orthorhombic transformation, with

$$\mathbf{U}_1 = \begin{pmatrix} \frac{\eta_1+\eta_3}{2} & \frac{\eta_1-\eta_3}{2} & 0 \\ \frac{\eta_1-\eta_3}{2} & \frac{\eta_1+\eta_3}{2} & 0 \\ 0 & 0 & \eta_2 \end{pmatrix}, \quad \mathbf{U}_2 = \begin{pmatrix} \frac{\eta_1+\eta_3}{2} & \frac{\eta_3-\eta_1}{2} & 0 \\ \frac{\eta_3-\eta_1}{2} & \frac{\eta_1+\eta_3}{2} & 0 \\ 0 & 0 & \eta_2 \end{pmatrix},$$

and the rest obtained by symmetry where the measured values in CuAlNi are $\eta_1 = 1.0619, \eta_2 = 0.9178, \eta_3 = 1.0231$.

Suppose we make a beam of the material in the austenite phase, and pick an orthonormal basis $\{\hat{\mathbf{e}}_1, \hat{\mathbf{e}}_2, \hat{\mathbf{e}}_3\}$ with $\hat{\mathbf{e}}_1$ the axis of the beam and $\hat{\mathbf{e}}_2$ the transverse direction. Now suppose the beam goes through a phase transformation (say due to cooling) and transforms

completely to a variant whose stress-free configuration is described by an affine deformation with gradient $\mathbf{U}_i$. The directions $\{\hat{\mathbf{e}}_i\}$ now are deformed to $\{\mathbf{U}_j\hat{\mathbf{e}}_i\}$. Suppose further that $\mathbf{U}_j$ and the directions $\{\hat{\mathbf{e}}_i\}$ were chosen such that this deformation is planar except for a uniform stretch in the $\hat{\mathbf{e}}_3$ direction, i.e.,

$$\hat{\mathbf{e}}_1 \cdot \mathbf{U}_j^2\hat{\mathbf{e}}_3 = \hat{\mathbf{e}}_2 \cdot \mathbf{U}_j^2\hat{\mathbf{e}}_3 = 0. \tag{4.24}$$

We can treat this now as a beam in the $\mathbf{U}_j\hat{\mathbf{e}}_1 - \mathbf{U}_j\hat{\mathbf{e}}_2$ plane. The stress-free configuration is described by

$$\lambda = |\mathbf{U}_j\hat{\mathbf{e}}_1|, \quad \beta = \arccos\left(\frac{\hat{\mathbf{e}}_2 \cdot \mathbf{U}_j^2\hat{\mathbf{e}}_1}{|\mathbf{U}_j\hat{\mathbf{e}}_1||\mathbf{U}_j\hat{\mathbf{e}}_2|}\right)$$

or equivalently

$$\alpha = \frac{1}{|\mathbf{U}_j^{-T}\hat{\mathbf{e}}_1|}, \quad \gamma = \frac{\hat{\mathbf{e}}_2 \cdot \mathbf{U}_j^2\hat{\mathbf{e}}_1}{|\mathbf{U}_j\hat{\mathbf{e}}_2|}.$$

Note that rigid body rotations of this beam $\mathbf{U}_j \to \mathbf{Q}\mathbf{U}_j$ do not change these quantities. Finally the moment-free curvature of this beam is zero.

Suppose we have a beam where only the austenite and the first variant of martensite are active, then we have to choose $\{\hat{\mathbf{e}}_i\}$ such that (4.24) holds for $j = 1$. We now have two phases with

$$\alpha_l = 1, \quad \alpha_h = \frac{1}{|\mathbf{U}_1^{-T}\hat{\mathbf{e}}_1|}, \quad \gamma_l = 0, \quad \gamma_h = \frac{\hat{\mathbf{e}}_2 \cdot \mathbf{U}_1^2\hat{\mathbf{e}}_1}{|\mathbf{U}_1\hat{\mathbf{e}}_2|},$$

and Φ_0 depends on temperature. Similarly, if we have a beam where only the first two variants are active. Then, we have to choose $\{\hat{\mathbf{e}}_i\}$ such that (4.24) holds for both $j = 1$ and $j = 2$. We now have two phases with

$$\alpha_l = \frac{1}{|\mathbf{U}_1^{-T}\hat{\mathbf{e}}_1|}, \quad \alpha_h = \frac{1}{|\mathbf{U}_2^{-T}\hat{\mathbf{e}}_2|}, \quad \gamma_l = \frac{\hat{\mathbf{e}}_2 \cdot \mathbf{U}_1^2\hat{\mathbf{e}}_1}{|\mathbf{U}_1\hat{\mathbf{e}}_2|}, \quad \gamma_h = \frac{\hat{\mathbf{e}}_2 \cdot \mathbf{U}_2^2\hat{\mathbf{e}}_1}{|\mathbf{U}_2\hat{\mathbf{e}}_2|},$$

and Φ_0 is zero. In either case, we have two distinct values for the stress-free values of α and γ. At the same time, the moment-free curvature is zero in each of these states. Therefore, it is natural to assume non-convexity of the energy in stretch and shear, but convexity in curvature.

We conclude by noting that even in one given material, one can freely change the stress-free values of α and γ by simply changing the crystallographic orientation of the beam $\{\hat{\mathbf{e}}_i\}$. Consider for example the material undergoing cubic to orthorhombic transformation as in

CuAlNi. Note that the following choice of $\{\hat{\mathbf{e}}_i\}$ satisfies (4.24) for both variants 1 and 2:

$$\hat{\mathbf{e}}_1 = \begin{pmatrix} \cos\xi \\ \sin\xi \\ 0 \end{pmatrix}, \qquad \hat{\mathbf{e}}_2 = \begin{pmatrix} -\sin\xi \\ \cos\xi \\ 0 \end{pmatrix}, \qquad \hat{\mathbf{e}}_3 = \begin{pmatrix} 0 \\ 0 \\ 1 \end{pmatrix}.$$

It is easy to verify that

$$\alpha_l = \frac{\sqrt{2}\eta_1\eta_3}{\sqrt{\eta_1^2+\eta_3^2+2\sin\xi\cos\xi(\eta_1^2-\eta_3^2)}}, \qquad \alpha_h = \frac{\sqrt{2}\eta_1\eta_3}{\sqrt{\eta_1^2+\eta_3^2+2\sin\xi\cos\xi(\eta_3^2-\eta_1^2)}}.$$

and

$$\gamma_l = \frac{4\sqrt{2}\eta_3^2\sin\xi\cos\xi}{\sqrt{\eta_1^2+\eta_3^2+2(\eta_1^2-\eta_3^2)\sin\xi\cos\xi}}, \qquad \gamma_h = -\frac{4\sqrt{2}\eta_1^2\sin\xi\cos\xi}{\sqrt{\eta_1^2+\eta_1^2+2(\eta_3^2-\eta_1^2)\sin\xi\cos\xi}}.$$

4.2.4 Kinetic relations

In addition to the constitutive assumptions above, we need to prescibe a kinetic relation that governs the propagation of phase boundaries (discontinuities in which the two end states are in different phases). This is necessary in quasistatic situations since the velocity of the phase boundary is indeterminate from the balance laws or equilibrium conditions as we will presently see in Section 4.3. This is exactly analogous to the situation in bars as pointed out by Ericksen (1975). Similarly in dynamics we shall soon see in Section 4.4 that unlike classical shocks, the jump conditions alone are *not* sufficient to uniquely determine the propagation velocity of phase boundaries. This information has to be provided from outside. We do so in the form of a kinetic relation: we assume that the propagation velocity of the phase boundary is a constitutive function of the driving force:

$$\dot{s} = V(f).$$

This notion of a kinetic relation was introduced by Abeyaratne and Knowles (see Abeyaratne and Knowles (1990,1991)) in their study of bars. We see that the dissipation inequality (4.19) imposes a restriction on the function V:

$$fV(f) \geq 0.$$

For future use, we calculate the driving force for our two-phase material. Substituting (4.21) and (4.22) in (4.18), a long but straightforward calculation shows that the driving force on a phase boundary with the high strain phase on the right is given by

$$f = EA[\,|\,\alpha^*\,|\,]\,(\langle\alpha^*\rangle - \langle\alpha\rangle) + \mu A[\,|\,\gamma^*\,|\,]\,(\langle\gamma^*\rangle - \langle\gamma\rangle) + \Phi_0. \tag{4.25}$$

Note that we have contributions from the stretch and shear, but none from the curvature.

4.3 Quasistatics

We now explore the behaviour of these beams by studying their equilibrium shapes. We find that the equilibrium shapes are characterized by sharp discontinuities in the tangent and jumps in curvature of the centerline at phase boundaries. We also find that the equilibrium conditions are insufficient to determine the position of the phase boundary, and this provides room for a kinetic relation. We propose a very simple experiment to verify this theory and determine the kinetic relation.

To obtain the equilibrium or quasistatic equations, we drop terms associated with inertia in equations (4.4), (4.6) and jump conditions (4.5), (4.7). We obtain

$$\mathbf{T}' + \mathbf{f} = \mathbf{0}, \qquad M' + \lambda\hat{\mathbf{t}} \times \mathbf{T} + l = 0, \tag{4.26}$$

$$[\,|\,\mathbf{T}\,|\,] = \mathbf{0}, \qquad [\,|\,M\,|\,] = 0 \tag{4.27}$$

where $'$ denotes partial differentiation with respect to x. We, however, allow the phase boundaries to propagate and therefore the kinematic jump conditions (4.1) and (4.2) hold unchanged.

4.3.1 Beam subjected to pure moments

Consider a beam subjected to a moment M at its two ends. We assume that there are no forces applied at the ends, and that the body force as well the body moment are zero. Then we see that $\mathbf{T} = \mathbf{0}$ satisfies $(4.26)_1$ and $(4.27)_1$ automatically. Invoking the moment-curvature relation (4.23), we see that (4.2),$(4.26)_2$ and $(4.27)_2$ reduce to

$$\theta'' = 0, \quad [\,|\,\theta'\,|\,] = 0, \quad [\,|\,\theta\,|\,] = 0$$

irrespective of whether the beam is entirely in the low strain phase or in the high strain phase, or whether the beam contains a phase boundary at some point s. Clearly the solution is

$$\theta = \frac{M}{EI}x + c$$

for some constant c. Therefore, the (inherent) curvature in $\kappa = \theta'$ is constant throughout the beam.

If this beam is entirely in the low strain phase, then we infer from $\mathbf{T} = \mathbf{0}$ and (4.22) that

$$\lambda = \lambda_l = \sqrt{\alpha_l^2 + \gamma_l^2}, \quad \beta = \beta_l = \text{arc tan}\frac{\gamma_l}{\alpha_l}.$$

Since β is the angle between the tangent and the director, we see that the angle ζ between the tangent and the horizontal is given by $\zeta = \frac{M}{EI}x + c - \beta_l$. Recalling that $\mathbf{y}' = \lambda\hat{\mathbf{t}}$, we see that

$$\mathbf{y} = \lambda_l \frac{EI}{M}\left(\sin\left(\frac{M}{EI}x + c - \beta_l\right)\mathbf{i} - \cos\left(\frac{M}{EI}x + c - \beta_l\right)\mathbf{j}\right) + \mathbf{d}$$

for some constant $\mathbf{d}$. Clearly, the centerline is deformed into a circular arc of radius $\frac{EI}{M}\lambda_l$.

Similarly if the beam is entirely in the high strain phase, we can follow the arguments above to see that

$$\mathbf{y} = \lambda_h \frac{EI}{M}\left(\sin\left(\frac{M}{EI}x + c - \beta_h\right)\mathbf{i} - \cos\left(\frac{M}{EI}x + c - \beta_h\right)\mathbf{j}\right) + \mathbf{d}$$

for some constant $\mathbf{d}$. Clearly, the centerline is deformed into a circular arc of radius $\frac{EI}{M}\lambda_h$.

Now assume that we have a phase boundary at s so that the left part $(0, s)$ of the beam is in the low strain phase while the right part (s, L) of the beam is in the high strain phase. Then arguing as above, we see

$$\mathbf{y} = \begin{cases} \lambda_l \frac{EI}{M}\left(\sin\left(\frac{M}{EI}x + c - \beta_l\right)\mathbf{i} - \cos\left(\frac{M}{EI}x + c - \beta_l\right)\mathbf{j}\right) + \mathbf{d}^- & 0 < x \leq s \\ \lambda_h \frac{EI}{M}\left(\sin\left(\frac{M}{EI}x + c - \beta_h\right)\mathbf{i} - \cos\left(\frac{M}{EI}x + c - \beta_h\right)\mathbf{j}\right) + \mathbf{d}^+ & s < x < L \end{cases}$$

for some constants $\mathbf{d}^-, \mathbf{d}^+$ chosen to satisfy $[\![\, \mathbf{y} \,]\!] = 0$ at s. Clearly, the centerline of the left portion of the beam deforms to circular arc of radius $\frac{EI}{M}\lambda_l$ while the centerline of the right portion deforms to a circular arc of radius $\frac{EI}{M}\lambda_h$. This is shown in Figure 4.2. While the inherent curvature is uniform, the centerline of the beam – which is the experimentally

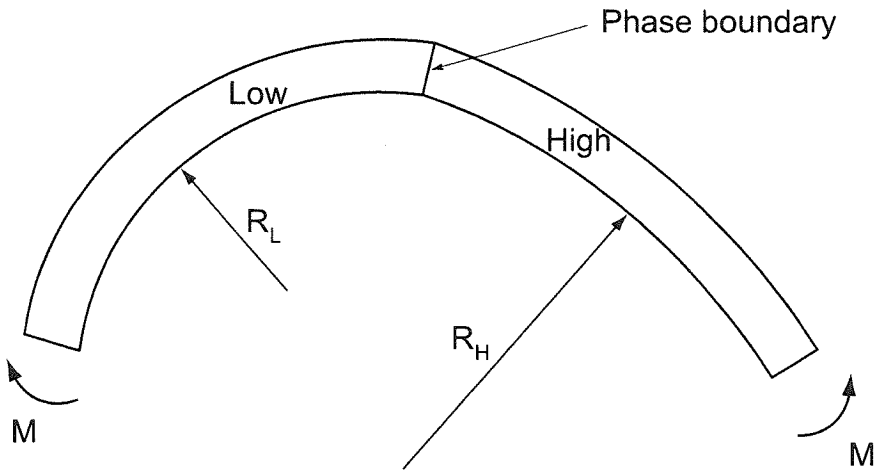

Figure 4.2: A beam with a phase boundary subjected to a constant moment.

observable quantity – has two distinct curvatures.

Further, notice that the tangent is discontinuous across the interface (with an angle of $\beta_h - \beta_l$ between them). In fact, this angle is independent of the applied moment and is present even at zero moment. Thus, we always expect a kink at the phase boundary.

Finally, we can verify from (4.25) that the driving force across this interface is exactly equal to Φ_0, and thus independent of the applied moment. This means that the propagation of the phase boundary, if any, would be independent of the applied moment.

Berg (1994,1995) designed a clever device to subject polycrystalline wires of NiTi to a pure moment. He observed that the deformed shape of the wire was very much like the predictions above with two distinct curvatures, and modelled it using the Euler-Bernoulli beam theory (which is based on an ansatz of zero stretch and shear) with a non-monotone moment-curvature relation. In other words, he assumed that the energy was convex with infinite modulus in the stretch and shear, while it is non-convex in curvature. This is exactly the opposite of what we have done here. We wonder whether the observations of different curvatures were mediated by different stretch as we have proposed here, or that the polycrystalline wires truly have a non-monotone moment curvature relation.

There is evidence for the latter in Berg's experiments. First there is no pronounced tangent discontinuity. Second, he could drive the phase boundary by increasing the applied moment in variance with the conclusions above. We note, however, that the phase boundary could have a non-zero driving force even if the moment-curvature relation were convex if the moduli of the two phases were different as in actual materials. It would be very interesting

to repeat Berg's experiments with single crystal wires so that these issues can be probed in detail. It also remains an interesting and open question, whether non-convexity in shear and stretch in single crystals can give rise to non-convexity in bending in a polycrystal made of multiple grains.

4.3.2 Cantilever with end load

Consider a cantilever with the end $x = 0$ fixed and with a dead load $-F\hat{\mathbf{j}}$ applied to the end $x = L$ as shown in Figure 4.3 (inset). We assume that there are no body forces or moments.

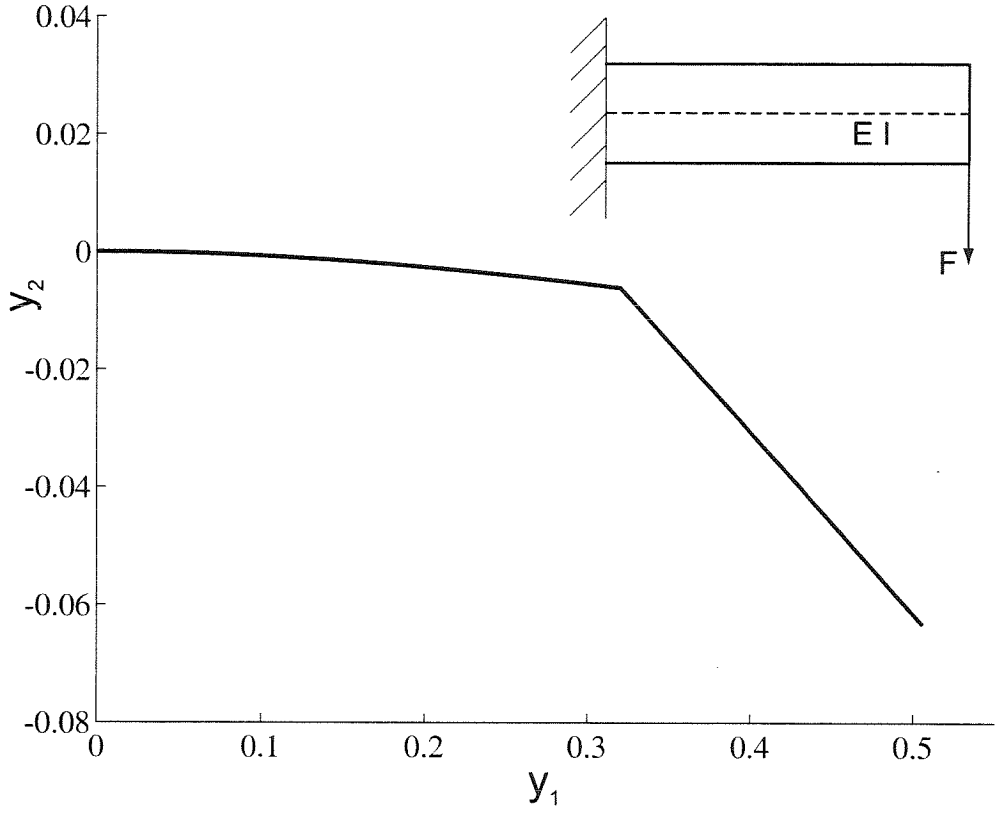

Figure 4.3: Typical deformed centerline of a cantilever with a phase boundary subjected to an end load.

The balance of forces ($(4.26)_1$ and $(4.27)_1$) then requires that $\mathbf{T}$ is constant. Therefore, we conclude from the constitutive relation (4.22) that

$$EA(\alpha - \alpha^*)\sin\theta + \mu A(\gamma - \gamma^*)\cos\theta = 0, \tag{4.28}$$

$$-EA(\alpha - \alpha^*)\cos\theta + \mu A(\gamma - \gamma^*)\sin\theta = -F. \tag{4.29}$$

Solving these simultaneously, we obtain

$$\alpha = \alpha^* + \frac{F}{EA}\cos\theta, \qquad \gamma = \gamma^* - \frac{F}{\mu A}\sin\theta. \tag{4.30}$$

In preparation for writing the balance of moments, we use the above to see that

$$\begin{aligned} \lambda\hat{\mathbf{t}} \times \mathbf{T} &= (-\gamma\hat{\mathbf{b}}^{\perp} + \alpha\hat{\mathbf{b}}) \cdot (-F\hat{\mathbf{j}}) \\ &= -F\left(\left(\alpha^* + \frac{F}{EA}\cos\theta\right)\sin\theta + \left(\gamma^* - \frac{F}{\mu A}\sin\theta\right)\cos\theta\right). \end{aligned}$$

We use this in the balance of moments $(4.26)_2$ and obtain

$$EI\theta'' - F\left(\left(\alpha^* + \frac{F}{EA}\cos\theta\right)\sin\theta + \left(\gamma^* - \frac{F}{\mu A}\sin\theta\right)\cos\theta\right) = 0. \tag{4.31}$$

We have to solve this ordinary differential equation subject to the following boundary conditions if the beam is entirely in one phase:

$$\theta(0) = \theta_0, \quad \theta'(L) = 0;$$

and the following boundary and jump conditions if the beam is in two phases:

$$\theta(0) = \theta_0, \quad \theta'(L) = 0, \quad [\![\,\theta\,]\!] = 0, \quad [\![\,\theta'\,]\!] = 0.$$

Above, $\theta_0 \neq 0$ depends on the experimental setup and is fixed for a given setup. In either case (one phase or two phases), this equation can be easily solved numerically by a shooting method. Figure 4.3 shows the deformed shape of a beam (centerline) with the following parameters: $E = 200.0GPa$, $\mu = 80.0GPa$, $\alpha_l = 1.0$, $\alpha_h = 1.043$, $\gamma_l = 0.0$, $\gamma_h = -0.28$, $L = 0.5m$, $A = 0.01m^2$, $I = 8.333 \times 10^{-6}m^4$ and $F = -50.0N$ with a phase boundary at $s = 0.3$ separating the low strain phase on the left from the high strain phase on the right. Furthermore, unlike the case of pure moments, we find that the phase boundary is subjected to a driving force that is linear in F. It also depends on the position of the phase boundary but only slightly (as shown in Figure 4.4).

This cantilever then provides a simple experiment to determine the kinetic relation. The phase boundary is characterised by a kink and is thus clearly visible. Thus the measurement

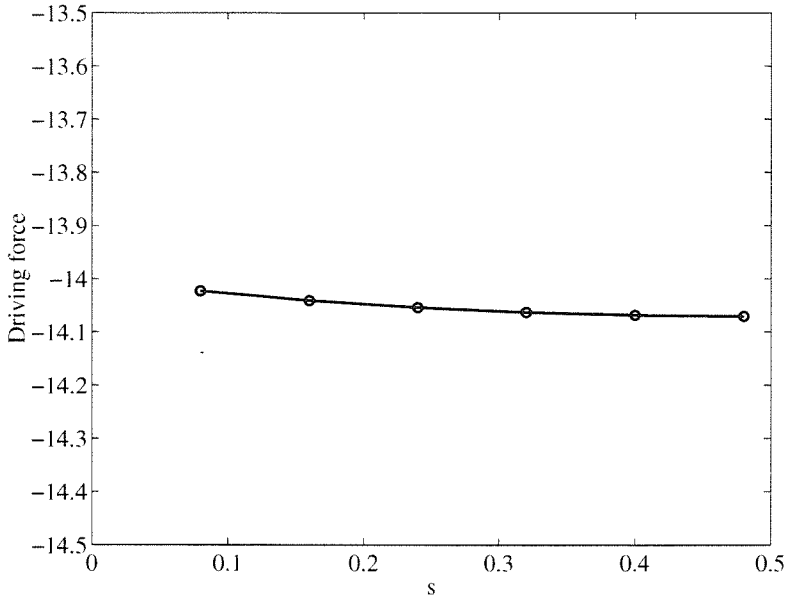

Figure 4.4: Driving force on the phase boundary.

of the propagation velocity is relatively easy. At the same time we can easliy control the driving force through the applied load F. Further α_h,α_l,γ_h,γ_l can be controlled through sample preparation and θ_0 by the clamping condition. This could enable detailed parametric studies.

We now discuss a few limiting cases. If the beam is very slender (i.e., $I/L^2 << A$), then we see that (4.31) is meaningful if and only if $F = O(EI/L^2)$, or if $F << EA, \mu A$. Therefore, $\alpha = \alpha^*$, $\gamma = \gamma^*$, and (4.31) reduces to

$$EI\theta'' - F\left(\alpha^* \sin\theta + \gamma^* \cos\theta\right) = 0.$$

We have to solve this subject to the same boundary and jump conditions above.

If, on the other hand, the beam is stubby (i.e., if $I/L^2 >> A$), then α, γ become too large to be meaningful unless $F = O(EA) = O(\mu A)$. Then, (4.31) with the appropriate boundary and jump conditions reduces to $\theta = \theta_0$. Therefore, (4.30) yields

$$\alpha = \alpha^* + \frac{F}{EA}\cos\theta_0, \qquad \gamma = \gamma^* - \frac{F}{\mu A}\sin\theta_0.$$

Suppose, now, that this beam has a phase boundary at point $x = s$ with the low strain phase on the left and the high strain phase on the right. The driving force on this interface

is given by (4.25) as

$$f = F\left(-(\alpha_h - \alpha_l)\cos\theta_0 + (\gamma_h - \gamma_l)\sin\theta_0\right) + \Phi_0.$$

Therefore, the experiment proposed above would be much simpler in this limit.

Finally, if the beam is stubby, and if the force is small, i.e., if $I/L^2 >> A$, $F/EA << \alpha^*$ and $F/\mu A << \gamma^*$, then we have piecewise rigid deformation,

$$\alpha \approx \alpha^*, \quad \beta \approx \beta^*, \quad \theta \approx \theta_0.$$

This deformation would be trivial in case the beam was made of a single phase. For example, if the beam was made of the low strain phase, the centerline is straight with an angle $\zeta = \theta_0 - \beta_l$ from the horizontal. The deformation is non-trivial in case the beam has a phase boundary at point $x = s$ with the low strain phase on the left and the high strain phase on the right. The centerline would then have a kink at $x = s$ with the left side making an angle $\zeta = \theta_0 - \beta_l$ from the horizontal and the right an angle $\zeta = \theta_0 - \beta_h$. Further, there is a non-trivial driving force on the phase boundary. The formula (4.25) can not be applied here; instead we have to go back to the more fundamental (4.18). We obtain

$$f = \Phi_0 - (-F\hat{\mathbf{j}}) \cdot \left([|\,\alpha^*\,|]\hat{\mathbf{b}}^{\perp} + [|\,\gamma^*\,|]\hat{\mathbf{b}}\right) = \Phi_0 - F[|\,\alpha^*\,|]\cos\theta_0 + F[|\,\gamma^*\,|]\sin\theta_0.$$

We see that there is a non-trivial driving force on the interface and that this depends on the applied load. James and Rizonni (2001) and James (2002) have discussed the use of the piecewise rigid approximation in the modelling of active materials.

4.4 Shocks and phase boundaries

We now turn to dynamics and study the restrictions imposed by the jump conditions on the propagation of discontinuities in a two phase material. We call a discontinuity a *shock* if there is no phase change across it and a *phase boundary* if there is. We show again that there is room for a kinetic relation.

We begin by combining the kinematic and momentum jump conditions. Eliminating

$[|\,\dot{\mathbf{y}}\,|]$ between (4.1) and (4.5), we obtain

$$[|\,\mathbf{T}\,|] = \rho A \dot{s}^2 [|\,\lambda \hat{\mathbf{t}}\,|].$$

Substituting for $\mathbf{T}$ from (4.22), we can expand this to be

$$EA(\hat{\mathbf{b}}^\perp \otimes \hat{\mathbf{b}}^\perp)[|\,\lambda \hat{\mathbf{t}}\,|] - EA[|\,\alpha^*\,|]\hat{\mathbf{b}}^\perp + \mu A(\hat{\mathbf{b}} \otimes \hat{\mathbf{b}})[|\,\lambda \hat{\mathbf{t}}\,|] - \mu A[|\,\gamma^*\,|]\hat{\mathbf{b}} = \rho A \dot{s}^2 [|\,\lambda \hat{\mathbf{t}}\,|].$$

Dividing by ρA yields

$$(\dot{s}^2 - c_1^2 \hat{\mathbf{b}}^\perp \otimes \hat{\mathbf{b}}^\perp)[|\,\lambda \hat{\mathbf{t}}\,|] = c_1^2 [|\,\alpha^*\,|]\hat{\mathbf{b}}^\perp + c_2^2 (\hat{\mathbf{b}} \otimes \hat{\mathbf{b}})[|\,\lambda \hat{\mathbf{t}}\,|] - c_2^2 [|\,\gamma^*\,|]\hat{\mathbf{b}}, \tag{4.32}$$

where

$c_1 = \sqrt{\frac{E}{\rho}}$ is the bar wave speed and

$c_2 = \sqrt{\frac{\mu}{\rho}}$ is the shear wave speed.

We deal similarly with the terms involving curvature and moment. Eliminating $[|\,\dot{\theta}\,|]$ between (4.2) and (4.7), we obtain

$$[|\,M\,|] = \rho I \dot{s}^2 [|\,\theta'\,|].$$

Substituting for M from (4.23), and dividing by ρI, we obtain

$$(\dot{s}^2 - c_1^2)[|\,\theta'\,|] = 0. \tag{4.33}$$

This clearly implies that discontinuities in the curvature θ' necessarily travel at the bar wave speed. This is true irrespective of whether the discontinuity is a shock (in either phase) or a phase boundary. Conversely, a discontinuity travelling at any other speed does *not* allow the curvature to jump.

There is a far richer class of discontinuities allowed by (4.32), as we presently see.

4.4.1 Shocks

We first look at discontinuities where both states are in the same phase so that $[\![\, \alpha^* \,]\!] = [\![\, \gamma^* \,]\!] = 0$. Substituting these in (4.32) reduces it to

$$\dot{s}^2[\![\, \lambda\hat{\mathbf{t}} \,]\!] = c_1^2(\hat{\mathbf{b}}^\perp \otimes \hat{\mathbf{b}}^\perp)[\![\, \lambda\hat{\mathbf{t}} \,]\!] + c_2^2(\hat{\mathbf{b}} \otimes \hat{\mathbf{b}})[\![\, \lambda\hat{\mathbf{t}} \,]\!] \tag{4.34}$$

in both the low strain and the high strain phase. Since we may assume without loss of generality that $[\![\, \lambda\hat{\mathbf{t}} \,]\!] \neq 0$ (else, we would have no discontinuity), we can obtain $\dot{s}^2$ and $[\![\, \lambda\hat{\mathbf{t}} \,]\!]$ as the eigenvalue and eigenvector of

$$c_1^2(\hat{\mathbf{b}}^\perp \otimes \hat{\mathbf{b}}^\perp) + c_2^2(\hat{\mathbf{b}} \otimes \hat{\mathbf{b}}). \tag{4.35}$$

We have two possible solutions,

$$\dot{s}^2 = c_1^2 \text{ with } [\![\, \lambda\hat{\mathbf{t}} \,]\!] || \hat{\mathbf{b}}^\perp \quad \text{and} \quad \dot{s}^2 = c_2^2 \text{ with } [\![\, \lambda\hat{\mathbf{t}} \,]\!] || \hat{\mathbf{b}}. \tag{4.36}$$

We can thus have shocks which propagate at either the bar or the shear wave speeds, but with constraints in the jump on $\frac{\partial \mathbf{y}}{\partial x} = \lambda\hat{\mathbf{t}}$.

To understand these a little more, let us specialize to the case when the tangent is continuous. Then, the first solutions tells us that arbitrary jumps in the stretch λ with no change of phase necessarily have no shear (since the tangent is necessarily perpendicular to the director $\hat{\mathbf{b}}$) and travel at the bar wave speed. These are exactly the shock waves that one has in bars. The second solution requires the tangent to be parallel to the director and thus requires an unphysically large amount of shear. Therefore, we believe that this solution is unphysical when the tangent is continuous.

It is interesting to compare these with the case of strings. There, shocks with discontinuous tangent necessarily have no discontinuity in stretch λ, and propagate at a velocity equal to $\sqrt{T(\lambda)/\lambda}$ (see chapter 2). There appears to be no direct analog of these in beams. We wonder if such solutions would appear as limits of certain travelling waves when the bending modulus goes to zero, or if such solutions are dispersive in beams.

4.4.2 Phase boundaries

We now consider discontinuities in which the two end states are in two different phases. We now have to study (4.32) in all generality. We can rewrite it as two scalar equations (components with respect to $\hat{\mathbf{b}}^{\perp}$ and $\hat{\mathbf{b}}$):

$$(\dot{s}^2 - c_1^2)[|\,\lambda\hat{\mathbf{t}}\,|]\cdot\hat{\mathbf{b}}^{\perp} = -c_1^2[|\,\alpha^*\,|], \tag{4.37}$$

$$(\dot{s}^2 - c_2^2)[|\,\lambda\hat{\mathbf{t}}\,|]\cdot\hat{\mathbf{b}} = -c_2^2[|\,\gamma^*\,|]. \tag{4.38}$$

Clearly these equations do *not* uniquely determine the velocity of the phase boundary. In fact, it can take a range of values depending on $[|\,\lambda\,|]$ and $[|\,\hat{\mathbf{t}}\,|]$. It therefore appears that the jump conditions alone are insufficient to determine the phase boundary velocity and that we need to invoke a kinetic relation.

There is an interesting exception, when we apriori know that the tangent is continuous. Then (4.37) and (4.38) reduce to

$$(\dot{s}^2 - c_1^2)[|\,\lambda\,|]\hat{\mathbf{t}}\cdot\hat{\mathbf{b}}^{\perp} = -c_1^2[|\,\alpha^*\,|], \tag{4.39}$$

$$(\dot{s}^2 - c_2^2)[|\,\lambda\,|]\hat{\mathbf{t}}\cdot\hat{\mathbf{b}} = -c_2^2[|\,\gamma^*\,|]. \tag{4.40}$$

We can solve these simultaneously for $\dot{s}^2$ and $[|\,\lambda\,|]$. In particular,

$$\dot{s}^2 = c_1^2c_2^2\frac{\cos\beta[|\,\gamma^*\,|] - \sin\beta[|\,\alpha^*\,|]}{c_2^2\cos\beta[|\,\gamma^*\,|] - c_1^2\sin\beta[|\,\alpha^*\,|]}.$$

The formulas for $[|\,\lambda\,|]$ are omitted for brevity. Thus, the velocity of a phase boundary would be completely determined by the jump conditions if we knew a priori that the tangent is continuous. This appears to be in contradiction to the behaviour of bars, where the jump conditions do not determine the velocity of the phase boundary. However, a bar is a beam with zero transformation strain in shear $[|\,\gamma^*\,|] = 0$ and infinite shear modulus $\mu = \infty$. Taking the limits $[|\,\gamma^*\,|] \to 0$, $\mu \to \infty$ in (4.40), we see that it reduces to the equation $\hat{\mathbf{t}}\cdot\hat{\mathbf{b}} = 0$, and we are now required to find both $\dot{s}^2$ and $[|\,\lambda\,|]$ from the equation (4.39) which reduces to

$$(\dot{s}^2 - c_1^2)[|\,\lambda\,|] = -c_1^2[|\,\alpha^*\,|].$$

This is exactly the situation in bars. Thus we see that the additional degree of freedom in

shear that beams possess breaks the degeneracy in bars and provides exactly the additional information to determine the phase boundary velocity.

Another noteworthy point here is that when the transformation shear strain $\gamma^* \approx 0$, we obtain $\dot{s}^2 \approx c_2^2$. This means that phase boundaries with continuous tangent in such materials would travel at nearly the shear wave speed.

Chapter 5

Propulsion

5.1 Introduction

Various micro-organisms propel through viscous media by beating flagella or cilia. In particular, a flagellum in eucaryotic cells is a slender structure (tens of microns long and tenths of microns wide) that achieves propulsion by actively deforming in a bending wave propagating from one end to the other (see for example, Bray, 1992). This deformation is resisted by the viscous fluid, and this in turn propels the organism. We wish to explore if it is possible to generate such propulsion by the propagation of phase boundaries through a string or a beam. A possible arrangement is to subject such a string in a viscous fluid to repeated thermal pulses (through the use of a laser for example), each pulse heating the string to nucleate and propagate some phase boundaries which then revert as the string is cooled by ambient environment. Since the phase change causes a change in the transformation strain, the string deforms back and forth as these phase boundaries are nucleated and propagated. We examine if we can arrange this in such a manner as to generate motion.

We first examine a one-dimensional bar with a single phase boundary and show that it cannot propel through a viscous medium. We then show that even multiple phase boundaries in a one-dimensional rod do not alter this conclusion. This leads us to the study of a shearble rod with two phase boundaries capable of moving on a plane, the idea being that we have to move away from one-dimensional motions. In this case again we find very little linear motion but significant rotational motion or 'tumbling'. Finally, we consider a beam with several phase boundaries and show how one can avoid tumbling by having them move in a certain way.

5.1.1 Motion of flagella

We begin by examining the force per unit length $\mathbf{b}$ that the fluid exerts on the string. Consider a flow past a long rigid rod of length L and radius a ($L >> a$). The Reynold's number of this flow is determined by the radius of the rod, and is thus very small for very thin rods. Therefore, we can consider the flow to be laminar. It is then known that the force exerted by the flowing fluid on the rod per unit length is given by

$$\mathbf{b} = d_t(\mathbf{v}\cdot\hat{\mathbf{t}})\hat{\mathbf{t}} + d_n(\mathbf{I}-\hat{\mathbf{t}}\otimes\hat{\mathbf{t}})\mathbf{v} \tag{5.1}$$

where $\mathbf{v}$ is the far-field velocity of the fluid and the coefficients d_t and d_n are given by

$$d_n \simeq 2d_t \simeq \frac{4\pi\mu}{[\log(L/2a)+p]}$$

where μ is the viscosity of the fluid and p is a constant of order 1 (see, for instance, Brennen and Winet (1977)).

Therefore, for a flagella moving with velocity $\dot{\mathbf{y}}$, we take the force per unit length to be

$$\mathbf{b} = -d_t(\dot{\mathbf{y}}\cdot\hat{\mathbf{t}})\hat{\mathbf{t}} - d_n(\mathbf{I}-\hat{\mathbf{t}}\otimes\hat{\mathbf{t}})\dot{\mathbf{y}}$$

for some constants d_t and d_n. The equation for the balance of momentum (2.9) now takes the form

$$\rho\ddot{\mathbf{y}} = \frac{\partial\mathbf{T}}{\partial x} - d_t(\dot{\mathbf{y}}\cdot\hat{\mathbf{t}})\hat{\mathbf{t}} - d_n(\mathbf{I}-\hat{\mathbf{t}}\otimes\hat{\mathbf{t}})\dot{\mathbf{y}}.$$

We now show that it is possible to neglect the inertial term. To see this, non-dimensionalize $\mathbf{y}$ by the length of the string L and t against (L/c) where $c^2 = \frac{E}{\rho}$. Denoting $\mathbf{y}/L$ by $\tilde{\mathbf{y}}$, the inertia and viscous terms respectively are

$$\text{Inertia term} \quad = \quad \frac{L^3\rho c^2}{L}\ddot{\tilde{\mathbf{y}}} \quad = \quad L^2\rho c^2\ddot{\tilde{\mathbf{y}}},$$

$$\text{Viscous term} \quad = \quad \frac{4\pi\mu}{[\log(L/2a)+p]}\frac{L}{L/c}\dot{\tilde{\mathbf{y}}} \quad = \quad \frac{4\pi\mu c}{[\log(L/2a)+p]}\dot{\tilde{\mathbf{y}}}.$$

Therefore, the ratio of the inertia to the drag forces is

$$R = \frac{L^2\rho c}{4\pi\mu}[\log(L/2a)+p].$$

Consider some typical numbers for a bacterial flagella: $L = 5\mu$m, $a = 0.3\mu m$, $c = 1000m/s$, $p = 1$, $\mu = 8.91 \times 10^{-4} Pa.s$. We assume that the density of the flagellar material is about $1000Kg/m^3$ and find $R = 19.7 \times 10^{-16}$. Clearly, the inertial forces are negligible. Therefore, we drop it and write the balance of momentum as

$$\frac{\partial \mathbf{T}}{\partial x} - d_t(\dot{\mathbf{y}} \cdot \hat{\mathbf{t}})\hat{\mathbf{t}} - d_n(\mathbf{I} - \hat{\mathbf{t}} \otimes \hat{\mathbf{t}})\dot{\mathbf{y}} = 0\,. \tag{5.2}$$

We are clearly in a *quasistatic* setting.

In this quasistatic setting, the kinematic jump condition (2.35) holds unaltered, but the momentum jump condition (2.36) simplifies to

$$[\![\, T\hat{\mathbf{t}} \,]\!] = \mathbf{0}\,.$$

This rules out tangent discontinuities (unless $T = 0$), and therefore the tension must be continuous and

$$[\![\, T \,]\!]\hat{\mathbf{t}} = \mathbf{0}\,.$$

For the trilinear material with no temperature jump this reduces to

$$[\![\, \lambda \,]\!] = \gamma_T\,.$$

We notice from (5.2) and the fact that there are no tangent discontinuities that if a string is initially straight, it remains straight for all subsequent times. Therefore, we shall confine ourselves to one-dimensional motions or to bars in what follows.

But before we do so, let us note that heat transfer is very rapid at small sizes, and consequently we may regard our string to be at a uniform temperature at any give time. Successive heating and cooling then uniformly change the temperature of the string, and thus alter the relative stability of the two phases. Therefore, simply by heating and cooling, one can freely change the driving force on phase boundary. Further, if we assume that our kinetic relation is invertible, then we can change the position of the phase boundary as desired by simply controlling the temperature of our string. Therefore, we regard the position of the phase boundaries to be prescribed functions of time in what follows.

5.1.2 Propulsion in bars

The deformation of a bar is axial so that $\mathbf{y}(x,t) = y(x,t)\hat{\mathbf{e}}$ where $\hat{\mathbf{e}}$ is the axis of the bar and y is scalar. It is conventional to work with the displacement $u = y - x$. The tension is clearly then of the form $\mathbf{T} = T\hat{\mathbf{e}}$. The momentum equation (5.2) then reduces to

$$T' - d_t\dot{u} = 0 \tag{5.3}$$

where we use ' to denote differentiation with respect to x. At discontinuities the jump conditions are

$$[\![\, \dot{u} \,]\!] = -\dot{s}[\![\, u' \,]\!] \quad \text{(kinematic)}, \tag{5.4}$$

$$[\![\, T \,]\!] = 0, \qquad \text{(equilibrium)}. \tag{5.5}$$

We now assume that our bar is made of the trilinear material described above, but with zero coefficient of thermal expansion (this is reasonable since the strains due thermal expansion is so much smaller than the transformation strain). The stress-strain relation is then

$$T = \begin{cases} E\epsilon & \text{low strain phase,} \\ E(\epsilon - \gamma_T) & \text{high strain phase.} \end{cases} \tag{5.6}$$

where $\epsilon = u'$ is the strain.

Consider now a bar of length L with stress free ends, with a phase boundary at the point $s(t)$ in $(0, L)$ separating the high strain phase to the left from the low strain phase to the right. From (5.3) and (5.6) governing equation is

$$d_t\dot{u} - Eu'' = 0 \tag{5.7}$$

with boundary conditions

$$u'(0,t) = \gamma_T, \quad u'(L,t) = 0$$

and jump conditions at $s(t)$

$$[\![\, u' \,]\!] = -\gamma_T, \qquad [\![\, \dot{u} \,]\!] = \dot{s}\gamma_T.$$

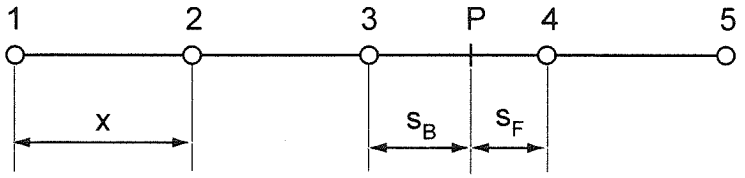

Figure 5.1: Phase boundary in a computational cell.

We consider the bar to be initially stationary and impose a $s(t)$ which sweeps back and forth through the specimen: $s(t)$ monotonically increases from L_0 to L_1 for $0 \leq t \leq t_1$, decreases monomotonically from L_1 to L_0 for $t_1 \leq t \leq t_2$ and then is repeated periodically. The problem of propulsion is to find the net movement $u(x, t + t_2) - u(x, t)$ at long times, and then to find $s(t)$ that maximizes it.

This problem is difficult to solve analytically, and therefore we solve it numerically. The problem above is to solve a heat equation with a moving sourse at the phase boundary $s(t)$. We do so by an explicit time stepping scheme based on finite differences. We have to be careful about the moving phase boundary since it leads to small cell-sizes and thus large errors. We do so as follows.

Figure 5.1 shows four cells with a phase boundary between grid-points 3 and 4. The variable u is evaluated at the grid points at each time step. Let us denote the value of u at grid-point k at the n^{th} time step by u_k^n. Then u_k^{n+1} is determined using

$$d_1 \Delta x \frac{u_k^{n+1} - u_k^n}{\Delta t} = E \frac{u_{k+1}^n - 2u_k^n + u_{k-1}^n}{\Delta x}$$

where Δx is the cell size and Δt is the time step. Both of them are chosen as constants. The above method for evaluating u_k^{n+1} is valid only for points like 1, 2, 5, etc., that are not neighbours of a phase boundary. Points like 3 and 4 that have a phase boundary between them need special treatment. Consider 3 for instance. Assuming that the left side of the phase boundary is in the high strain phase, we can write

$$d_t \Delta x \frac{u_3^{n+1} - u_3^n}{\Delta t} = E\Big(\frac{u_P^n - u_3^n}{s_B} - \gamma_T\Big) - E\Big(\frac{-u_2^n + u_3^n}{\Delta x} - \gamma_T\Big)$$

where u_P^n denotes the displacement at the phase boundary at the n^{th} time step. The difficulty with using this scheme for u_3 is that we have to divide by s_B which may become a very small quantity at some time. This problem is circumvented by making use of the

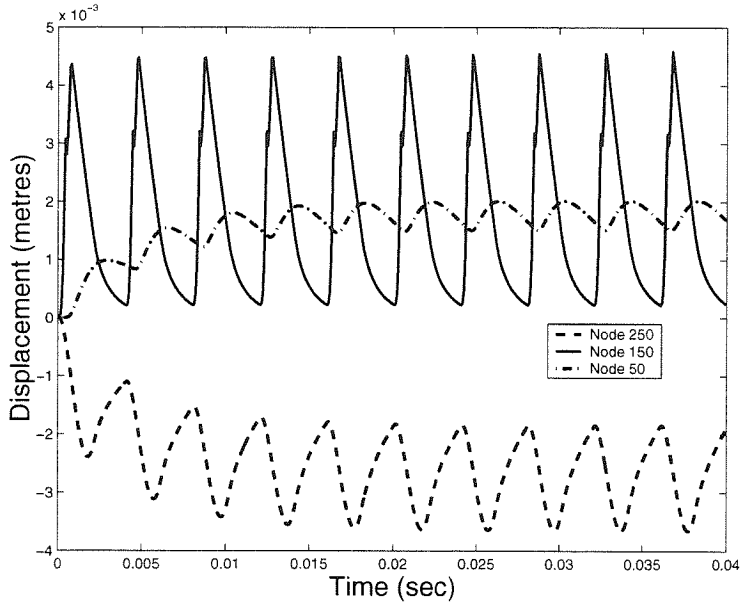

Figure 5.2: Displacement histories of points on the bar.

jump condition $[|\,T\,|] = 0$. In the above case where the high strain phase is on the left, we have

$$\begin{aligned} \frac{u_4^n - u_P^n}{s_F} + \gamma_T &= \frac{u_P^n - u_3^n}{s_B}, \\ s_F + s_B &= \Delta x. \end{aligned}$$

Combining these,

$$\frac{u_P^n - u_3^n}{s_B} = \frac{u_4^n}{\Delta x} - \frac{u_3^n}{\Delta x} + \frac{\gamma_T s_F}{\Delta x}.$$

Using this we can rewrite the equation for u_3^{n+1} as

$$d_t \Delta x \frac{u_3^{n+1} - u_3^n}{\Delta t} = E \frac{u_4^n - 2u_3^n + u_2^n + \gamma_T s_F}{\Delta x}.$$

Note that we are no longer dividing by s_B, thus avoiding errors coming from division by small numbers. A similar equation can be written for u_4^{n+1}. We have

$$d_t \Delta x \frac{u_4^{n+1} - u_4^n}{\Delta t} = E \frac{u_5^n - 2u_4^n + u_3^n + \gamma_T s_B}{\Delta x}.$$

Figure 5.2 shows the results of a calculation of a bar with 300 nodes where the phase boundary is swept back and forth between nodes 120 to 180. It is easily seen that after

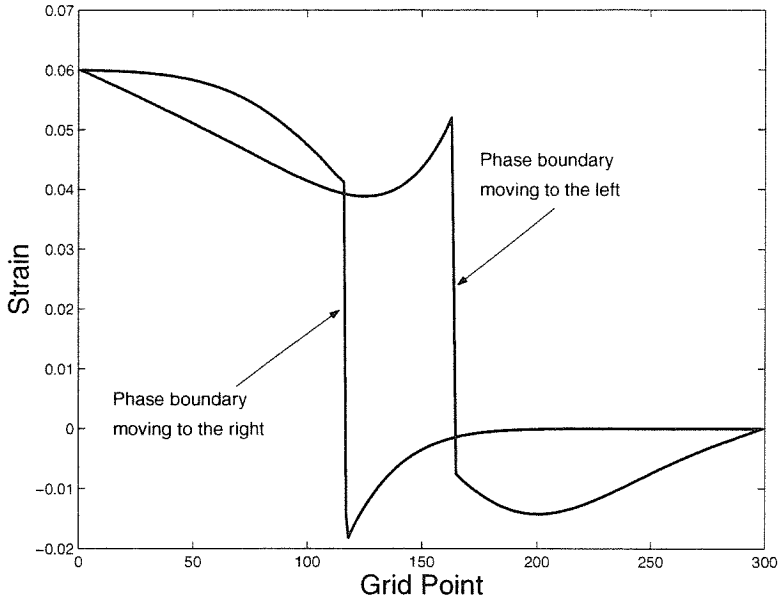

Figure 5.3: Strain profiles of the bar with the phase boundary.

a brief transient various points on the bar just oscillate about a mean position with *no propulsion*. During the transient the bar gets stretched to the equilibrium length. Thereafter, it oscillates about this equilibrium and it does not propel itself. Two typical strain profiles during this oscillation are shown in Figure 5.3. We find very similar results for various different trajectories of the phase boundary. In fact, we have found in our numerical explorations that the result (of no propulsion) remains unchanged even if we have two or more phase boundaries instead of one.

5.1.3 Piecewise rigid body dynamics

In order to understand the results above, we study the motion of a piecewise rigid bar which one would obtain in the limit $E \to 0$. Here the bar is divided into segments by the moving phase boundaries, and the particle velocity as well as the strain is uniform in each segment. Furthermore, the strain can only take the values 0 and γ_T depending on the phase.

Let us begin with a single phase boundary with a given trajectory $s(t)$. Then, the particle velocity and strain are given by

$$\dot{u}(x,t) = \begin{cases} \dot{u}^+(t) & 0 < x < s(t), \\ \dot{u}^-(t) & s(t) < x < L, \end{cases}$$

$$u'(x,t) = \begin{cases} \gamma_T & 0 < x < s(t), \\ 0 & s(t) < x < L. \end{cases}$$

The field equation is then meaningless, and therefore we have to consider the integral version of the balance law,

$$T(x_2) - T(x_1) = d_t \int_{x_1}^{x_2} \dot{u} dx, \tag{5.8}$$

from which we conclude that

$$T(s^-) = d_t \dot{u}^+ s, \quad T(s^+) = -d_1 \dot{u}^- (L - s).$$

Applying the jump conditions (which remain the same), we obtain

$$d_t \dot{u}^+ s = -d_t \dot{u}^- (L - s), \qquad \dot{u}^+ - \dot{u}^- = \dot{s}\gamma_T \tag{5.9}$$

which we can solve for the unknowns $\dot{u}^\pm$ to obtain

$$\dot{u}^- = \frac{\dot{s}\gamma_T}{L} s, \quad \dot{u}^+ = -\frac{\dot{s}\gamma_T}{L}(L - s)$$

For a given pulse $s(t)$, we can now find the displacement

$$\begin{aligned} u_0 &= \int_0^{t_2} \dot{u}^+(t) dt \\ &= -\frac{\gamma_T}{L} \int_0^{t_1} \dot{s}(t)(L - s(t)) dt - \frac{\gamma_T}{L} \int_{t_1}^{t_2} \dot{s}(t)(L - s(t)) dt \\ &= -\frac{\gamma_T}{L} \left\{ \left(L(s(t_1) - s(0)) - \int_{s(0)}^{s(t_1)} s ds \right) + \left(L(s(t_2) - s(t_1)) - \int_{s(t_1)}^{s(t_2)} s ds \right) \right\} \\ &= -\frac{\gamma_T}{L} \left\{ L(L_1 - L_0) - \frac{1}{2}(L_1^2 - L_0^2) + L(L_0 - L_1) - \frac{1}{2}(L_0^2 - L_1^2) \right\} \\ &= 0 \end{aligned}$$

where we have only used the facts $s(0) = s(t_2) = L_0$, $s(t_1) = L_1$. Thus, it is *impossible* to produce a net displacement: the bar moves in one direction as the phase boundary sweeps across the bar. but moves an equal amount in the opposite direction as the phase boundary sweeps back. Indeed, we could have predicted this from the governing equations (5.9): they are invariant under time reversal.

Now consider n phase boundaries at $s_i(t)$, $i = 1, \ldots n$ separating the high and low strain phases (with the high strain phase at the extreme left). From the momentum jump condition (5.5) at each phase boundary, we obtain

$$u_i' - u_{i+1}' = (-1)^{i-1}\gamma_T, \qquad i = 1, \ldots n.$$

Combining these with the kinematic jump condition (5.4) at each phase boundary, we obtain

$$\dot{u}_i - \dot{u}_{i+1} = (-1)^i \dot{s}_n \gamma_T, \qquad i = 1, \ldots n. \tag{5.10}$$

We now apply (5.8) to the entire bar and recall that $T(0) = T(L) = 0$. We obtain

$$0 = T(L) - T(0) = c\int_0^L \dot{u} dx = \dot{u}_1 s_1 + \dot{u}_2(s_2 - s_1) + \ldots \dot{u}_n(s_n - s_{n-1}) + \dot{u}_{n+1}(L - s_n) \tag{5.11}$$

since the velocity is piecewise constant. Equations (5.10) and (5.11) constitute a system of $n+1$ linear equations for the $n+1$ variables $\dot{u}_1, \dot{u}_2, \ldots\ldots, \dot{u}_{n+1}$. The solution of these equations is

$$\begin{aligned} \dot{u}_p &= K + \gamma_T \sum_{i=p}^{n} (-1)^i \dot{s}_{n-i} \qquad (p = 1, 2, \ldots., n) \\ \dot{u}_{n+1} &= K, \end{aligned}$$

where

$$K = \frac{1}{L}(s_1\dot{s}_1 - s_2\dot{s}_2 + \ldots\ldots + (-1)^{n-1} s_n \dot{s}_n). \tag{5.12}$$

We can now find the propulsion from the displacement of the particle $x = L$. We have

$$u(L,t) = \int_0^t \dot{u}_{n+1}\, dt = \int_0^t \mathbf{a}\cdot\mathbf{s}\, dt = \int_{\mathbf{s}(0)}^{\mathbf{s}(t)} \mathbf{a}\cdot d\mathbf{s}$$

where $\mathbf{a} = [s_1, -s_2, s_3, \ldots, (-1)^n s_n]^T$ and $\mathbf{s} = [s_1, s_2, \ldots, s_n]^T$. We assume that $\mathbf{s}(t)$ is periodic with period T, so that we can find $u(L,T)$ from the above by integrating over a closed loop in the n-dimensional s-space. However, notice that

$$\mathbf{a} = \nabla_{\mathbf{s}}\phi \qquad \text{where} \qquad \phi = \frac{1}{2}(s_1^2 - s_2^2 + \ldots + (-1)^{n-1} s_n^2).$$

Therefore,

$$u(L,T) = \oint \mathbf{a} \cdot d\mathbf{s} = \oint \nabla_{\mathbf{s}}\phi \cdot d\mathbf{s} = 0.$$

Therefore, there can be no propulsion with bars undergoing piecewise rigid motion. Therefore, one can have no significant propulsion in bars with a finite but large elastic modulus. In fact, we believe that there is no propulsion for any finite elastic modulus as suggested by the numerical study in the previous sub-section but have been unable to prove it.

5.2 Beam with piecewise rigid body dynamics

One-dimensional motions do not generate propulsion. So, in this section we consider planar motions of a beam with phase boundaries. We saw in chapter 4 that there is large shear associated with these phase boundaries. We intend to exploit this feature to generate propulsion. We assume that the deformation of the beam is piecewise rigid so that θ is uniform (i.e., $\theta(x,t) = \theta(t)$). Consequently, the angle that the tangent to the centerline makes with the horizontal is $\zeta(t) + \zeta_0$ in the high strain phase and $\zeta(t) - \zeta_0$ in the low strain phase. The stretch is λ_h in the high strain phase and λ_l in the low strain phase. We assume that the position and evolution of the phase boundaries is a given input, and try to determine the overall motion of the beam. We do not discuss how one may generate such phase boundaries. Finally, we only consider quasistatics.

Suppose we have a beam with two phase boundaries moving periodically in a prescribed manner. Let $s_1(t)$ and $s_2(t)$ denote the positions of the phase boundaries in the reference configuration, and let the leftmost part of the beam be in the low strain phase. Then given the position $\mathbf{y}_0(t)$ of the leftmost point $x = 0$, and $\zeta(t)$, we can use the piecewise rigid assumption to write down the position of the centerline as

$$\mathbf{y}(x,t) = \begin{cases} \mathbf{y}_0(t) + \lambda_l x\, \hat{\mathbf{t}}^- & 0 \le x \le s_1, \\ \mathbf{y}_0(t) + \lambda_l s_1\, \hat{\mathbf{t}}^- + \lambda_h (x - s)\, \hat{\mathbf{t}}^+ & s_1 \le x \le s_2, \\ \mathbf{y}_0(t) + \lambda_l s_1\, \hat{\mathbf{t}}^- + \lambda_h (s_2 - s_1)\, \hat{\mathbf{t}}^+ + \lambda_l (x - s_2) \hat{\mathbf{t}}^- & s_2 \le x \le L \end{cases} \tag{5.13}$$

where $\hat{\mathbf{t}}^- = \cos(\zeta - \zeta_0)\hat{\mathbf{i}} + \sin(\zeta - \zeta_0)\hat{\mathbf{j}}$ and $\hat{\mathbf{t}}^+ = \cos(\zeta + \zeta_0)\hat{\mathbf{i}} + \sin(\zeta + \zeta_0)\hat{\mathbf{j}}$ respectively.

Differentiating with respect to t, we obtain the particle velocity

$$\dot{\mathbf{y}}(x,t) = \begin{cases} \dot{\mathbf{y}}_0(t) + \dot{\zeta}\lambda_l x\ \hat{\mathbf{n}}^- & 0 \le x \le s_1, \\ \dot{\mathbf{y}}_0(t) + \lambda_l \dot{s_1}\ \hat{\mathbf{t}}^- + \dot{\zeta}\lambda_l s_1\ \hat{\mathbf{n}}^- - \lambda_h \dot{s_1}\ \hat{\mathbf{t}}^+ + \dot{\zeta}\lambda_h(x - s_1)\ \hat{\mathbf{n}}^+ & s_1 \le x \le s_2, \\ \dot{\mathbf{y}}_0(t) + \lambda_l \dot{s_1}\ \hat{\mathbf{t}}^- + \dot{\zeta}\lambda_l s_1\ \hat{\mathbf{n}}^- + \lambda_h(\dot{s_2} - \dot{s_1})\ \hat{\mathbf{t}}^+ + \dot{\zeta}\lambda_h(s_2 - s_1)\ \hat{\mathbf{n}}^+ & \\ \qquad -\lambda_l \dot{s_2}\ \hat{\mathbf{t}}^- + \dot{\zeta}\lambda_l(x - s_2)\ \hat{\mathbf{n}}^- & s_2 \le x \le L. \end{cases} \tag{5.14}$$

where $\hat{\mathbf{n}}^- = -\sin(\zeta-\zeta_0)\hat{\mathbf{i}}+\cos(\zeta-\zeta_0)\hat{\mathbf{j}}$ and $\hat{\mathbf{n}}^+ = -\sin(\zeta+\zeta_0)\hat{\mathbf{i}}+\cos(\zeta+\zeta_0)\hat{\mathbf{j}}$ are perpendicular to $\hat{\mathbf{t}}^-$ and $\hat{\mathbf{t}}^+$ respectively. We seek to obtain the unknowns $\dot{\mathbf{y}}_0(t)$ and $\dot{\zeta}(t)$ using the balance of forces and moments,

$$\mathbf{0} = \int_0^L \{d_t(\dot{\mathbf{y}} \cdot \hat{\mathbf{t}})\hat{\mathbf{t}} + d_n(\dot{\mathbf{y}} - (\dot{\mathbf{y}} \cdot \hat{\mathbf{t}})\hat{\mathbf{t}})\}dx \tag{5.15}$$

and

$$0 = \int_0^L (\mathbf{y}(x) - \mathbf{y}(0)) \times \{d_t(\dot{\mathbf{y}} \cdot \hat{\mathbf{t}})\hat{\mathbf{t}} + d_n(\dot{\mathbf{y}} - (\dot{\mathbf{y}} \cdot \hat{\mathbf{t}})\hat{\mathbf{t}})\}\ dx. \tag{5.16}$$

A long and cumbersome but unenlightening calculation then yields

$$\mathbf{A}(\mathbf{s})\mathbf{R}(\zeta)\mathbf{v} = \mathbf{B}(\mathbf{s})\dot{\mathbf{s}}. \tag{5.17}$$

where $\mathbf{A}(\mathbf{s})$ is a 3×3 matrix, $\mathbf{s} = \{s_1, s_2\}^T$, $\mathbf{R}(\zeta)$ is a 3×3 rotation matrix of angle ζ about the axis perpendicular to the plane of the beam, $\mathbf{v} = \{\dot{y}_1(0,t), \dot{y}_2(0,t), \dot{\zeta}(t)\}^T$, $\mathbf{B}(\mathbf{s})$ is a 3×2 matrix and $\dot{\mathbf{s}} = \{\dot{s}_1, \dot{s}_2\}^T$. Assuming that $\mathbf{A}$ is invertible [1] this equation can be solved to obtain

$$\mathbf{v} = \mathbf{R}^T\mathbf{A}^{-1}\mathbf{B}\dot{\mathbf{s}} \tag{5.18}$$

Since the phase boundary motion is periodic with period T, we integrate this from time 0 to T to see if there is any propulsion. This integration becomes a contour integration on the (s_1, s_2)–plane. The presence of $\mathbf{R}$ makes it impossible to do the integrations explicitly. The integrations are therefore performed numerically over contours that avoid the singular curve of $\mathbf{A}$. It is possible to integrate the equations even if one chooses a trajectory that crosses (non-tangentially) the singular curve at a finite number of points by requiring the continuity of $\mathbf{y}_0$ and ζ. The results from one of these calculations are shown in Figure 5.4.

[1] $\mathbf{A}$ is invertible except on a certain curve in the (s_1, s_2)–plane. We will call this curve the *singular curve* of $\mathbf{A}$.

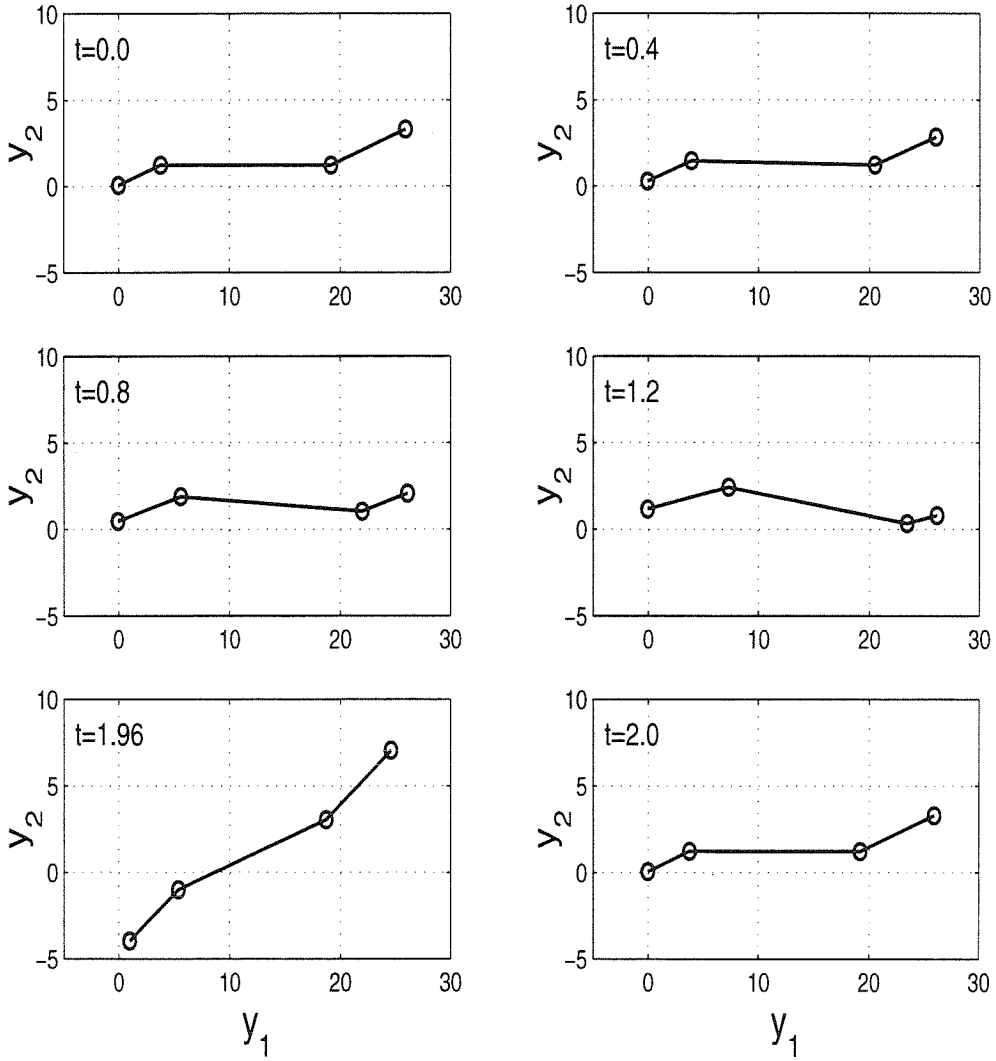

Figure 5.4: Positions in space of a beam with two phase boundaries. There is a lot of tumbling and very little linear motion.

We see that we have significant tumbling, but very little linear motion. While we have not made any systematic attempt to optimize the propulsion by proper choice of trajectory, our numerical experiments suggest that this behaviour is typical. The relatively short length of the beam makes it easy to tumble unless the phase boundaries are perfectly symmetric; and any propulsive gains made in one part of the period are reversed in the other part as the phase boundaries reset. It will be interesting to study this in greater detail, perhaps using the framework of geometric phases developed by Kelly and Murray (1998) and Marsden and Ostrowski (1995).

We now propose a strategy to overcome the difficulties above. We show that it is possible

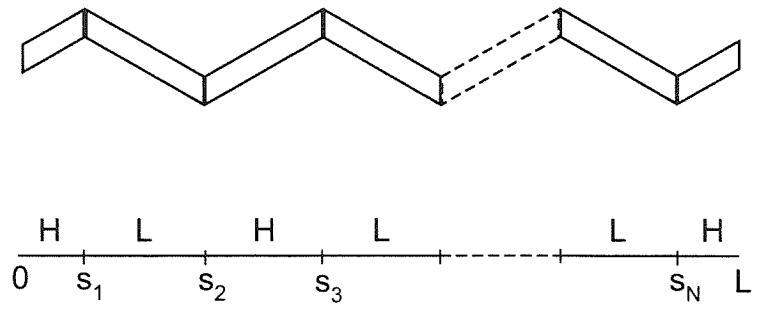

Figure 5.5: Beam with multiple phase boundaries.

to generate linear propulsion with little tumbling by having multiple phase boundaries moving from one end of the beam to the other. Suppose we have a long beam, and we periodically nucleate a phase boundary on the left ($x = 0$), and have them propagate to the right with a propagation velocity v till they traverse through the entire beam and exit at the right ($x = L$). Clearly we have to alternately nucleate a low/high and a high/low phase boundary. Then at any instance of time t, the beam is composed of alternating segments of the low and high strain phase separated by phase boundaries which have a uniform spacing. This is shown in Figure 5.5. Suppose at the instant t the beam has N phase boundaries at the positions $s_1(t), s_2(t), \ldots, s_N(t)$ with

$$s_i - s_{i-1} = d, \quad i = 2, \ldots, N.$$

We refer to the segment of the beam $(0, s_1)$ the first segment, and the segment (s_{i-1}, s_i) to be the ith segment for $i = 2, \ldots N$.

Let us first assume that the first segment is in the high strain phase; subsequent segments alternate between the low and high strain phases. Therefore,

$$\lambda(x,t) = \lambda_i, \quad \zeta(x,t) = \zeta_i \quad s_{i-1} < x < s_i$$

where

$$\lambda_i = \begin{cases} \lambda_h & i \text{ odd}, \\ \lambda_l & i \text{ even}, \end{cases} \qquad \zeta_i = \begin{cases} \zeta_h = \zeta + \zeta_0 & i \text{ odd}, \\ \zeta_l = \zeta - \zeta_0 & i \text{ even}. \end{cases}$$

The tangent and the normal to the centerline of the beam are

$$\hat{\mathbf{t}} = \cos\zeta_i\hat{\mathbf{i}} + \sin\zeta_i\hat{\mathbf{j}},\ \ \hat{\mathbf{n}} = -\sin\zeta_i\hat{\mathbf{i}} + \cos\zeta_i\hat{\mathbf{j}}$$

in the ith segment. Note that $\dot{\hat{\mathbf{t}}}_i = \dot{\zeta}\hat{\mathbf{n}}_i$. For future use, we set

$$\alpha_{ij} = \hat{\mathbf{t}}_i \cdot \hat{\mathbf{t}}_j = \hat{\mathbf{n}}_i \cdot \hat{\mathbf{n}}_j = \begin{cases} 1 & i+j \text{ even}, \\ -\sin 2\zeta_0 & i+j \text{ odd}, \end{cases}$$

$$\beta_{ij} = \hat{\mathbf{t}}_i \cdot \hat{\mathbf{n}}_j = \hat{\mathbf{n}}_i \cdot \hat{\mathbf{t}}_j = \begin{cases} 0 & i+j \text{ even}, \\ \sin 2\zeta_0 & i+j \text{ odd}. \end{cases}$$

The position of the centerline of the beam is given by

$$\begin{aligned} \mathbf{y}(x,t) &= \mathbf{y}_0(t) + \lambda_1 s_1 \hat{\mathbf{t}}_1 + \sum_{i=2}^{k} \lambda_i (s_i - s_{i-1})\hat{\mathbf{t}}_i + \lambda_{k+1}(x - s_k)\hat{\mathbf{t}}_{k+1} \qquad (5.19) \\ &= \mathbf{y}_0(t) + \lambda_1 s_1 \hat{\mathbf{t}}_1 + \sum_{i=2}^{k} \lambda_i d\hat{\mathbf{t}}_i + \lambda_{k+1}(x - s_k)\hat{\mathbf{t}}_{k+1} \end{aligned}$$

for $s_k < x \le s_{k+1}$. Therefore, the velocity of a point on the centerline is given by

$$\dot{\mathbf{y}}(x,t) = \dot{\mathbf{y}}_0(t) + \dot{\zeta}\left(\lambda_1 s_1 \hat{\mathbf{n}}_1 + \sum_{i=2}^{k} \lambda_i d\hat{\mathbf{n}}_i + \lambda_{k+1}(x - s_k)\hat{\mathbf{n}}_{k+1}\right) + v\left(\lambda_1 \hat{\mathbf{t}}_1 - \lambda_{k+1}\hat{\mathbf{t}}_{k+1}\right) \quad (5.20)$$

for $s_k < x \le s_{k+1}$.

We shall first use the balance of angular momentum to show that if N is large, then $\dot{\zeta} = 0$, or that the tumbling is eliminated by putting a large number of interfaces. To that end, we calculate

$$\begin{aligned} l_f(x,t) &= (\mathbf{y}(x,t) - \mathbf{y}_0(t)) \times \mathbf{f} \\ &= \left(\left((\mathbf{y} - \mathbf{y}_0)\cdot\hat{\mathbf{t}}\right)\hat{\mathbf{t}} + \left((\mathbf{y} - \mathbf{y}_0)\cdot\hat{\mathbf{n}}\right)\hat{\mathbf{n}}\right) \times \left(d_t(\dot{\mathbf{y}}\cdot\hat{\mathbf{t}})\hat{\mathbf{t}} + d_n(\dot{\mathbf{y}}\cdot\hat{\mathbf{n}})\hat{\mathbf{n}}\right) \\ &= d_n\left((\mathbf{y} - \mathbf{y}_0)\cdot\hat{\mathbf{t}}\right)(\dot{\mathbf{y}}\cdot\hat{\mathbf{n}}) - d_t\left((\mathbf{y} - \mathbf{y}_0)\cdot\hat{\mathbf{n}}\right)(\dot{\mathbf{y}}\cdot\hat{\mathbf{t}}) \\ &= d_n\left(\lambda_1 s_1 \alpha_{1\,k+1} + \sum_{i=1}^{k} \lambda_i d\alpha_{i\,k+1} + \lambda_{k+1}(x - s_k)\right) \\ &\quad \left(\dot{\mathbf{y}}\cdot\hat{\mathbf{n}}_{k+1} + \dot{\zeta}\left(\lambda_1 s_1 \alpha_{1\,k+1} + \sum_{i=1}^{k} \lambda_i d\alpha_{i\,k+1} + \lambda_{k+1}(x - s_k)\right) + v\lambda_1\beta_{1\,k+1}\right) \end{aligned}$$

$$
\begin{aligned}
& -d_t\left(\lambda_1 s_1 \beta_{1\,k+1} + \sum_{i=1}^{k} \lambda_i d\beta_{i\,k+1}\right) \\
& \quad \left(\dot{\mathbf{y}}\cdot\hat{\mathbf{t}}_{k+1} + \dot{\zeta}\left(\lambda_1 s_1 \beta_{1\,k+1} + \sum_{i=1}^{k} \lambda_i d\beta_{i\,k+1}\right) + v(\lambda_1\alpha_{1\,k+1} - \lambda_{k+1})\right) \\
= \;& \dot{\zeta} d^2\left(d_n\left(\sum_{i=1}^{k}\lambda_i\alpha_{i\,k+1}\right)^2 - d_t\left(\sum_{i=1}^{k}\lambda_i\beta_{i\,k+1}\right)^2\right) \\
& + d_n\left(\sum_{i=1}^{k}\lambda_i d\alpha_{i\,k+1}\right)(a_{k+1} + b_{k+1}(x-s_k)) - d_t\left(\sum_{i=1}^{k}\lambda_i d\beta_{i\,k+1}\right)c_{k+1} \\
& + e_{k+1} + f_{k+1}(x-s_k) + g_{k+1}(x-s_k)^2
\end{aligned}
$$

for $s_k < x \le s_{k+1}$. Therefore,

$$
\begin{aligned}
\int_{s_k}^{s_{k+1}} l_f dx \;=\; & \dot{\zeta} d^3\left(d_n\left(\sum_{i=1}^{k}\lambda_i\alpha_{i\,k+1}\right)^2 - d_t\left(\sum_{i=1}^{k}\lambda_i\beta_{i\,k+1}\right)^2\right) \\
& + d_n\left(\sum_{i=1}^{k}\lambda_i d\alpha_{i\,k+1}\right)\left(a_{k+1}d + b_{k+1}\frac{d^2}{2}\right) - d_t d\left(\sum_{i=1}^{k}\lambda_i d\beta_{i\,k+1}\right)c_{k+1} \\
& + d e_{k+1} + f_{k+1}\frac{d^2}{2} + g_{k+1}\frac{d^3}{3}. \qquad (5.21)
\end{aligned}
$$

Now note that

$$
\lambda_i\alpha_{i\,k+1} = \begin{cases} \lambda_h & i \text{ odd} \quad k+1 \text{ odd} \\ -\lambda_h \sin 2\zeta_0 & i \text{ odd} \quad k+1 \text{ even} \\ -\lambda_l \sin 2\zeta_0 & i \text{ even} \quad k+1 \text{ odd} \\ \lambda_l & i \text{ even} \quad k+1 \text{ even} \end{cases}
$$

so that

$$
\sum_{i=1}^{k}\lambda_i\alpha_{i\,k+1} \approx \frac{k}{4}\left(\lambda_h(1-\sin 2\zeta_0) + \lambda_l(1-\sin 2\zeta_0)\right)
$$

for k large enough and averaged over k odd and even. Similarly,

$$
\sum_{i=1}^{k}\lambda_i\beta_{i\,k+1} \approx \frac{k}{4}\left(\lambda_h \sin 2\zeta_0 + \lambda_l \sin 2\zeta_0\right)
$$

for k large enough and averaged over k odd and even. Substituting these in (5.21), we see

that

$$\int_{s_k}^{s_{k+1}} l_f dx = \frac{\dot{\zeta} d^3 \langle \lambda^* \rangle}{16} k^2 \left(d_n (1 - 2\sin 2\zeta_0 + \sin^2 2\zeta_0) - d_t \sin^2 2\zeta_0 \right) + O(k).$$

Therefore, if the number of phase boundaries N is large enough,

$$\int_0^L l_f dx \approx \sum_{k=1}^{N} \int_{s_k}^{s_{k+1}} l_f dx \approx \frac{\dot{\zeta} d^3 N^3 \langle \lambda^* \rangle}{48} \left(d_n (1 - 2\sin 2\zeta_0 + \sin^2 2\zeta_0) - d_t \sin^2 2\zeta_0 \right) + O(N^2).$$

Therefore, we see that if N is large enough, the balance of angular momentum,

$$\int_0^L l_f dx = 0$$

implies that

$$\dot{\zeta} = 0.$$

Now, according to (5.1) and (5.20), the body force per unit length,

$$\begin{aligned} \mathbf{f} &= d_t (\dot{\mathbf{y}}_0 \cdot \hat{\mathbf{t}}_{k+1}) \hat{\mathbf{t}}_{k+1} + d_n (\dot{\mathbf{y}}_0 \cdot \hat{\mathbf{n}}_{k+1}) \hat{\mathbf{n}}_{k+1} \\ &\quad + v \left(d_t \left(\lambda_1 \alpha_{1\,k+1} - \lambda_{k+1} \right) \hat{\mathbf{t}}_{k+1} + d_n \lambda_1 \beta_{1\,k+1} \hat{\mathbf{n}}_{k+1} \right) \end{aligned}$$

for $s_k < x \leq s_{k+1}$. Therefore, for N large enough,

$$\int_0^L \mathbf{f} dx = \sum_{k=1}^{N} \int_{s_k}^{s_{k+1}} \mathbf{f} dx \approx \mathbf{A}\dot{\mathbf{y}} - v\mathbf{a}_h$$

where

$$\begin{aligned} \mathbf{A} &= d_t \langle \hat{\mathbf{t}} \otimes \hat{\mathbf{t}} \rangle + d_n \langle \hat{\mathbf{n}} \otimes \hat{\mathbf{n}} \rangle, \\ \mathbf{a}_h &= \frac{1}{2} \left(d_t (\lambda_h \sin 2\zeta_0 + \lambda_l) \hat{\mathbf{t}}_l - d_n \lambda_h \sin 2\zeta_0 \hat{\mathbf{n}}_l \right). \end{aligned}$$

Therefore, the balance of forces gives us

$$\dot{\mathbf{y}} = v\mathbf{A}^{-1}\mathbf{a}_h.$$

This gives the velocity as long as the first segment is in the high strain phase.

We can do a similar calculation when the first segment is in the low strain phase. We obtain

$$\dot{\mathbf{y}} = v\mathbf{A}^{-1}\mathbf{a}_l.$$

where

$$\mathbf{a}_l = \frac{1}{2}\left(d_t(\lambda_l \sin 2\zeta_0 + \lambda_h)\hat{\mathbf{t}}_h - d_n\lambda_l \sin 2\zeta_0 \hat{\mathbf{n}}_h\right).$$

Therefore, we obtain a propulsion with overall velocity

$$\frac{v}{2}\mathbf{A}^{-1}(\mathbf{a}_h + \mathbf{a}_l).$$

Two aspects were crucial above. First, that the beam was long with a large number of interfaces. This seems important for preventing tumbling. Second, all the phase boundaries moved in one direction. This is consistent with the behavior observed in flagella.

Bibliography

[1] Abeyaratne, R. and Knowles, J.K., 1990. On the driving traction on a surface of a strain discontinuity in a continuum. *J. Mech. Phys. Solids*, **38**, 345.

[2] Abeyaratne, R. and Knowles, J.K., 1991. Kinetic realtions and the propagation of phase boundaries in solids *Arch. Rational Mech. Anal.*, **114**, 119.

[3] Abeyaratne, R. and Knowles, J.K., 1993. A continuum model of a thermoelastic solid capable of undergoing phase transitions. *J. Mech. Phys. Solids*, **41**, 541.

[4] Abeyaratne, R. and Knowles, J.K., 1994. Dynamics of propagating phase boundaries: thermoelastic solids with heat conduction. *Arch. Rational Mech. Anal.*, **126**, 203-230.

[5] Abeyaratne, R. and Knowles, J.K., 1997. Impact-induced phase transitions in thermoelastic solids. *Phil. Trans. R. Soc. Lond. A*, **355**, 843.

[6] Antman, S.S., 1995. *Non-linear problems of elasticity*, Springer-Verlag, New York.

[7] Ball, J.M. and James, R.D., 1992. Proposed experimental tests of a theory of fine microstructure and the two-well problem, *Phil. Trans. Royal Soc. London A* **338**, 389-450.

[8] Balk, A.M., Cherkaev, A.V. and Slepyan, L.I., 2001a. Dynamics of chains with non-monotone stress-strain relations - I, Model and numerical experiments. *J. Mech. Phys. Solids*, **49**, 131.

[9] Balk, A.M., Cherkaev, A.V. and Slepyan, L.I., 2001b. Dynamics of chains with non-monotone stress-strain relations - II, Nonlinear waves and waves of phase transition. *J. Mech. Phys. Solids*, **49**, 149.

[10] Berg, B.T., 1994. Thermomechanics of shape memory alloy rods, Ph.D. Thesis, University of Minnesota.

[11] Berg, B.T., 1995. Bending of superelastic wires 1 - Experimental aspects, *J. Appl. Mech.* **62**(2), 459-465.

[12] Bhattacharya, K. 1991. Wedge-like micro-structure in martensites, *Acta Metall. Mater.* **39**, 2431-2444.

[13] Bhattacharya, K. 2001. A direct derivation of a theroy of rods with application to shape-memory alloys, In preparation.

[14] Bhattacharya, K. and James, R.D., 1999. A theory of thin films of martensitic materials with applications to microactuators, *J. Mech. Phys. Solids.* **47**, 531-576.

[15] Bray, D. 1992. *Cell Movements*, Garland Publishing, New York.

[16] Brennen, C. and Winet, H., 1977. Fluid mechanics of propulsion by cilia and flagella. *Ann. Rev. Fluid Mech.* **9**, 339-398.

[17] Chin, R.C.Y., 1975. Dispersion and Gibbs phenomenon associated with difference approximations to initial-boundary value problems for hyperbolic equations. *Journal of Computational Physics* **18**, 233-247.

[18] Coleman, B.D. and Noll, W., 1963. The thermodynamics of elastic materials with heat conduction and viscosity. *Arch. Rational Mech. Anal.*, **13**, 167-178.

[19] Ericksen, J.L., 1975. Equilibrium of bars. *Journal of Elasticity*, **5**, 191.

[20] Escobar, J. and Clifton, R., 1993. On pressure-shear plate impact for studying the kinetics of stress-induces phase transitions. *Mater. Sci. Engng. A* **170**, 125-142.

[21] Eshelby, J.D., 1956. *Solid state physics*, Vol. 3, pages 17-144. Academic press, New York.

[22] Eshelby, J.D., 1975. The elastic energy-momentum tensoir. *Journal of Elasticity*, **5**, 321.

[23] Gurtin, M.E., 1995. The nature of configurational forces. *Arch. Rational Mech. Anal.*, **131**, 67-100.

[24] Gurtin, M.E., 2000. *Configurational forces as basic concepts of continuum physics*, Springer-Verlag, New York.

[25] James, R.D., 2002. I. Real and configurational forces in magnetism, and II. Analysis of a microscale cantilever. To appear in *Continuum Mech. and Thermodynamics* (issue in honor of Ingo Müller).

[26] James, R.D. and Rizzoni, R., 2001. Piecewise rigid body mechanics. In preparation.

[27] Kelly, S.D. and Murray, R.M., 1995. Geometric phases and robotic locomotion. *J. of Robotic Systems.*, **12**(6), 417-431.

[28] Krumhansl, J.A. and Schrieffer, J.R., 1975. Dynamics and statistical mechanics of a one-dimensional model Hamiltonian for structural phase transitions. *Phys. Rev. Letters*-B, **11**, 3535-3545.

[29] Marsden, J.E. and Ostrowski, J., 1998. Symmetries in motion: Geometric foundations of motion control, *Nonlinear Sci. Today.*

[30] Ngan, S. and Truskinovsky, L., 1998. Thermal trapping and kinetics of martensitic phase boundaries. *J. Mech. Phys. Solids*, **47**, 141.

[31] Puglisi, G. and Truskinovsky, L., 2000. Mechanics of a discrete chain with bi-stable elastic elements. *J. Mech. Phys. Solids*, **48**, 1.

[32] Rice, J.R., 1971. An internal variable theory and its application to metal plasticity. *J. Mech. Phys. Solids*, **19**, 433.

[33] Rosakis, P. and Knowles, J.K., 1997. Unstable kinetic relations and the dynamics of solid-solid phase transitions. *J. Mech. Phys. Solids*, **45**, 1055.

[34] Simha, N.K. and Bhattacharya, K., 1998. Kinetics of phase boundaries with edges and junctions. *J. Mech. Phys. Solids*, **46**, 2323.

[35] Simha, N.K. and Bhattacharya, K., 2000. Kinetics of phase boundaries with edges and junctions in a three-dimensional multiphase body. *J. Mech. Phys. Solids*, **48**, 2619-2641.

[36] Slemrod, M., 1983. Admissibility criteria for propagating phase boundaries in a Van der Waals fluid. *Arch. Rational Mech. Anal.*, **81**, 301.

[37] Slemrod, M., 1984. Dynamic phase transitions in a Van der Waals fluid. *J. Diff. Eqs.*, **52**, 1.

[38] Truskinovsky, L., 1987. Dynamics of nonequilibrium phase boundaries in a heat conducting non-linear elastic medium. *J. Appl. Math and Mech.*(PMM) **51**, 777-784.

[39] Turteltaub, S. 1997. Viscosity and strain gradient effects on the kinetics of propagating phase boundaries. *Journal of Elasticity*, **46**, 53.

[40] Wegner, J., Haddow, J.B. and Tait, R.J., 1989. *Elastic wave propagation*, pages 161-166. Elsevier Science Publishers B.V. (North Holland).

[41] Zhong, X., Hou, T.Y. and LeFloch, P. 1996. Computational methods for propagating phase boundaries. *Journal of Computational Physics*, **124**, 192.